Supplementary Information

Stabilizing microbial communities by looped mass transfer

Shuang Li[a], Nafi'u Abdulkadir[a], Florian Schattenberg[a], Ulisses Nunes da Rocha[a], Volker Grimm[b,c], Susann Müller[a*] and Zishu Liu[d]

[a]Helmholtz Centre for Environmental Research-UFZ, Department of Environmental Microbiology, Permoserstr. 15, 04318 Leipzig, Germany.

[b]Helmholtz Centre for Environmental Research-UFZ, Department of Ecological Modelling, Permoserstr. 15, 04318 Leipzig, Germany.

[c]University of Potsdam, Plant Ecology and Nature Conservation, Am Mühlenberg 3, 14476 Potsdam, Germany

[d]College of Environmental and Resource Sciences, Zhejiang University, 866 Yuhangtang Rd, Hangzhou 310058, China

Content

S1: Bioreactor setup

The bioreactors were constructed and handled as described previously (1). In short, a microbial community from an activated sludge basin of a wastewater treatment plant (Eilenburg, Saxonia, Germany, 51°27′39.4″N, 12°36′17.5″E) was pre-cultivated in a medium mixture of peptone medium and synthetic wastewater [v:v = 2%:98%; 0.198 g L^{-1} peptone (from meat), 0.2 g L^{-1} meat extract, 0.219 g L^{-1} yeast extract, 0.1 g L^{-1} glucose, 0.49 g L^{-1} Na-propionate (filtered), 0.0059 g L^{-1} $CaCl_2.2H_2O$, 0.0294 g L^{-1} KCl, 0.06 g L^{-1} NaCl, 0.04 g L^{-1} K_2HPO_4, 0.2156 g L^{-1} KH_2PO_4 and 0.0196 g L^{-1} $MgSO_4.7H_2O$; chemicals were purchased from: Merck KGaA (Darmstadt, Germany), SERVA Electrophoresis GmbH (Heidelberg, Germany) and Carl Roth GmbH (Karlsruhe, Germany)]. This pre-cultivation was started by mixing 10 mL thawed activated sludge samples (from frozen aliquots) with 100 mL medium mixture in a 500 mL Erlenmeyer flask, and the cultivation was carried out on a rotary shaker at 125 rpm and 30°C for 24 h (Incubator Hood TH 25; Edmund Bühler GmbH, Hechingen, Germany). Five bioreactors were then setup in parallel and the same volume of the preculture was used for inoculation for each 1 L bioreactor filled with the medium mixture to a final volume of 800 mL (initial $OD_{600,\ d=5mm} = 0.057 \pm 0.003$). Effluents of each of the five reactors were collected by a sixth bioreactor, and this reactor was operated in exactly the same way as the other five reactors, only without the addition of fresh medium (Fig. 1).

All six connected reactors were run at 27°C (thermostat with Incubator Hood TH 25) and 350 rpm using a multipoint magnetic stirrer (Thermo Electron LED GmbH, Langenselbold, Germany) and stirrer bars (45 × 8 mm, Labsolute®; Th. Geyer GmbH, Renningen, Germany), and at an aeration rate of 150 mL min^{-1} with compressed sterile filtered ambient air controlled by a rotor gas flowmeter (six measuring channels; Analyt-MTC GmbH, Müllheim, Germany). The fluidic system of the bioreactors was controlled through a set of microprocessor-controlled dispensing pumps IPC-N 12 (Ismatec®; Cole-Parmer GmbH, Wertheim, Germany), and the continuously running mode was maintained over time.

S2: Experimental setup

The local communities L1-L5 and the regional pool R together formed a metacommunity (Fig. S2.1). The rates of effluents and influents among the local communities L1-L5 and also for the regional pool R were controlled manually. The flow rate of the total influent (medium plus recycling flow) into each of the local communities L1-L5 was set at a constant 0.4 mL min^{-1}, a dilution rate

of 0.72 d^{-1} and a hydraulic retention time of 33.3 h. The setup for the regional pool R differed from that of local communities L1-L5. The influent of the regional pool R was the sum of effluents from the five local communities L1-L5 without additional nutrients. This setup caused a fivefold higher dilution rate than for the local communities. Owing to $5D$ (i.e., 3.6 d^{-1}), the cells entered and left the regional pool R at a fivefold higher rate than for the five local communities L1-L5.

The six reactors were run for 110 days. The days were sub-grouped into five phases according to increasing recycling flow rates (Table S2.1). The first phase was the Insular I phase, in which no exchange with the other reactors was allowed. The reactor serving as the regional pool R was run as a sink for local community effluents starting at day 9, which were not recycled back to the local communities L1-L5. The second phase RC_{10} (i.e. recycling rate RC 10%) started at day 26 in which the regional pool R and the local communities L1-L5 were interconnected. The third phase RC_{50} (i.e. recycling rate RC 50%) was started at day 47 and the fourth phase RC_{80} (i.e. recycling rate RC 80%) at day 64. In phases 2-4, the inflow from the regional pool R, increasing from 0.04, 0.2 and 0.32 mL min^{-1}, was compensated for by decreasing the amounts of medium. Therefore, the medium flow rates were lowered to 0.36, 0.2 and 0.08 mL min^{-1} (Table S2.1). To maintain the nutrient load rate for the local communities L1-L5 under the recycling flow rate conditions, the nutrients in the medium were concentrated 1.1 times, 2 times and 5 times, accordingly. In the fifth Insular II phase starting at day 89, all recycling from the regional pool R to local communities L1-L5 was stopped and conditions returned back to how they were in the first phase. Within each of the five phases, the first 7 days were defined as an adaptation period in which the medium volume of the reactors was exchanged five times. Afterwards, balanced growth conditions were assumed. A total of 448 samples were collected from the six bioreactors in 110 days, with 76 samples from each of the local communities L1-L5 and 68 samples from the regional pool R. The number of samples, recycling flow rate settings and time intervals per phase are summarized in Table S2.1.

Table S2.1 Summary of sample numbers, recycling rate (RC) setting and time intervals per phase

phase	number of samples per reactor	medium flow rate (mL min^{-1})	recycling flow rate (mL min^{-1})	medium factor	adaptation period (d)	balanced period (d)
Insular I	18 (10 for R)	0.4	0	1	0-8	8-26
RC_{10}	14	0.36	0.04	1.1	26-33	33-47
RC_{50}	13	0.2	0.2	2	47-54	54-64
RC_{80}	15	0.08	0.32	5	64-71	71-89
Insular II	16	0.4	0	1	89-96	96-110

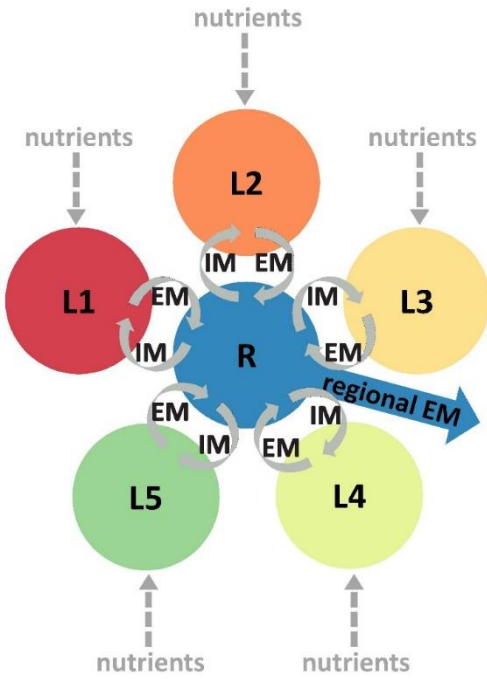

Figure S2.1 Conceptual setup of the metacommunity investigated in this study. Local communities L1-L5 assembled in identical localities, and all were connected to a community in the regional pool R. Microbial immigration (IM) and emigration (EM) of local communities occurred between each of the local communities and the regional pool R. In addition, cells were emigrated via the regional pool R.

S3: Analysis and calculation of functional parameters

For each sample, 7 mL of cell culture was taken, of which 0.2 mL was used for counting total cell number (CN), 1 mL for DNA extraction (centrifuged at 21,000×g for 10 min and 4°C, and pellet stored at -20°C), and 5.8 mL for the measurements of optical density (OD), pH and electrical conductivity (EC), as well as for the flow cytometric analysis of the cells. In addition, 5 mL was collected two to five times a week per reactor to analyze the chemical oxygen demand of the supernatant (CODs) and of the total sample (CODt), ammonium-nitrogen (NH4, supernatant) and

total phosphate, calculated as phosphor (PHOt, total sample). The dry weight (DW) was measured once a week using a 20 mL sample.

The optical density ($OD_{600, d=5\ mm}$, Ultraspec 1100pro; Amersham Biosciences, Little Chalfont, UK), pH (EL 20; Mettler-Toledo, Greifensee, Switzerland) and electrical conductivity (EC, inolab Cond7110; WTW, Germany) were measured daily in all reactors. Additionally, COD, NH4 and PHOt were measured daily in the first 7 days (i.e., adaptation period) and once every 3 or 4 days during the balanced period per phase. CODs and CODt (DIN ISO 15705:2002) and NH4 (DIN 38406-E5) were analyzed with NANOCOLOR® test tubes (Macherey-Nagel GmbH, Düren, Germany) following the manufacturer's instructions. CODb (chemical oxygen demand of biomass) was calculated by subtracting CODs from CODt. PHOt (phosphate) was measured by phosphomolybdate blue spectrophotometry. Briefly, after a pre-heating treatment (120°C, 30 min), 500 µL diluted supernatant was treated with 800 µL reagent [stock solution: 125 mL H_2O, 25 mL 9N H_2SO_4, 25 mL $Mo_7O_{24}^{-6}$ solution (1.65 g $(NH_4)_6Mo_7O_{24}{\cdot}4H_2O$ in 25 mL H_2O), and 25 mL Fe (II) solution (3.89 g $(NH_4)_2Fe(SO_4)_2{\cdot}6H_2O$ in 25 mL H_2O)] for 10 minutes. The dry weight (DW) of the biomass was measured once a week during the balanced growth conditions of each phase. Briefly, the cell solution was centrifuged at 5,000×g for 10 min at 4°C (Centrifuge 5804R; Eppendorf, Hamburg, Germany). The supernatant was discarded and the residual pellet was transferred to a 2 mL tube and centrifuged at 20,000×g for 10 min at 4°C (Heraeus Fresco 21 centrifuge; Thermo Scientific, Langenselbold, Germany). Finally, the pellet was dried at 50°C for 4 days. In addition to CODb and DW, biomass was also evaluated by counting the total number of cells mL^{-1} (CN) by flow cytometry (Supplementary Information S5). All other supernatants measured in this study were obtained by centrifuging the samples at 3,200×g for 10 min and 4°C. The OD, pH, EC and PHOt measurements were performed in triplicate, while COD and NH4 were measured in duplicates. A graphical overview of all parameters is shown in Fig. S3.1. All data of the parameters are listed in Dataset S1.

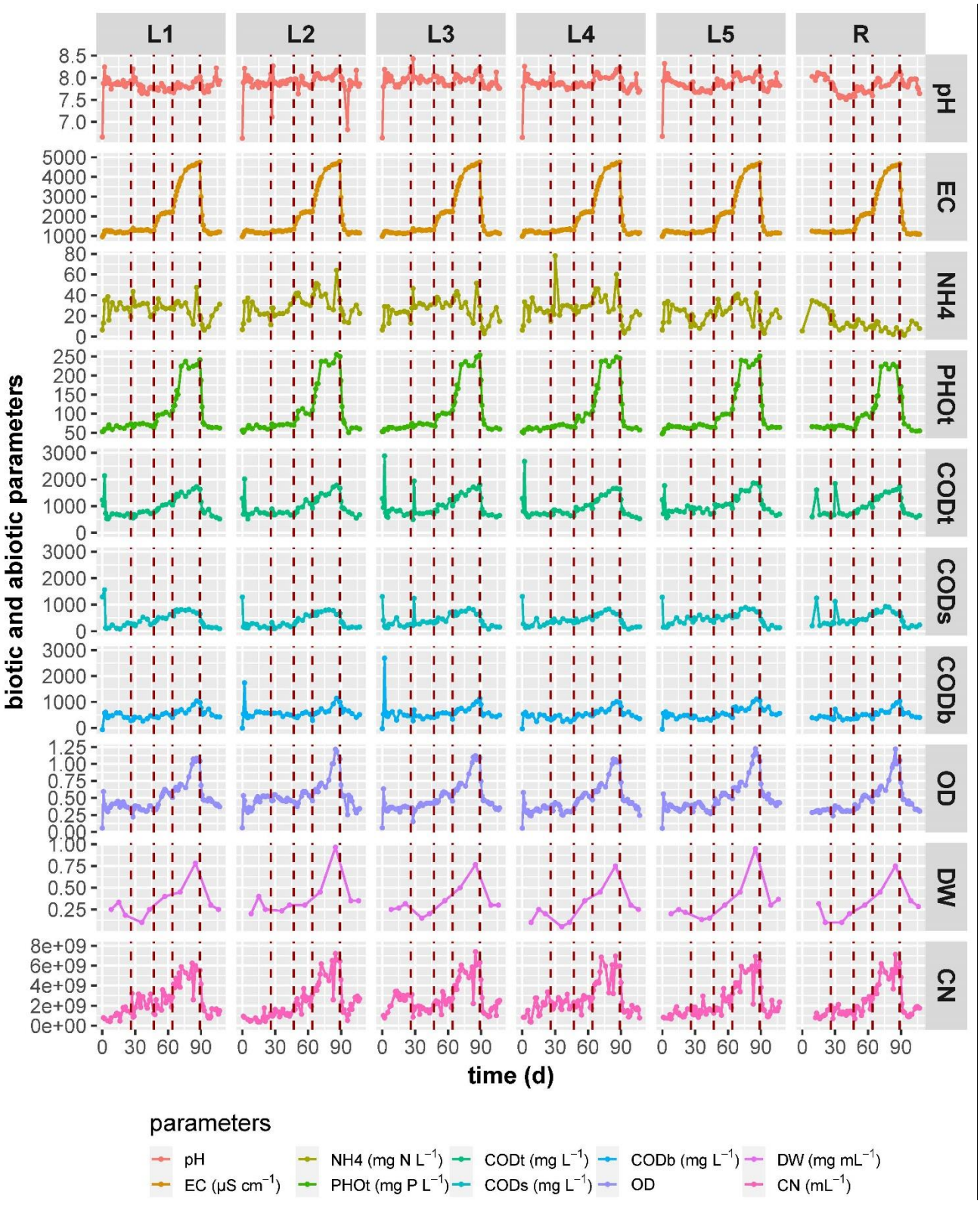

208
209

210 **Figure S3.1** Overview of the bulk biotic and abiotic parameters measured for the local communities L1-L5
211 and the regional pool R. Parameters were pH, EC (electrical conductivity, µS cm^{-1}), NH4 (ammonium, mg

N L^{-1}), PHOt (phosphate of total sample, mg P L^{-1}), CODt (chemical oxygen demand of total sample, mg L^{-1}), CODs (chemical oxygen demand of supernatant, mg L^{-1}), CODb (chemical oxygen demand of biomass, mg L^{-1}), $OD_{600,\ d=5mm}$ (optical density), DW (dry weight, g L^{-1}) and CN (cell number, mL^{-1}). The dashed red lines indicate the times at which the next phase begins.

With the increase of RC_{10} to RC_{80} the values for the abiotic parameter EC and phosphate also increased, while the values for ammonium and pH remained constant in local communities L1-L5. The biotic parameter showed increased values for biomass (CODb, OD, dry weight and cell number; comparisons between successive phases, Wilcoxon test: $p \leqslant 0.01$). The regional pool R showed similar trends, with the exception of ammonium, which decreased. In all reactors, the highest biomass values were found in RC_{80} and the lowest in Insular I phase and Insular II phase (Fig. S3.1, Dataset S1).

Effects of mass transfer on the universal functions of wastewater communities

Wastewater communities have the function to remove carbon, nitrogen and phosphorus from the wastewater. Carbon is taken up into biomass or degraded to CO_2. Ammonium-nitrogen is originating from the destruction of biomass (especially from proteins: amino-acids) and is removed mainly via nitrification and denitrification. Phosphorus is released during anaerobic conditions and by cell destruction into the wastewater and can be removed by biomass production and accumulation as polyphosphates in the biomass under mainly aerobic conditions. Produced biomass is finally taken out from the wastewater treatment process as biosolids which are finally either burned or used for other purposes. In this study removal of carbon is measured by various COD values, the removal of nitrogen by NH4 values and the removal of phosphorus as PHOt values. To evaluate the influences of mass transfer on these functional parameters, we summarized the measured values as average ± standard deviations per balanced period per phase and per reactor, which are shown in Table S3.1. Due to the looped mass transfer, medium and biomass recycled between local communities L1-L5 and the regional pool R (Supplementary Information S2) with increasing mass transfer rates in phases 2, 3 and 4. The average NH4 values in the wastewater supernatant remained roughly unchanged while CODs values and PHOt values of the total biomass increased with mass transfer rates. The increase in total biomass (CN: cell number; CODb: carbon bound in biomass) also increased with mass transfer rates.

Table S3.1 Average values of changes in CODs (chemical oxygen demand of the supernatant), CODb (chemical oxygen demand of biomass), NH4 (ammonium-nitrogen in supernatant), PHOt (total phosphate)

CN (cell number) and DW (dry weight) per local communities L1-L5 and regional pool R, determined for the balanced period per phase. The CODs, NH4, and PHOt values for the medium are also given.

phase	reactor	CODs (mg L^{-1})	CODb (mg L^{-1})	NH4 (mg N L^{-1})	PHOt (mg P L^{-1})	CN ($\times 10^9$ L^{-1})	DW (mg L^{-1})
Insular I	L1	192.0 ± 92.1	489.4 ± 86.9	29.3 ± 3.3	64.5 ± 4.5	1.3 ± 0.4	258.3 ± 106.1
	L2	196.2 ± 78.2	566.2 ± 74.8	24.9 ± 5.0	63.6 ± 4.2	0.7 ± 0.4	325.0 ± 106.1
	L3	274.7 ± 136.7	503.5 ± 132.0	23.9 ± 1.1	63.3 ± 2.2	2.9 ± 0.4	291.7 ± 35.4
	L4	280.5 ± 123.9	423.3 ± 115.6	27.6 ± 5.7	61.1 ± 3.3	2.0 ± 0.9	225.0 ± 35.4
	L5	395.2 ± 118.1	452.0 ± 64.5	25.6 ± 3.9	64.6 ± 2.2	1.2 ± 0.4	233.3 ± 23.6
RC_{10}	L1	399.5 ± 118.1	372.8 ± 85.6	28.4 ± 6.1	72.0 ± 2.5	2.5 ± 0.5	175.0 ± 106.1
	L2	223.0 ± 57.8	513.8 ± 58.8	25.1 ± 4.3	71.7 ± 1.0	1.2 ± 0.2	266.7 ± 47.1
	L3	328.0 ± 44.9	413.0 ± 48.4	30.3 ± 2.0	73.0 ± 1.8	1.6 ± 0.3	175.0 ± 35.4
	L4	395.0 ± 59.7	331.8 ± 112.6	27.4 ± 4.5	69.1 ± 2.8	2.3 ± 0.5	75.0 ± 35.4
	L5	493.5 ± 94.9	326.3 ± 30.2	16.4 ± 7.6	68.6 ± 3.6	1.5 ± 0.6	141.7 ± 11.8
	R	335.0 ± 51.8	360.0 ± 51.7	9.5 ± 2.8	66.1 ± 3.5	1.4 ± 0.3	150.0 ± 70.7
RC_{50}	L1	541.3 ± 86.3	535.3 ± 42.7	27.7 ± 0.8	99.9 ± 3.8	2.6 ± 0.7	400.0
	L2	534.0 ± 110.5	566.7 ± 42.1	31.5 ± 1.5	104.2 ± 8.1	2.5 ± 0.8	300.0
	L3	509.7 ± 175.3	566.0 ± 23.4	30.2 ± 2.3	101.1 ± 1.2	2.4 ± 0.7	350.0
	L4	478.0 ± 52.5	508.3 ± 49.1	29.5 ± 0.9	93.3 ± 10.9	2.3 ± 0.7	350.0
	L5	521.5 ± 85.0	527.5 ± 45.0	24.5 ± 3.0	98.7 ± 0.9	2.5 ± 0.8	300.0
	R	502.7 ± 107.2	505.7 ± 20.5	9.8 ± 3.0	95.5 ± 4.3	2.1 ± 0.7	300.0
RC_{80}	L1	768.5 ± 57.7	783.9 ± 185.8	28.9 ± 13.0	226.6 ± 6.7	5.0 ± 1.3	783.3
	L2	748.0 ± 70.9	815.2 ± 222.8	39.6 ± 15.1	238.0 ± 10.6	5.5 ± 1.5	966.7
	L3	762.0 ± 84.0	810.8 ± 145.5	29.5 ± 14.4	233.0 ± 9.8	5.4 ± 1.5	766.7
	L4	733.0 ± 82.2	802.2 ± 172.6	36.8 ± 14.3	237.1 ± 8.9	5.5 ± 1.5	750.0
	L5	826.0 ± 57.7	862.0 ± 190.4	29.2 ± 12.1	233.9 ± 7.7	5.1 ± 1.6	950.0
	R	788.0 ± 122.7	739.0 ± 163.4	5.7 ± 2.8	224.6 ± 5.1	5.4 ± 1.0	750.0
Insular II	L1	327.3 ± 274.3	428.2 ± 268.4	21.6 ± 12.6	84.2 ± 75.3	2.2 ± 1.6	275.0 ± 35.4
	L2	297.5 ± 265.1	474.6 ± 282.4	22.9 ± 14.2	86.2 ± 79.6	2.0 ± 1.8	350.0 ± 0
	L3	331.8 ± 262.9	440.3 ± 272.9	20.8 ± 12.7	85.0 ± 77.9	2.4 ± 1.7	300.0 ± 0
	L4	327.7 ± 253.3	405.0 ± 267.6	22.4 ± 13.8	84.2 ± 79.1	2.3 ± 1.7	275.0 ± 35.4
	L5	387.8 ± 285.4	436.0 ± 295.9	18.7 ± 11.2	84.8 ± 78.1	2.0 ± 1.6	333.3 ± 47.1
1× medium		1262.1 ± 30.4	-	6.5 ± 0.2	52.4 ± 3.3	-	-

To reveal how mass transfer affected community functions, the efficiency of CODs removal (CODs: Function 1), ammonium-nitrogen removal (NH4: Function 2) and phosphate removal (PHOt: Function 3) were calculated (see Eq. S3.1- Eq. S3.29).

Function 1: CODs removal by the local communities L1-L5, the regional pool R, and the metacommunity

The CODs removal was calculated on the basis of CODs inflow (CODs of the medium feed) and the CODs in the effluent. For each phase, the CODs removal efficiency (%) was determined. The used terms for the metacommunity are:

$CODs_{remove}$ is the CODs removed per minute by microbial communities L1-L5 and R;

$CODs_{inflow}$ is the CODs of the medium feed per minute;

$CODs_{effluent}$ is the CODs of the effluent per minute;

5 is the number of local communities L1-L5;

medium flow rate per phase is shown in Table S2.1;

effluent flow rate (5 × medium flow rate) per phase is shown in Fig. 1;

$CODs_R$ is the average CODs of the regional pool R per each phase shown in Table S3.1;

$CODs_{medium}$ is the carbon content of the medium:

insular phases I & II: ×1 (1,262.1 ± 30.4 mg L^{-1}, Table S3.1).

mass transfer RC_{10}: ×1.1 (1,388.3 mg L^{-1})

mass transfer RC_{50}: ×2 (2,524.2 mg L^{-1})

mass transfer RC_{80}: ×5 (6,310.4 mg L^{-1})

$$CODs_{inflow} = 5 \times \text{medium flow rate} \times CODs_{medium} \quad \text{Eq. S3.1}$$

$$CODs_{effluent} = \text{effluent flow rate} \times CODs_R \quad \text{Eq. S3.2}$$

$$CODs_{remove} = CODs_{inflow} - CODs_{effluent} \quad \text{Eq. S3.3}$$

$$\text{efficiency} = CODs_{remove} / CODs_{inflow} \times 100\% \quad \text{Eq. S3.4}$$

The used terms for the local communities L1-L5 are:

$CODs_{L,remove}$ is the CODs removed per minute by each of the microbial communities L1-L5;

$CODs_{L,inflow}$ is the CODs of the medium feed per minute plus the inflow from the regional pool;

$CODs_{L,effluent}$ is the CODs of the effluent per local community per minute;

medium flow rate per phase is shown in Table S2.1;

effluent flow rate is 0.4 mL min^{-1};

recycling flow rate per phase is shown in Table S2.1;

$CODs_R$ is the average CODs of the regional pool R per each phase shown in Table S3.1;

$CODs_L$ is the average CODs for each of the local communities per each phase (Table S3.1);

$CODs_{medium}$ is the carbon content of the medium:

insular phases I & II: ×1 (1,262.1 ± 30.4 mg L^{-1}, Table S3.1).

mass transfer RC_{10}: ×1.1 (1,388.3 mg L^{-1})

mass transfer RC_{50}: ×2 (2,524.2 mg L^{-1})

mass transfer RC_{80}: ×5 (6,310.4 mg L^{-1})

$$CODs_{L,inflow} = \text{medium flow rate} \times CODs_{medium} + \text{recycling flow rate x } CODs_R \quad \text{Eq. S3.5}$$

$$CODs_{L,effluent} = \text{effluent flow rate} \times CODs_L \quad \text{Eq. S3.6}$$

$$CODs_{L,remove} = CODs_{L,inflow} - CODs_{L,effluent} \quad \text{Eq. S3.7}$$

$$\text{efficiency} = CODs_{L,remove} / CODs_{L,inflow} \times 100\% \quad \text{Eq. S3.8}$$

The used terms for the regional pool R are:

$CODs_{R,remove}$ is the CODs removed by the microbial community of R per minute;

$CODs_{R,inflow}$ is the CODs of the sum of the inflow of the local communities L1-L5 per minute;

$CODs_{R,effluent}$ is the CODs of the effluent of the regional pool R plus recycled flow to local communities L1-L5 per minute;

effluent flow rate is 2.0 mL min^{-1} which is the sum of the effluent and the recycling flow rate;

medium flow rate per phase is shown in Table S2.1;

recycling flow rate per phase is shown in Table S2.1;

$CODs_R$ is the average CODs of the regional pool R per each phase shown in Table S3.1;

$CODs_{L1\text{-}L5}$ is the sum of CODs of all 5 local communities L1-L5 per each phase (Table S3.1);

$$CODs_{R,inflow} = (\text{medium flow rate} + \text{recycling flow rate}) \times CODs_{L1\text{-}L5} \quad \text{Eq. S3.9}$$

$$CODs_{R,effluent} = \text{effluent flow rate} \times CODs_R \quad \text{Eq. S3.10}$$

$$CODs_{R,remove} = CODs_{R,inflow} - CODs_{R,effluent} \quad \text{Eq. S3.11}$$

$$\text{efficiency} = CODs_{R,remove} / CODs_{R,inflow} \times 100\% \quad \text{Eq. S3.12}$$

Table S3.2 CODs removal efficiency (%) from the metacommunity, the local communities L1-L5 and the regional pool R per phase. The CODs inflow ($CODs_{inflow}$), CODs effluent ($CODs_{effluent}$) and removed COD (COD_{remove}) were also given.

phase	system	$CODs_{inflow}$ (mg min^{-1})	$CODs_{effluent}$ (mg min^{-1})	$CODs_{remove}$ (mg min^{-1})	removal efficiency (%)
Insular I	L1	0.5048	0.0768	0.4280	84.8
	L2		0.0785	0.4264	84.5
	L3		0.1099	0.3950	78.2
	L4		0.1122	0.3926	77.8
	L5		0.1581	0.3468	68.7
RC_{10}	metacommunity	2.5242	0.6030	1.9212	76.1
	L1	0.5132	0.1598	0.3534	68.9
	L2		0.0892	0.4240	82.6
	L3		0.1312	0.3820	74.4
	L4		0.1580	0.3552	69.2
	L5		0.1974	0.3158	61.5
	R	0.7356	0.6700	0.0656	8.9
RC_{50}	metacommunity	2.5242	0.5027	2.0215	80.1
	L1	0.6054	0.2165	0.3889	64.2
	L2		0.2136	0.3918	64.7
	L3		0.2039	0.4015	66.3
	L4		0.1912	0.4142	68.4
	L5		0.2086	0.3968	65.5
	R	1.0338	1.0054	0.0284	2.7
RC_{80}	metacommunity	2.5242	0.3152	2.2090	87.5

	L1	0.7885	0.3074	0.4811	61.0
	L2		0.2992	0.4893	62.1
	L3		0.3048	0.4837	61.3
	L4		0.2932	0.4953	62.8
	L5		0.3304	0.4581	58.1
	R	1.5350	1.5760	-0.0410	-2.7
Insular II	L1	0.5048	0.1309	0.3739	74.1
	L2		0.1190	0.3858	76.4
	L3		0.1327	0.3721	73.7
	L4		0.1311	0.3738	74.0
	L5		0.1551	0.3497	69.3

As shown in Table S3.2, the CODs removal efficiency of the single local communities L1-L5 decreased slightly from the average values of Insular I and Insular II phases (78.8 ± 6.6% and 73.5 ± 2.6%) with 71.3 ± 7.8% in RC_{10}, 65.8 ± 1.6% in RC_{50} and 61.1 ± 1.8% in RC_{80}. In the regional pool R the removal efficiency is very low or not existent because a balance between the inflow carbon ($CODs_{R,inflow}$) and the carbon lost to the outflow ($CODs_{R,effluent}$) is reached. The CODs removal for the whole metacommunity increased with mass transfer from 76.1% in RC_{10} to 87.5% in RC_{80}. We assume that on metacommunity scale, the significant increases in biomass (about twofold CODb value, Table S3.1) accompanied by the higher recycling rates had allowed the input nutrients to be mineralized more completely. Therefore, the function of carbon removal was enhanced by the looped mass transfer approach.

Function 2: NH4 removal by the local communities L1-L5, the regional pool R, and the metacommunity

NH4 removal from local communities L1-L5, the regional pool R, and the metacommunity was calculated similar to the CODs removal and the same basic equations were used (Eq. S3.1-12, Table S3.1). First, we estimated the organic N content of the three different organic sources of nitrogen in our medium [peptone from meat (CAS 91079-38-8): 11.0-14.0 w/w %; meat extract (CAS 68990-09-0): 11.5-12.5 w/w %; yeast extract (CAS 8013-01-2): ≥ 10.5 w/w %; Merck KGaA, Darmstadt, Germany]. The estimated organic N content in the 1 × medium (Insular I and II) was about 67.8 mg L^{-1}, for 1.1 × medium (RC_{10}) 74.6 mg L^{-1}, for 2 × medium (RC_{50}) 135.6 mg L^{-1}, and for 5 × medium (RC_{80}) 339.0 mg L^{-1}. This ammonium bound in organic sources was set free by the activity of the wastewater community, thereby increasing the concentration of ammonium in the medium manifold. These amounts of ammonium were also metabolized to nitrogen by the activity of the wastewater communities. Therefore, the measured NH4 values are a result of the activity of all microbial communities and the nitrogen that was provided by the medium. For the calculation of the removal efficiency we used the measured NH4 values in the local communities

L1-L5 and the regional pool R, as well as the estimated NH4 from organic N in medium. For each phase, the NH4 removal efficiency (%) was determined with the basic equations used for CODs removal (Eq. S3.1-12). The used terms for the metacommunity and the local communities L1-L5 are:

$NH4_{inflow}$ is the measured NH4 plus the estimated NH4 converted from the organic-N of the medium feed per minute;

$NH4_{L,inflow}$ is the measured NH4 plus estimated NH4 converted from the organic-N of the medium free per minute plus the inflow from the regional pool;

$NH4_{medium}$ is the measured NH4 of the medium.

insular phases I & II: ×1 (6.5 ± 0.2 mg L^{-1}, Table S3.1):

mass transfer RC_{10}: ×1.1 (7.2 mg L^{-1})

mass transfer RC_{50}: ×2 (13.0 mg L^{-1})

mass transfer RC_{80}: ×5 (32.5 mg L^{-1})

$N_{organic}$ is the estimated NH4 converted from organic-N of the medium:

insular phases I & II: ×1 (67.8 mg L^{-1}).

mass transfer RC_{10}: ×1.1 (74.6 mg L^{-1})

mass transfer RC_{50}: ×2 (135.6 mg L^{-1})

mass transfer RC_{80}: ×5 (339.0 mg L^{-1})

$NH4_R$ is the average NH4 of the regional pool R per each phase shown in Table S3.1;

5 is the number of local communities L1-L5;

medium flow rate per phase is shown in Table S2.1;

recycling flow rate per phase is shown in Table S2.1;

for the NH4 removal of metacommunity, Eq. S3.1 was exchange to

$$NH4_{inflow} = 5 \times \text{medium flow rate} \times (NH4_{medium} + N_{organic}) \quad \text{Eq. S3.13}$$

for the NH4 removal per each of local communities L1-L5, Eq. S3.5 was exchange to

$$NH4_{L,inflow} = \text{medium flow rate} \times (NH4_{medium} + N_{organic}) + \text{recycling flow rate} \times NH4_R \quad \text{Eq. S3.14}$$

Table S3.3 NH4 removal efficiency (%) from the metacommunity, the local communities L1-L5 and the regional pool R per phase. The measured NH4 values, the estimated organic N in medium ($N_{organic}$), NH4 inflow ($NH4_{inflow}$), NH4 effluent ($NH4_{remain}$) and removed NH4 ($NH4_{remove}$) were also given.

phase	system	NH4 (mg N L^{-1})	$N_{organic}$ (mg N L^{-1})	$NH4_{inflow}$ (× 10^{-3} mg N min^{-1})	$NH4_{effluent}$ (× 10^{-3} mg N min^{-1})	$NH4_{remove}$ (× 10^{-3} mg N min^{-1})	removal efficiency (%)
Insular I	L1	29.3 ± 3.3	67.8	29.7	11.7	18.0	60.6
	L2	24.9 ± 5.0			10.0	19.7	66.3
	L3	23.9 ± 1.1			9.6	20.1	67.7
	L4	27.6 ± 5.7			11.0	18.7	63.0
	L5	25.6 ± 3.9			10.2	19.5	65.7
RC_{10}	metacommunity	-	74.6	148.5	17.1	131.4	88.5

	L1	28.4 ± 6.1	74.6	30.3	11.4	19.0	62.7
	L2	25.1 ± 4.3			10.0	20.3	67.0
	L3	30.3 ± 2.0			12.1	18.2	60.1
	L4	27.4 ± 4.5			11.0	19.4	64.0
	L5	16.4 ± 7.6			6.6	23.8	78.5
	R	9.5 ± 2.8	0	51.0	19.0	32.0	62.7
RC_{50}	metacommunity	-	135.6	148.5	9.8	138.7	93.4
	L1	27.7 ± 0.8	135.6	34.3	11.1	23.2	67.6
	L2	31.5 ± 1.5			12.6	21.7	63.3
	L3	30.2 ± 2.3			12.1	22.2	64.7
	L4	29.5 ± 0.9			11.8	22.5	65.6
	L5	24.5 ± 3.0			9.8	24.5	71.4
	R	9.8 ± 3.0	0	57.4	19.6	37.8	65.9
RC_{80}	metacommunity	-	339.0	148.5	2.3	146.2	98.5
	L1	28.9 ± 13.0	339.0	42.0	11.6	30.4	72.4
	L2	39.6 ± 15.1			15.8	26.1	62.1
	L3	29.5 ± 14.4			11.8	30.1	71.7
	L4	36.8 ± 14.3			14.7	27.2	64.8
	L5	29.2 ± 12.1			11.7	30.2	71.9
	R	5.7 ± 2.8	0	65.6	11.4	54.2	82.6
Insular II	L1	84.2 ± 75.3	67.8	29.7	8.6	21.1	71.0
	L2	86.2 ± 79.6			9.2	20.5	69.0
	L3	85.0 ± 77.9			8.3	21.4	72.1
	L4	84.2 ± 79.1			9.0	20.7	69.7
	L5	84.8 ± 78.1			7.5	22.2	74.7

As shown in Table S3.3, the NH4 removal efficiency of the single local communities L1-L5 (67.5 ± 4.7%) did not change from the average values of Insular I and Insular II phases (64.6 ± 2.8% and 71.3 ± 2.3%) with 66.5 ± 7.2% in RC_{10}, 66.5 ± 3.2% in RC_{50} and 68.6 ± 4.8% in RC_{80}. In the regional pool R the removal efficiency is on average 70.4 ± 10.7%. The NH4 removal for the whole metacommunity increased with mass transfer from 62.7% in RC_{10} to 98.5% in RC_{80}. Therefore, the function of the nitrogen removal was enhanced by the looped mass transfer approach.

Function 3: PHOt removal by the local communities L1-L5, the regional pool R, and metacommunity

PHOt removal by the local communities L1-L5, the regional pool R, and the metacommunity was calculated as follows: The measured PHOt values are the measured phosphate values calculated to elementary phosphorus [PHOt (mg P L^{-1})]. This value does not include phosphorus bound in biomass, which is calculated as DWP (mg P L^{-1}) based on an estimated phosphorus content in biomass of 4% (2). In our study, DWP is then calculated using the average value of measured dry weight per reactor per phase (DW, Table S3.1). The flow rate $P_{PHOt+DWP}$ is calculated per

minute and regards both the PHOt and the P-biomass values. The $PHOt_{effluent}$ values are representing the phosphate (as phosphorus) values still in the flow of effluent per minute. For each phase, the removal efficiency (%) for PHOt were determined. The used terms for the metacommunity are:

DW_R is the average DW of the regional pool R per each phase shown in Table S3.1;

4% is the estimate proportion of phosphorus in biomass (dry weight);

DWP_R is the estimated bound P in biomass for regional pool R per each phase;

$PHOt_R$ is the average PHOt for regional pool R per each phase (Table S3.1);

$P_{PHOt+DWP}$ is the value of PHOt plus DWP flow through metacommunity per min;

5 is the number of local communities L1-L5;

medium flow rate per phase is shown in Table S2.1;

effluent flow rate (5 × medium flow rate) per phase is shown in Fig. 1;

$PHOt_{effluent}$ is the PHOt still in the effluent from metacommunity per minute;

$PHOt_{remove}$ is the PHOt removed per minute by microbial communities for L1-L5 and R;

$$DWP_R = 4\% \times DW_R \quad \text{Eq. S3.15}$$

$$P_{PHOt+DWP} = 5 \times \text{medium flow rate} \times (PHOt_R + DWP_R) \quad \text{Eq. S3.16}$$

$$PHOt_{effluent} = \text{effluent flow rate} \times PHOt_R \quad \text{Eq. S3.17}$$

$$PHOt_{remove} = P_{PHOt+DWP} - PHOt_{effluent} \quad \text{Eq. S3.18}$$

$$\text{efficiency} = PHOt_{remove} / P_{PHOt+DWP} \times 100\% \quad \text{Eq. S3.19}$$

The used terms for the local communities L1-L5 are:

DW_L is the average DW of the each of local communities L1-L5 per each phase shown in Table S3.1;

4% is the estimate proportion of phosphorus in biomass (dry weight);

DWP_L is the estimated bound P in biomass for each of local communities L1-L5 per each phase;

$PHOt_L$ is the average PHOt for each of local communities L1-L5 per each phase (Table S3.1);

$P_{L,PHOt+DWP}$ is the value of PHOt plus DWP flow through each of local communities L1-L5 per min;

medium flow rate per phase is shown in Table S2.1;

recycling flow rate per phase is shown in Table S2.1;

effluent flow rate is 0.4 mL min^{-1};

$PHOt_{L,effluent}$ is the PHOt still in the effluent from each of local communities L1-L5 per minute;

$PHOt_{L,remove}$ is the PHOt removed per minute by each of microbial communities L1-L5;

$$DWP_L = 4\% \times DW_L \quad \text{Eq. S3.20}$$

$$P_{L,PHOt+DWP} = (\text{medium flow rate} + \text{recycling flow rate}) \times (PHOt_L + DWP_L) \quad \text{Eq. S3.21}$$

$$PHOt_{L,effluent} = \text{effluent flow rate} \times PHOt_L \quad \text{Eq. S3.22}$$

$PHOt_{L,remove} = P_{L,PHOt+DWP} - PHOt_{L,effluent}$ Eq. S3.23

$efficiency = PHOt_{L,remove} / P_{L,PHOt+DWP} \times 100\%$ Eq. S3.24

The used terms for the regional pool R are:

DW_R is the average DW of the regional pool R per each phase shown in Table S3.1;

4% is the estimate proportion of phosphorus in biomass (dry weight);

DWP_R is the estimated bound P in biomass for the regional pool R per each phase;

$PHOt_R$ is the average PHOt for the regional pool R per each phase (Table S3.1);

$P_{R,PHOt+DWP}$ is the value of PHOt plus DWP flow through the regional pool R per min;

5 is the number of local communities L1-L5;

medium flow rate per phase is shown in Table S2.1;

recycling flow rate per phase is shown in Table S2.1;

effluent flow rate is 2.0 mL min^{-1} which is the sum of the effluent and the recycling flow rate;

$PHOt_{R,effluent}$ is the PHOt still in the effluent from the regional pool R per minute plus recycled flow to local communities L1-L5 per minute;

$PHOt_{R,remove}$ is the PHOt removed per minute by microbial community of the regional pool R;

$DWP_R = 4\% \times DW_R$ Eq. S3.25

$P_{R,PHOt+DWP} = 5 \times (\text{medium flow rate} + \text{recycling flow rate}) \times (PHOt_R + DWP_R)$ Eq. S3.26

$PHOt_{R,effluent} = \text{effluent flow rate} \times PHOt_R$ Eq. S3.27

$PHOt_{R,remove} = P_{R,PHOt+DWP} - PHOt_{R,effluent}$ Eq. S3.28

$efficiency = PHOt_{R,remove} / P_{R,PHOt+DWP} \times 100\%$ Eq. S3.29

Table S3.4 PHOt removal efficiency (%) from the metacommunity, the local communities L1-L5 and the regional pool R per phase. The measured PHOt (phosphate calculated to phosphorus) values, estimated P bound to biomass (DWP), PHOt plus DWP flow ($P_{PHOt+DWP}$), PHOt effluent ($PHO_{effluent}$) and removed PHOt ($PHOt_{remove}$) were also given.

phase	system	PHOt (mg P L^{-1})	DWP (mg P L^{-1})	$P_{PHOt+DWP}$ (× 10^{-3} mg P min^{-1})	$PHOt_{effluent}$ (× 10^{-3} mg P min^{-1})	$PHOt_{remove}$ (× 10^{-3} mg P min^{-1})	removal efficiency (%)
Insular I	L1	64.5 ± 4.5	10.3	29.9	25.8	4.1	13.8
	L2	63.6 ± 4.2	13.0	30.6	25.4	5.2	17.1
	L3	63.3 ± 2.2	11.7	30.0	25.3	4.7	15.6
	L4	61.1 ± 3.3	9.0	28.0	24.4	3.6	13.0
	L5	64.6 ± 2.2	9.3	29.6	25.8	3.8	12.8
RC_{10}	metacommunity	-	-	129.7	119.0	10.7	8.3
	L1	72.0 ± 2.5	7.0	31.6	28.8	2.8	8.9
	L2	71.7 ± 1.0	10.7	32.9	28.7	4.2	12.9
	L3	73.0 ± 1.8	7.0	32.0	29.2	2.8	8.7
	L4	69.1 ± 2.8	3.0	28.8	27.6	1.2	4.3
	L5	68.6 ± 3.6	5.7	29.7	27.4	2.3	7.8

	R	66.1 ± 3.5	6.0	144.1	132.2	11.9	8.3
RC_{50}	metacommunity	-	-	111.9	95.5	16.4	14.7
	L1	99.9 ± 3.8	16.0	46.4	40.0	6.4	13.7
	L2	104.2 ± 8.1	12.0	46.5	41.7	4.8	10.3
	L3	101.1 ± 1.2	14.0	46.0	40.4	5.6	12.2
	L4	93.3 ± 10.9	14.0	42.9	37.3	5.6	13.1
	L5	98.7 ± 0.9	12.0	44.3	39.5	4.8	10.8
	R	99.9 ± 3.8	12.0	223.8	191.0	32.8	14.7
RC_{80}	metacommunity	-	-	101.8	89.8	12.0	11.8
	L1	226.6 ± 6.7	31.3	103.2	90.6	12.6	12.2
	L2	238.0 ± 10.6	38.7	110.7	95.2	15.5	14.0
	L3	233.0 ± 9.8	30.7	105.5	93.2	12.3	11.6
	L4	237.1 ± 8.9	30.0	106.9	94.8	12.1	11.3
	L5	233.9 ± 7.7	38.0	108.8	93.6	15.2	14.0
	R	224.6 ± 5.1	30.0	509.2	449.2	60.0	11.8
Insular II	L1	84.2 ± 75.3	11.0	38.1	33.7	4.4	11.5
	L2	86.2 ± 79.6	14.0	40.1	34.5	5.6	14.0
	L3	85.0 ± 77.9	12.0	38.8	34.0	4.8	12.4
	L4	84.2 ± 79.1	11.0	38.1	33.7	4.4	11.5
	L5	84.8 ± 78.1	13.3	39.3	33.9	5.4	13.7

As shown in Table S3.4, the PHOt removal efficiency of the single local communities L1-L5 was low with average value 12.0 ± 2.6%: in Insular I and Insular II phases the removal efficiencies were 14.5 ± 1.9% and 12.6 ± 1.2%, and remained nearly unchanged with 8.5 ± 3.1% in RC_{10}, 12.0 ± 1.5% in RC_{50} and 12.6 ± 1.3% in RC_{80}. In the regional pool R the removal efficiency was on average 10.6 ± 3.2%. The PHOt removal for the whole metacommunity was also not affected by mass transfer with average value 11.3 ± 3.2%. Therefore, the function of the PHOt removal was not change by the looped mass transfer approach.

S4: Flow cytometric analysis of community structure

Preparation of cell samples

Step 1: Cell sample fixation

For fixation, 2 × 2.5 mL samples were taken from each reactor and placed in glass tubes. Supernatants were removed after centrifugation at 3,200×g for 10 min at 4°C. For every tube, the cells in the pellet were suspended in 2 mL paraformaldehyde solution [PFA, 2% in phosphate-buffered saline (PBS, 6 mM Na_2HPO_4, 1.8 mM NaH_2PO_4, 145 mM NaCl, pH 7)] and incubated for 30 min at room temperature (RT). Afterwards, the cells were centrifuged again (3,200×g, 10 min, 4°C), resuspended in 4 mL 70% ethanol, and then stored at -20°C.

Step 2: DNA staining with DAPI

An aliquot of the fixed sample was taken into a glass tube and washed twice with PBS (3,200×g, 10 min, 4°C), and then adjusted with PBS to an $OD_{700,\ d=5\ mm}$ of 0.035. Two mL of the adjusted cell solution was centrifuged (3,200×g, 10 min, 4°C), and the pellet was resuspended in 1 mL solution A (0.11 M citric acid and 4.1 mM Tween 20 in bidistilled water) and incubated at RT for 20 min, the first 10 min in an ultrasonication bath (35 kHz; Merck Eurolab, Darmstadt, Germany). Solution A was discarded after centrifugation (3,200×g, 10 min, 4°C). The cells were resuspended in 2 mL solution B [0.24 µM DAPI (4',6-diamidino-2-phenylindole, Lot. 118M4025V; Sigma-Aldrich, St. Louis, MO, USA) in phosphate buffer (289 mM Na_2HPO_4 and 128 mM NaH_2PO_4 in bidistilled water)] and incubated overnight at RT and in the dark before flow cytometric measurement.

Cytometric analysis

Step 1: Instrumental setup

The cells were flow cytometrically measured in a MoFlo Legacy Cell Sorter using the software Summit v4.3 (Beckman Coulter, Brea, CA, USA). The instrument was equipped with a 488 nm argon laser (400 mW; Coherent, Santa Clara, CA, USA) and a 355 nm UV laser (150 mW, Xcyte CY-355-150; Lumentum, Milpitas, CA, USA). The 488 nm laser light was used for detection of the forward scatter (FSC, 488/10 nm band pass) and the side scatter (SSC, 488/10 nm band pass, trigger signal). The DAPI fluorescence was measured at signal channel FL4 (450/65 nm band pass) after excitation with the UV laser.

The fluidic system was run at constant sheath pressure of 56.0 psi with a 70 µm nozzle. The sample pressure was adjusted within the range of 55.8-56.2 psi, in order to obtain a stable event measurement of around 3,500 events per second. The sheath fluid was composed of 10-fold sheath buffer (19 mM KH_2PO_4, 38 mM KCl, 166 mM Na_2HPO_4 and 1.39 M NaCl with 0.13 µm filtrated Millipore water) and further diluted with filtrated Millipore water to a 0.2-fold working solution (for cell sorting: 0.5-fold working solution).

For the daily optical calibration of the cytometer in the linear range, 1 µm blue fluorescent FluoSpheres (F-8815; Molecular Probes, Eugene, OR, USA) and 2 µm yellow-green fluorescent FluoSpheres (F8827; ThermoFisher Scientific, Waltham, MA, USA) were used. For calibration in the logarithmic range, 0.5 µm and 1.0 µm UV Fluoresbrite Microspheres (18339 and 17458, respectively; Polysciences, Warrington, PA, USA) were used.

To ensure the reliability and comparability of the cell fixation and staining procedures, a microbial cytometric mock community (mCMC) (3) was used each day. The cells of the mCMC were

handled identically to the staining protocol in the section S4 (steps 1 & 2: Preparation of cell samples). The use of the mCMC guaranteed a high resolution by ensuring optimal optical settings of the flow cytometer and comparable cytometric measurements of bioreactor samples, even if they were measured over months.

Step 2: Measuring community samples

Prior to measurement, DAPI-stained cells were filtered to remove larger particles by using a nylon filter (CellTrics® 50 µm; Sysmex Partec GmbH, Görlitz, Germany) and were spiked with 0.5 µm and 1 µm UV Fluoresbrite Microspheres (18339 and 17458, respectively; Polysciences). The microspheres served as internal standards to monitor instrument stability and to allow the correct comparison of samples (Fig. S4.1a). Cell data were collected in logarithmically scaled 2D-dot plots according to DAPI fluorescence for DNA content and forward scatter (FSC) for cell size-related information. A cell gate was defined, which comprised 200,000 virtual cells for each measurement (cell gate; Fig. S4.1a). An overview of all measured samples from each bioreactor can be seen in Movie S1.

Movie S1 Overview on all measured samples from each bioreactor. All cells are analyzed according to their DAPI fluorescence for DNA content and forward scatter (FSC) for cell size-related information. 200,000 cells per analysis were measured.

Step 3: Creation of the gate-template to determine the community structure

According to the measured samples, apparent cell clusters in 2D-dot plots (FSC and DAPI fluorescence) were gated sample per sample (4) and all defined gates were combined together to create the gate template. In this study, the gate template included 80 gates (G1 to G80; Fig. S4.1b), and we defined the cell population in each of the gates as a subcommunity (SC). The relative cell abundance per SC (G1-G80) within the cell gate was computed using FlowJo™ v10 (FlowJo LLC, Ashland, OR, USA) automatically. A list of the data on relative cell abundance per gate per sample is given in the Dataset S2.

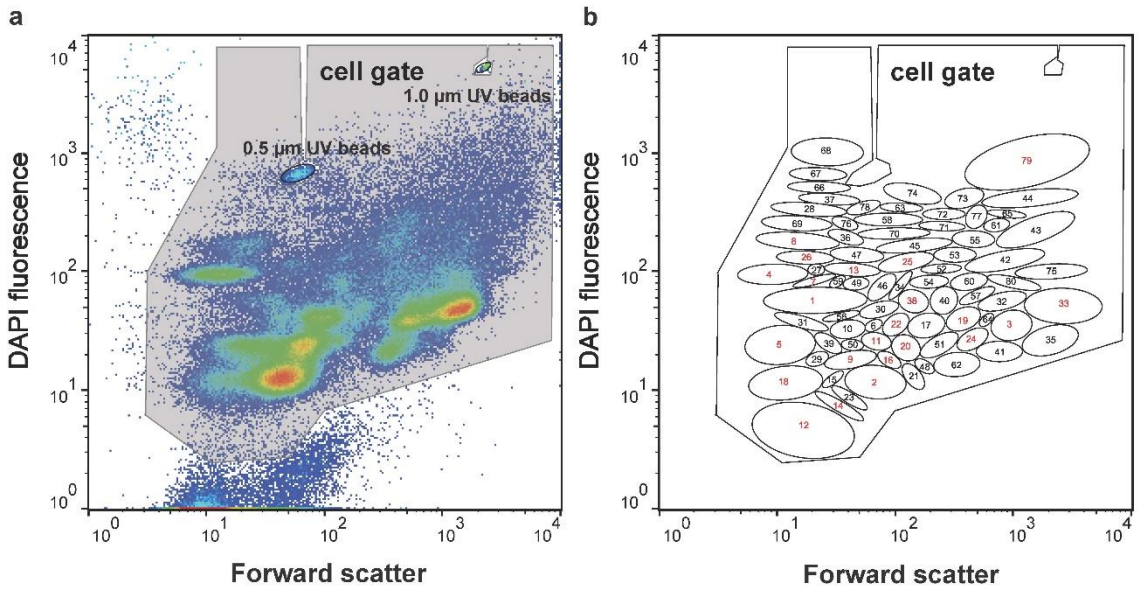

Figure S4.1 Gating strategy. First, a cell gate was defined for the measurement of 200,000 cells. Calibration beads were excluded. Afterwards, the gate template was created by defining 80 gates (i.e., G1-G80), based on forward scatter (Forward scatter) and DAPI fluorescence (DAPI fluorescence). The cell numbers per gate and sample were used for evaluations in further data evaluation pipelines. Sorted gates are marked by red numbers.

Step 4: Cell sorting

To determine the taxonomic affiliation of selected SCs, cell sorting was performed. The cell sorting procedure was carried out in accordance with the work of Cichocki et al. (3). Briefly, the positions of gates to be sorted were defined and assigned using the Summit software (V4.3; Beckman Coulter, Brea, CA, USA). The cell sorting was performed using the four-way-sort option and the '1.0 Drop Pure' sort mode. A total of 500,000 cells of each selected gate were sorted into a 1.5 mL Eppendorf tube at an event rate of not more than 1,500 events per second. Sorted cells were harvested from the sheath buffer by centrifugation (20,000×g, 6°C, 25 min), and the cell pellets were stored at -20°C for subsequent DNA isolation.

S5: Cell counting by flow cytometry

Preparation of cells for the determination of cell numbers

Step 1: Cell sample dilution

Live cells (0.2 mL) were sampled from the bioreactors and directly diluted in three standardized steps (all in all 1/500-fold) to about 10^7 cells per mL using 0.85% saline solution.

Step 2: DNA staining with SYTO®9

SYTO®9 (Lot. 2088729; ThermoFisher Scientific, Eugene, OR, USA) is a cell-permeant nucleic acid stain, which was used in this study to stain fresh cell samples to distinguish cells from medium particles. A 35 µM stock solution of SYTO®9 was prepared daily and stored on ice. The final cell solution contained 950 µL diluted cell sample and 50 µL 35 µM SYTO®9, with a final concentration of 1.75 µM SYTO®9. The cell solution was mixed and incubated for 15 min at RT before cell counting. The diluted and stained cell samples were measured on the same day.

Counting cell numbers

Step 1: Instrumental setup

The cell counting was performed with the flow cytometer CyFlow®Space (Sysmex Partec GmbH, Görlitz, Germany) using the True Volumetric Absolute Counting mode, which counts cells in a fixed volume (0.2 mL). This device was equipped with a 488 nm argon laser (50mW; Sapphire, Coherent, Santa Clara, CA, USA). The fluorescence of the stained cells was measured using the filters 536/40 nm band pass for green fluorescence and 610/30 nm band pass for red fluorescence. For the daily optical calibration of the flow cytometer in the linear range, 0.5 µm yellow-green fluorescent FluoSpheres (F8827; ThermoFisher Scientific, Waltham, MA, USA) and 1.0 µm yellow-green fluorescent FluoSpheres (F13081; ThermoFisher Scientific, Waltham, MA, USA) were used. These latter FluoSpheres were also added to each sample to ensure comparability of measurements.

Step 2: Determination of total cell number

Before determining the total cell number (CN, mL^{-1}), the cell suspension was filtered to remove larger particles by using a nylon filter (CellTrics® 50 µm; Sysmex Partec GmbH, Görlitz, Germany). The measuring rate was adjusted to below 1,500 events per second. Dependent on the cell concentration, 100-200 µL of the cell solution was added to 1-1.1 mL Millipore water to maintain the measuring rate. A cell gate was defined on the basis of SYTO®9 green and red fluorescence (Fig. S5.1) to differentiate the cells from instrumental and background noise. Total cell numbers

were counted automatically using the software FloMax (V2.4; Sysmex Partec GmbH, Germany). Based on the cell numbers in diluted samples and the actual dilution factor, the CNs in local communities L1-L5 and the regional pool R were calculated. In total, 421 values (71 per local community and 66 per regional pool) were measured, as shown in Dataset S1 and visualized in Fig. S5.2. In Table S5.1, the mean values and the standard deviation of cell numbers per phase (balanced period) are shown for the local communities L1-L5 and the regional pool R, respectively. The CN per SC was calculated by multiplying relative cell numbers per SC (Dataset S2) by cell number per community (Dataset S3).

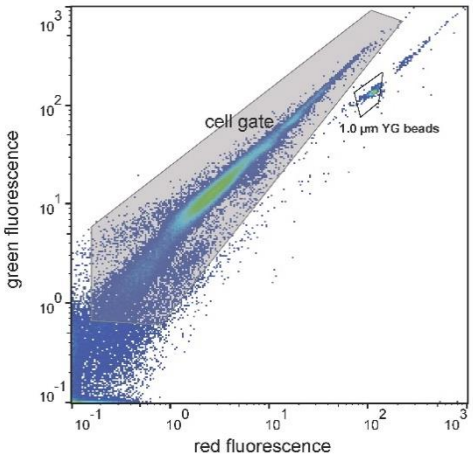

Figure S5.1. Cell gate for cell counting. The cell gate was set apart from instrumental noise, background noise and calibration beads.

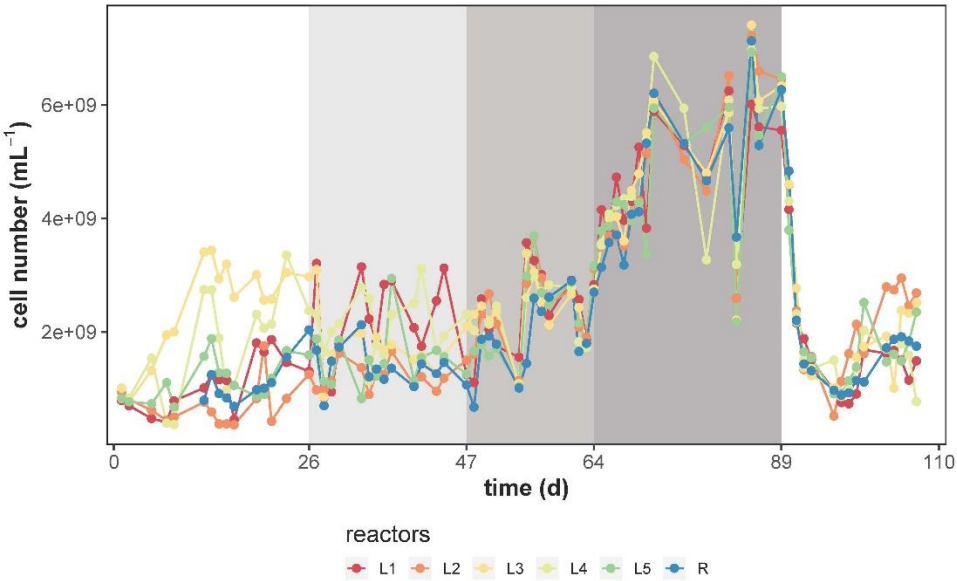

Figure S5.2 Analysis of cell numbers (CN, mL^{-1}) in the local communities L1-L5 and the regional pool R. The shaded areas represent different phases with changed RC.

Table S5.1 Summary of mean values and standard deviation (sd) of cell numbers ($\times 10^9$ cells mL^{-1}) per balanced period and phase of the local communities (L1-L5) and the regional pool (R).

reactor	Insular I		RC_{10}		RC_{50}		RC_{80}		Insular II	
	mean	sd	mean	sd	mean	sd	mean	sd	mean	sd
local communities (L1-L5)	1.60	0.93	1.82	0.65	2.46	0.71	5.29	1.39	1.58	0.62
regional pool (R)	1.02	0.26	1.38	0.31	2.05	0.67	5.40	1.02	1.41	0.44

S6: DNA extraction and 16S rRNA gene amplicon sequencing

The 16S rRNA gene amplicon sequencing analysis was performed as follows:

Step 1: DNA extraction

The DNA was extracted in accordance with a protocol from Cichocki et al. (3). In short, 70 µL of Chelex 100 solution [Chelex 100 sodium form, Sigma-Aldrich, CAS no. 11139-85-8, preparation of 10% (wt/vol) with molecular-biology-grade water] was added to each frozen cell pellet from whole communities or sorted cells of SCs (Supplementary Information S4, Cytometric analysis, step 4). Whole-community pellets were thawed, $OD_{700,\ d=5mm}$ adjusted to 0.01 with sterile PBS and centrifuged at 20,000×g for 25 min at 4°C prior to the Chelex addition. Negative controls (14 controls, sheath buffer and 300 µL of Chelex solution) and a positive control (ZymoBIOMICS™ Microbial Community Standard; Zymo Research Europe GmbH, Freiburg, Germany) were included in the analysis. Each of the solutions was vortexed for 10 s, incubated at 95°C for 45 min and centrifuged at 7,000×g at 4°C for 5 min. Fifty µL of the supernatant, which contained the extracted DNA, was transferred to a new pre-chilled tube. Samples were stored at -20°C before further use.

Step 2: DNA quality testing and library preparation for Illumina MiSeq sequencing

DNA yield was determined using Qubit 3.0 (Thermo Fisher Scientific, Waltham, MA, USA). DNA extracts with more than 0.1 ng of DNA per µL were amplified for 25 PCR cycles and those with less than 0.1 ng per µL were amplified for 35 PCR cycles. Table S6.1 indicates the number of cycles used for PCR amplification of the different samples. 16S rRNA gene amplicon sequencing was performed on the V3-V4 region of the 16S rRNA gene region using the primers Pro341F 5'-CCTACGGGNBGCASCAG-3' (5) and Pro805R 5'-GACTACNVGGGTATCTAATCC-3' (6). These

primers and the barcoded primers used for the library were synthesized by Eurofins (Eurofins Scientific, Luxembourg City, Luxembourg). PCR amplification was performed in accordance with the procedure of Liu et al. (1) and checked for the presence of single band PCR products by gel electrophoresis (1.5% agarose). For each PCR batch, a negative control without any DNA was amplified for up to 35 cycles and checked by gel electrophoresis (1.5% agarose) to ensure that no contamination was present. In the absence of contamination, the samples were purified, quantified and equimolarly pooled in accordance with the work of Liu et al. (1). The pooled amplicon samples were sequenced with MiSeq (Illumina®, San Diego, CA, USA).

Step 3: Processing of raw sequencing data, denoising and selection of 16S rRNA gene amplicon sequencing variants

The raw sequence reads from Illumina Miseq were checked and separated according to their number of PCR cycles (Table S6.1) by using manifest files as indicated by the QIIME2 v2020.2, following the instructions of the developers (7). The paired-end sequence reads fastq files were demultiplexed using q2-demux. Subsequently, the primers were trimmed and low-quality reads were removed as defined by QIIME2 (7). Denoising and selection of amplicon sequencing variants were performed separately for samples amplified for 25 or 35 PCR cycles using DADA2, in accordance with the instructions of the developers (8).

Table S6.1. Metadata of different libraries from whole communities and sorted gates amplified based on 25 and 35 PCR cycles. Run: the sequencing round in which the group of samples was sequenced; Type: the different sorted gates (G) and the whole-community (WC) samples; Identity: which samples were sorted or kept as a whole-community; PCR cycles: the number of cycles for which the different samples were amplified during PCR.

sample ID	reactor	days	run	type	identity	PCR-Cycles	sample ID	reactor	days	run	type	identity	PCR-Cycles
Samp01	R	85	Run1	G5	sorted	35	Samp80	R	97	Run2	WC	Community-88	25
Samp02	R	85	Run1	G12	sorted	35	Samp81	L1	100	Run2	WC	Community-89	25
Samp03	L2	86	Run1	G18	sorted	35	Samp82	L3	100	Run2	WC	Community-90	25
Samp04	L3	61	Run1	G7	sorted	35	Samp83	L1	107	Run2	WC	Community-91	25
Samp05	L3	61	Run1	G12	sorted	35	Samp84	L2	107	Run2	WC	Community-92	25
Samp06	L3	63	Run1	G8	sorted	35	Samp85	L3	107	Run2	WC	Community-93	25
Samp07	L1	100	Run1	G7	sorted	35	Samp86	L4	107	Run2	WC	Community-94	25
Samp08	L2	47	Run1	G16	sorted	35	Samp87	L5	107	Run2	WC	Community-95	25
Samp09	L2	47	Run1	G22	sorted	35	Samp88	L2	86	Run1	G25	sorted	35
Samp10	L1	34	Run1	G4	sorted	35	Samp89	L3	61	Run1	G18	sorted	35
Samp11	L1	99	Run1	G8	sorted	35	Samp90	L3	63	Run1	G4	sorted	35
Samp12	L5	44	Run1	G7	sorted	35	Samp91	L3	63	Run1	G9	sorted	35
Samp13	L3	100	Run1	G5	sorted	35	Samp99	L1	0	Run1	WC	Community_01	35
Samp14	L1	71	Run1	G4	sorted	35	Samp100	L1	1	Run1	WC	Community_02	25
Samp15	L2	44	Run1	G1	sorted	35	Samp101	L2	1	Run1	WC	Community_03	25
Samp16	L2	44	Run1	G24	sorted	35	Samp102	L3	1	Run1	WC	Community_04	25
Samp17	L2	44	Run1	G26	sorted	35	Samp103	L4	1	Run1	WC	Community_05	25
Samp18	L4	86	Run1	G13	sorted	35	Samp104	L5	1	Run1	WC	Community_06	25
Samp19	L5	71	Run1	G2	sorted	35	Samp105	L1	8	Run1	WC	Community_07	25
Samp20	L5	71	Run1	G4	sorted	35	Samp106	L2	8	Run1	WC	Community_08	25
Samp21	L1	99	Run1	G20	sorted	35	Samp107	L3	8	Run1	WC	Community_09	25
Samp22	R	85	Run1	G14	sorted	35	Samp108	L4	8	Run1	WC	Community_10	25
Samp23	L1	85	Run1	G5	sorted	35	Samp109	L5	8	Run1	WC	Community_11	25
Samp24	L1	85	Run1	G12	sorted	35	Samp110	R	9	Run1	WC	Community_12	25
Samp25	L1	85	Run1	G14	sorted	35	Samp111	L1	26	Run1	WC	Community_13	25

Samp26	L3	85	Run1	G5	sorted	35	Samp112	L2	26	Run1	WC	Community_14	25
Samp27	L3	85	Run1	G12	sorted	35	Samp113	L3	26	Run1	WC	Community_15	25
Samp28	L3	85	Run1	G14	sorted	35	Samp114	L4	26	Run1	WC	Community_16	25
Samp29	L2	86	Run1	G9	sorted	35	Samp115	L5	26	Run1	WC	Community_17	25
Samp34	L3	61	Run1	G5	sorted	35	Samp116	R	26	Run1	WC	Community_18	25
Samp35	L3	99	Run1	G12	sorted	35	Samp117	L1	27	Run1	WC	Community_19	25
Samp36	L1	34	Run1	G19	sorted	35	Samp118	L2	27	Run1	WC	Community_20	25
Samp37	R	85	Run1	G33	sorted	35	Samp119	L3	27	Run1	WC	Community_21	25
Samp38	L1	85	Run1	G33	sorted	35	Samp120	L4	27	Run1	WC	Community_22	25
Samp39	L3	85	Run1	G33	sorted	35	Samp121	L5	27	Run1	WC	Community_23	25
Samp40	L2	86	Run1	G1	sorted	35	Samp122	R	27	Run1	WC	Community_24	25
Samp41	L5	55	Run2	WC	Community_49	25	Samp123	L1	34	Run1	WC	Community_25	25
Samp42	R	55	Run2	WC	Community_50	25	Samp124	L2	34	Run1	WC	Community_26	25
Samp43	L3	61	Run2	WC	Community_51	25	Samp125	L3	34	Run1	WC	Community_27	25
Samp44	L5	61	Run2	WC	Community_52	25	Samp126	L4	34	Run1	WC	Community_28	25
Samp45	L1	64	Run2	WC	Community-53	25	Samp127	L5	34	Run1	WC	Community_29	25
Samp46	L2	64	Run2	WC	Community-54	25	Samp128	R	34	Run1	WC	Community_30	25
Samp47	L3	64	Run2	WC	Community-55	25	Samp129	L2	44	Run1	WC	Community_31	25
Samp48	L4	64	Run2	WC	Community-56	25	Samp130	L5	44	Run1	WC	Community_32	25
Samp49	L5	64	Run2	WC	Community-57	25	Samp131	L1	47	Run1	WC	Community_33	25
Samp50	R	64	Run2	WC	Community-58	25	Samp132	L2	47	Run1	WC	Community_34	25
Samp51	L1	65	Run2	WC	Community-59	25	Samp133	L3	47	Run1	WC	Community_35	25
Samp52	L2	65	Run2	WC	Community-60	25	Samp134	L4	47	Run1	WC	Community_36	25
Samp53	L3	65	Run2	WC	Community-61	25	Samp135	L5	47	Run1	WC	Community_37	25
Samp54	L4	65	Run2	WC	Community-62	25	Samp136	R	47	Run1	WC	Community_38	25
Samp55	L5	65	Run2	WC	Community-63	25	Samp137	L1	48	Run1	WC	Community_39	25
Samp56	R	65	Run2	WC	Community-64	25	Samp138	L2	48	Run1	WC	Community_40	25
Samp57	L1	72	Run2	WC	Community-65	25	Samp139	L3	48	Run1	WC	Community_41	25
Samp58	L2	72	Run2	WC	Community-66	25	Samp140	L4	48	Run1	WC	Community_42	25
Samp59	L3	72	Run2	WC	Community-67	25	Samp141	L5	48	Run1	WC	Community_43	25
Samp60	L4	72	Run2	WC	Community-68	25	Samp142	R	48	Run1	WC	Community_44	25
Samp61	L5	72	Run2	WC	Community-69	25	Samp143	L1	55	Run1	WC	Community_45	25
Samp62	R	72	Run2	WC	Community-70	25	Samp144	L2	55	Run1	WC	Community_46	25
Samp63	L1	89	Run2	WC	Community-71	25	Samp145	L3	55	Run1	WC	Community_47	25
Samp64	L2	89	Run2	WC	Community-72	25	Samp146	L4	55	Run1	WC	Community_48	25
Samp65	L3	89	Run2	WC	Community-73	25	Samp154	L1	99	Run2	G38	sorted	35
Samp66	L4	89	Run2	WC	Community-74	25	Samp155	L1	63	Run2	G2	sorted	35
Samp67	L5	89	Run2	WC	Community-75	25	Samp156	L1	63	Run2	G3	sorted	35
Samp68	R	89	Run2	WC	Community-76	25	Samp157	L1	63	Run2	G11	sorted	35
Samp69	L1	90	Run2	WC	Community-77	25	Samp158	L1	100	Run2	G3	sorted	35
Samp70	L2	90	Run2	WC	Community-78	25	Samp159	L1	100	Run2	G4	sorted	35
Samp71	L3	90	Run2	WC	Community-79	25	Samp160	L1	100	Run2	G24	sorted	35
Samp72	L4	90	Run2	WC	Community-80	25	Samp161	L2	47	Run2	G33	sorted	35
Samp73	L5	90	Run2	WC	Community-81	25	Samp162	L2	47	Run2	G79	sorted	35
Samp74	R	90	Run2	WC	Community-82	25	Samp163	L2	26	Run2	G33	sorted	35
Samp75	L1	97	Run2	WC	Community-83	25	Samp164	L5	47	Run2	G3	sorted	35
Samp76	L2	97	Run2	WC	Community-84	25	Samp165	L3	100	Run2	G18	sorted	35
Samp77	L3	97	Run2	WC	Community-85	25	Samp166	L3	58	Run2	G19	sorted	35
Samp78	L4	97	Run2	WC	Community-86	25	Samp167	L3	58	Run2	G24	sorted	35
Samp79	L5	97	Run2	WC	Community-87	25	Samp168	R	107	Run2	WC	Community_96	25

Step 4: Taxonomic classification

To perform taxonomic classification of the amplicon sequence variants (ASVs), feature classifiers were trained with the q2-feature-classifier provided by the QIIME2 using the instructions from the developers (7). To this end, the SILVA database v132 (9) was used as a reference database and the primers (Pro341F and Pro805R) were used to trim the reference database. After the taxonomic classification, samples amplified for 25 or 35 PCR cycles were merged using q2-feature-table merge (7).

Step 5: Removing contaminants and setting relative abundance thresholds based on positive and negative controls.

A two-fold approach was used to determine which ASVs should be removed based on negative (two sets) and positive controls (one set). For the first set of negative controls, 14 DNA extractions of the sheath buffer were sequenced to account for potential contamination during the DNA

extraction. The second set of negative controls consisted of one extraction using the Chelex 100 solution as template for the PCR. All ASVs present in the sheath buffer DNA extracts or Chelex 100 solution were removed from the analysis. As a positive control, the ZymoBIOMICS™ Microbial Community Standard (Zymo Research Europe GmbH Freiburg, Germany) was sequenced in triplicate (Fig. S6.1). Then, the ASVs from the eight different species were identified as present in this community using BLAST (10). BLAST used as the q2-feature-classifier was unable to determine the phylogeny of all ASVs present in the ZymoBIOMICS™ Microbial Community Standard at the species level. The highest relative abundance of ASVs that did not belong to the ZymoBIOMICS™ Microbial Community Standard ASVs was 0.1%. Therefore, every ASV with a relative abundance of 0.1% or lower was removed from the 16S rRNA gene amplicon sequencing dataset.

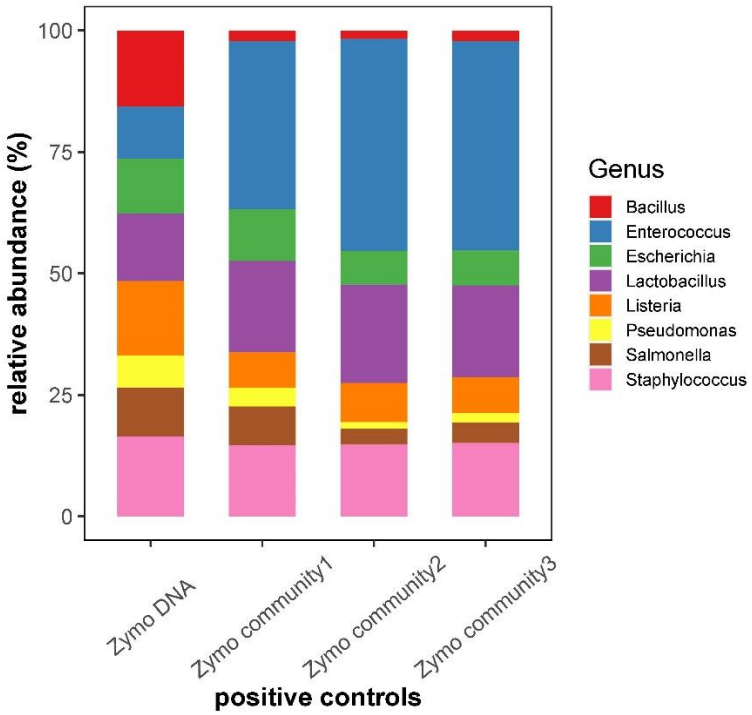

Figure S6.1 Positive control for 16S rRNA gene amplicon sequencing. The ZymoBIOMICS™ Microbial Community Standard ASVs were used for this purpose (left column: data provided by the company) and three sets were run in parallel in accordance with the protocol described in this paper. The highest relative abundance of other strains not belonging to the standard was 0.1%. Therefore, every ASV with a relative abundance of 0.1% or lower was removed from the 16S rRNA gene amplicon sequencing dataset.

Step 6: Visualization of the amplicon sequencing data.

We used the 'phyloseq' R package to visualize the taxonomic composition of the different samples used for 16S rRNA gene amplicon sequencing, in accordance with the instructions of the developers (11).

S7: Stability of communities under the influence of RC_{10}, RC_{50} and RC_{80}

The stability properties of constancy, resistance RS and recovery RV were calculated for all SCs per community per phase and reactor in accordance with previous studies (1, 12). Community stability was tested during Insular I phase, RC_{10}, RC_{50}, RC_{80} and Insular II phase based on the Canberra distance measure.

Step 1: Constancy spaces for determining changes in microbial community composition caused by increasing $\boldsymbol{RC}$

Constancy space reveals the fluctuation of community structure without the influence of external disturbance, thus indicating the inherent community variation. To investigate whether the shift in recycling rates RC caused essential changes in microbial community compositions, and if so, to what extent, the deviations of the community structures of L1-L5 and of R from either the inoculum or start and end of the recycling phases were calculated using the Canberra distance (Fig. 2b; R-script v1.0, GitHub: https://github.com/fcentler/EcologicalStabilityPropertiesComputation). When the deviation of the community structure leaves the constancy space, the community is defined as unstable (1, 12). The constancy space can be calculated in accordance with the procedure described by Liu et al. (12). Briefly, the relative cell abundance data of all SCs of all samples from the balanced periods per phase and per reactor were included in the calculation of Canberra distances. This resulted, first, in an average sampling point, which described the mean of all samples. Second, Canberra distances from all samples to the average sampling point were calculated. Third, the constancy space was defined by determining the maximum Canberra distance per phase, which was possible due to the undisturbed balanced phases from which the samples were taken from. The mean value of the constancy space per phase was calculated for each of the five local communities L1-L5 (dashed lines in Fig. 2b).

A small value between 0 and 1 mirrors only small intrinsic fluctuations of a community and thus high constancy. Increased recycling rates resulted in a smaller constancy space of community structures of L1-L5, while no recycling allowed for higher fluctuations and a larger constancy

space. The mean values of constancy spaces for the local communities L1-L5 were 0.44, 0.34, 0.26 and 0.27 for phases 1 to 4, respectively. In the Insular II phase, when recycling rates were stopped, the constancy values were similarly high as in Insular I phase (0.43, Table S7.1). The phase-to-phase variation was confirmed by Wilcoxon test (p = 0.008, 0.008, 0.841 and 0.008 respectively), with the exception of that between RC_{50} and RC_{80}.

Table S7.1 Constancy space calculated based on Canberra distance.

reactor	Insular I	RC_{10}	RC_{50}	RC_{80}	Insular II
L1	0.44	0.33	0.26	0.27	0.50
L2	0.46	0.34	0.25	0.32	0.48
L3	0.41	0.33	0.28	0.27	0.37
L4	0.46	0.34	0.28	0.24	0.39
L5	0.43	0.37	0.22	0.25	0.41
mean ± sd	0.44 ± 0.02	0.34 ± 0.02	0.26 ± 0.02	0.27 ± 0.03	0.43 ± 0.06
R	0.28	0.25	0.22	0.26	0.39

Step 2: Resistance RS and recovery RV for determining changes in microbial community composition caused by increasing RC

The values for resistance RS and recovery RV were used to determine whether microbiomes change in composition between the phases, that is, Insular I phase to RC_{10}, RC_{10} to RC_{50}, RC_{50} to RC_{80} and RC_{80} to Insular II phase. The values were calculated by the degree of deviation from the starting point (resistance RS) and the ability of the microbiome to return to the starting point (recovery RV). The deviation from the inoculum (day 0) or from the respective endpoints of previous balanced phases (days 26, 47, 64, and 89, respectively; Fig. 2b) were used to calculate the deviations that occurred. These phase-to-phase variations were confirmed by significance testing (Wilcoxon test, p = 0.0079, 0.1508 and 0.008 respectively; Fig. S7.2). The RS value was lowest during the shift from Insular I phase to RC_{10} (mean 0.46 ± 0.05 for L1-L5) suggesting the greatest changes in community composition under these conditions. The shifts RC_{10} to RC_{50} and RC_{50} to RC_{80} showed the highest RS (mean 0.57 ± 0.03 and 0.60 ± 0.03, respectively, for L1-L5) and therefore indicated small changes of microbiome structures. We did not observe much changes in RV in all phases and for all communities (Table S7.2).

Table. S7.2 Resistance (RS) and recovery (RV) for the shifts between phases in L1-L5 and R based on Canberra distance.

reactor	Insular I to RC_{10}		RC_{10} to RC_{50}		RC_{50} to RC_{80}		RC_{80} to Insular II	
	RS	RV	RS	RV	RS	RV	RS	RV
L1	0.52	0.06	0.57	0.23	0.61	0.03	0.44	0.19

L2	0.41	0.02	0.53	0	0.61	0.01	0.52	0.11
L3	0.47	0.02	0.6	0	0.6	0.14	0.52	0.04
L4	0.39	0.07	0.59	0.14	0.55	0.12	0.5	0.12
L5	0.49	0.01	0.58	0.01	0.62	0.02	0.5	0.09
mean ± sd	0.46 ± 0.05	0.04 ±0.03	0.57 ± 0.03	0.08 ± 0.10	0.60 ± 0.03	0.06 ± 0.06	0.50 ± 0.03	0.11 ± 0.05
R	0.57	0.18	0.67	0.08	0.6	0.01	0.53	0.15

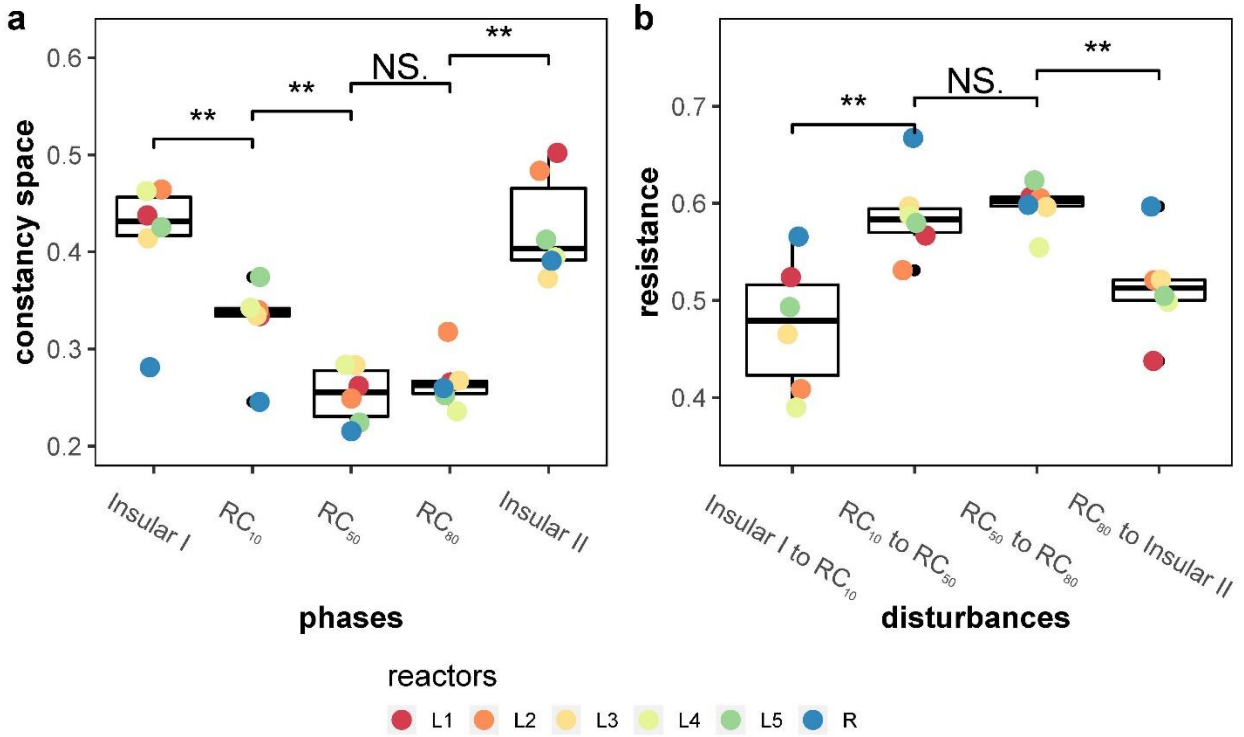

Figure S7.1 The stability properties of **a)** constancy and **b)** resistance RS were calculated for the local microbiomes L1-L5 and the regional pool R. A small constancy space marks a high constancy and high resistance values mark a high resistance behaviour. The stars indicate a significant difference in stability properties of local communities L1-L5 between two successive phases (Wilcoxon; *$p \leqslant 0.05$ and **$p \leqslant 0.01$).

S8: Analysis of microbial community composition

Step 1: Visualization of microbial community composition

The microbial community composition (i.e. fingerprint) was determined by flow cytometry. The variations in the composition of the six communities were shown by the relative cell abundance and absolute cell abundance variations for the dominant SCs (Figs. S8.1, S8.2; dominant SC:

relative cell abundance >1/number of gates = 1.25% or absolute cell abundance > cell number of total community/number of gates).

The fate of all dominant SCs through time (Fig. S8.3) was shown based on relative cell abundance. Using the R package 'vegan' (13), the dissimilarity of the samples was shown as NMDS plots based on the Bray-Curtis distance measure calculated based on relative cell abundance in Fig. 2a.

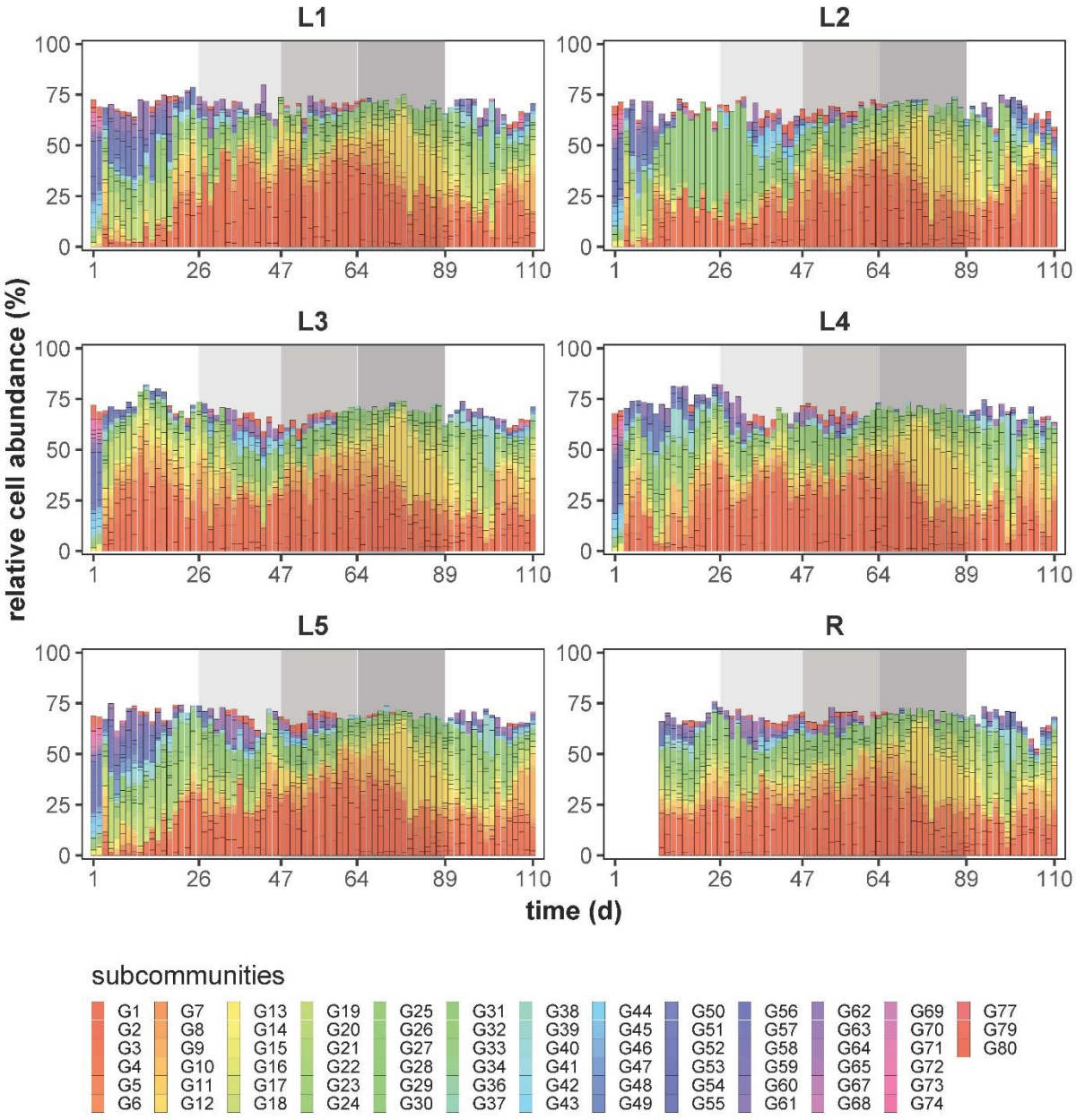

Figure S8.1 The relative cell abundance distribution per dominant SC and reactors (relative abundance > 1/number of gates = 1.25% in the corresponding community sample) over time. Each SC is represented

by a different colour. The relative abundance of each SC is given in %. The shaded areas represent different phases with changed RC.

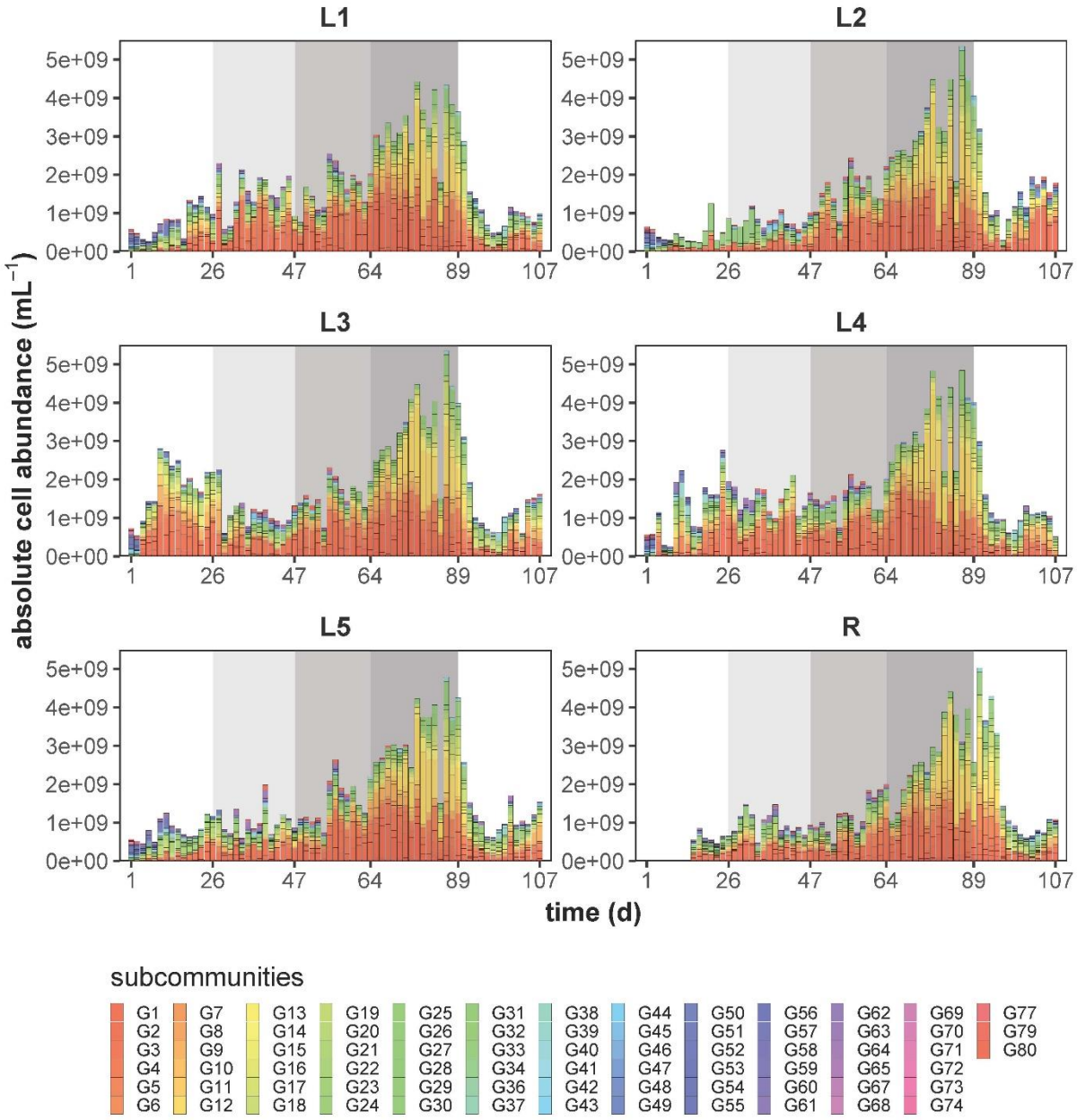

Figure S8.2 The absolute cell abundance distribution per dominant SCs and reactors (absolute cell abundance > cell number of total community/number of gates) over time. Each SC is represented by a different colour. The absolute cell abundance of each SC is given in cells mL^{-1}. The shaded areas represent different phases with changed RC.


L1
L2
L3
L4
L5
R
G2
G3
G4
G9
G12
G1
G18
G5
G33
G24
G19
G32
G11
G22
G8
G20
G64
G17
G16
G79
G13
G10
G51
G26
G38
G39
G62
G30
G50
G41
G40
G7
G25
G15
G47
G29
G23
G6
G45
G14
relative cell abundance per subcommunity (%)
50
0
0 551100 551100 551100 551100 551100 55110
time (d)

772

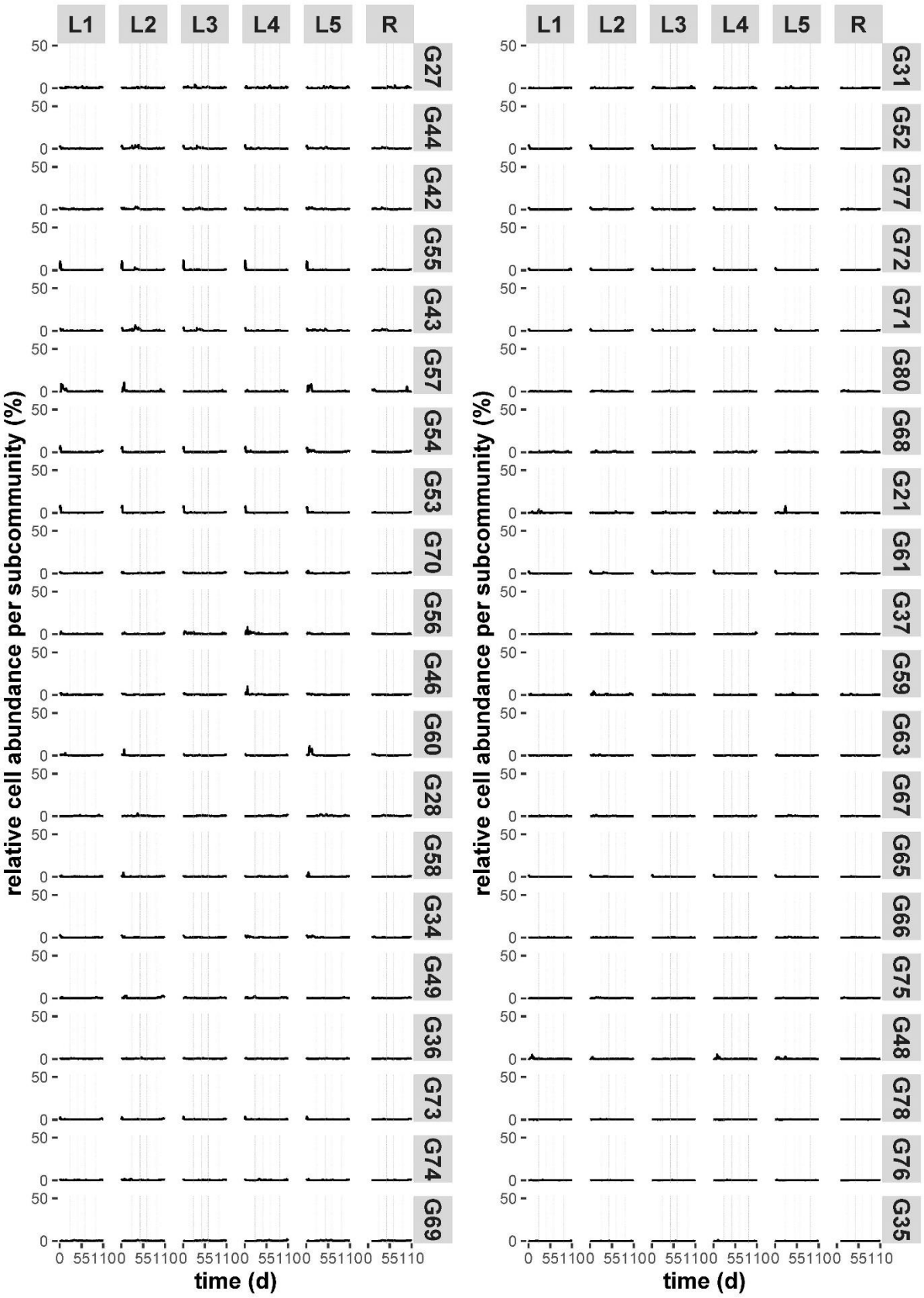
L1
L2
L3
L4
L5
R
G27
G44
G42
G55
G43
G57
G54
G53
G70
G56
G46
G60
G28
G58
G34
G49
G36
G73
G74
G69
G31
G52
G77
G72
G71
G80
G68
G21
G61
G37
G59
G63
G67
G65
G66
G75
G48
G78
G76
G35
relative cell abundance per subcommunity (%)
50
0
0 551100 551100 551100 551100 551100 55110
time (d)

773

Figure S8.3 The fate of SCs according to relative cell abundance. SCs are ranked in descending order of mean relative cell abundance over the whole experiment. The dashed lines indicate the different phases with changed RC.

Step 2: Comparison of effluents between local communities L1-L5 and the regional pool R

A PERMANOVA (permutational multivariate analysis of variance) was applied using the R package 'vegan' (13) to determine the difference between the effluents from the local communities L1-L5 and the regional pool R. We wanted to know whether the microbial composition of R was similar to the sum of effluents from L1-L5. Briefly, samples from day 12 to day 23 (Insular I phase) were used. For each day, the values of absolute cell abundance per SC from L1-L5 were summed up and then normalized to relative cell abundance to simulate the sum of L1-L5 effluents. The sum of L1-L5 effluents was compared with the R community of the same days (permutations = 9999, method = 'bray'). The results showed that the composition of the R community was divergent from that of L1-L5 (PERMANOVA, $F = 8.452$, $p = 0.0002$, $R^2 = 0.346$). Thus, the composition of the R community was not only determined by the immigration from L1-L5, but also by its unique operational parameters (e.g., dilution time, no nutrient feeding).

Step 3: α-, γ- and β-diversity values of microbial communities L1-L5 and R

The α-diversity was determined by counting the numbers of dominant SCs (relative cell abundance > 1/number of gates = 1.25%, Fig. S8.4) per local community L1-L5 and the regional pool R.

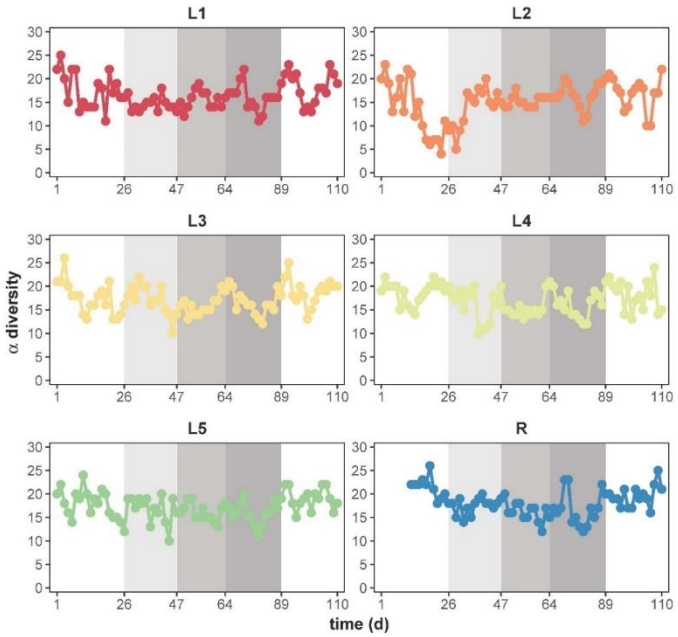

Figure S8.4 α-diversity of the composition of the five local communities L1-L5 and the regional pool R. The α-diversity was determined by counting the numbers of dominant SCs (relative cell abundance $>$ 1/number of gates $=$ 1.25%) in each community. The color indicates the respective community as specified in Fig. 1. The shaded areas represent different phases with changed RC.

The γ-diversity was determined by counting the numbers of SCs among a total of 80 SCs that were dominant (relative cell abundance > 1/number of gates = 1.25%) in at least one local community within the whole metacommunity, which was expressed as the richness of SCs in the metacommunity. The γ-diversity showed remarkable phase-to-phase variation (Wilcoxon test, $p = 3.416\times10^{-4}$, 6.258×10^{-4}, 0.045, 3.605×10^{-4}, respectively; Fig. S8.5). The γ-diversity declined from 39.73 ± 3.17 SCs in Insular I phase to 18.8 ± 3.85 SCs in RC_{80} and increased again to 33.11 ± 3.62 SCs in Insular II phase (Table 1). Thus, the γ-diversity decreased with increasing RC values, but recovered to a level when the recycling flow was stopped.

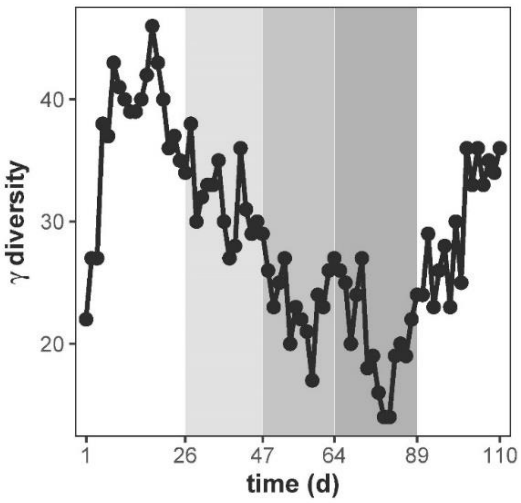

Figure S8.5 γ-diversity of the metacommunity composed of five local communities (L1-L5). The γ-diversity was determined by counting the numbers of SCs among a total of 80 SCs that were dominant (relative cell abundance > 1/number of gates = 1.25%) in at least one local community. The shaded areas represent different phases with changed RC.

The β-diversity was computed as the number of unique dominant SCs, which were not shared by pairwise samples. Intra-community β-diversity compared samples from successive time points per reactor (Fig. 3a), while inter-community β-diversity compared samples from the same time point but from different reactors (Fig. 3b). Significant differences of intra-community β-diversity

between RC_{50} and zero or low recycling phases were found ($p = 5.505\times10^{-5}$ for Insular I, 8.016×10^{-4} for RC_{10}, 1.625×10^{-7} for Insular II), as well as between RC_{80} and these phases respectively ($p = 3.737\times10^{-8}$ for Insular I, 1.753×10^{-6} for RC_{10}, 1.983×10^{-11} for Insular II). Wilcoxon test also showed significant differences of inter-community β-diversity between successive phases for L vs. L ($p = 3.848\times10^{-14}$, 2.2×10^{-16}, 1.033×10^{-8}, 2.2×10^{-16}) and L vs. R ($p = 3.203\times10^{-8}$, 5.086×10^{-10}, 4.838×10^{-10}, 3.203×10^{-8}, 2.2×10^{-16}). A summary of α-, γ- and β-diversity values is shown in Table 1.

Drift events were calculated from balanced periods when the temporal community composition variation (i.e. intra-community β-diversity) was higher than a defined threshold (Fig. 3a and Table S8.1). The threshold was set to 8.76 and was calculated as the mean value for intra-community β-diversity of L1-L5 of the Insular I phase during the balanced periods. To investigate which microorganisms were involved in the drift events, we sorted the relevant SCs that massively changed their relative cell abundance. After cell sorting, 16S rRNA gene sequencing analysis was performed (Supplementary Information S9). We studied three drift events: drift1 (RC_{10}) in L2 and L5 at day 47, drift2 (RC_{50}) in L3 and L5 at day 61 and drift3 (Insular II) in L1 and L3 at day 100. For comparison of community states between before and after the drifts, day 44, day 58 and day 99 were taken as before-drift community states, respectively, for drift1, 2 and 3 (Table S8.2).

Table S8.1 Drifts occurring on certain days in local communities L1-L5. The values showed the intra-community β-diversity between two successive time points. The drifts were identified by intra-community β-diversity values being above a threshold of > 8.76 (i.e. mean intra-community β-diversity value during the balanced periods of Insular I phase of all five local communities). A dash (-) means that no drift occurred in the respective communities at the time. The drifts in bold were chosen for cell sorting (Supplementary Information S9).

time (d)	Insular I												RC_{10}								RC_{50}				RC_{80}		Insular II									
	8	*9*	*12*	*13*	*14*	*15*	*16*	*19*	*20*	*21*	*23*	*26*	*34*	*35*	*36*	*40*	*41*	*43*	*44*	***47***	*58*	***61***	*62*	*63*	*76*	*89*	*97*	*98*	*99*	***100***	*103*	*104*	*105*	*106*	*107*	*110*
L1	-	-	10	10	13	-	-	19	15	-	9	20	-	-	-	-	9	9	-	-	9	-	-	-	-	9	-	-	15	**20**	9	-	-	10	10	12
L2	19	15	11	9	11	-	-	-	-	-	-	-	13	11	-	-	11	-	15	**24**	-	10	10	10	11	-	11	-	19	9	19	10	-	9	-	9
L3	-	-	-	-	-	-	-	-	12	12	11	-	-	16	-	9	9	-	-	-	-	**18**	-	-	-	-	-	15	-	**20**	20	15	-	-	-	14
L4	13	15	13	13	-	11	15	12	-	9	-	9	9	10	12	-	-	14	14	12	-	11	-	-	-	-	-	15	-	17	13	12	-	20	16	9
L5	9	10	10	9	13	11	11	10	-	-	-	-	-	10	-	12	10	10	13	**15**	-	**13**	-	-	-	-	-	9	-	16	9	9	10	11	-	10

Table S8.2 Relative cell abundance of SCs (%) before and after drift1 (day 47, RC_{10}) in L2 and L5, drift2 (day 61, RC_{50}) in L3 and L5, and drift3 (day 100, Insular II) in L1 and L3. The pink background of squares marks the dominance of the SCs (relative cell abundance > 1/number of gates = 1.25%). A dash (-) means that the SC was not involved in the drift in the corresponding reactor. The SCs in bold were chosen for cell sorting (Supplementary Information S9).

drift 1 (day 47)	reactor	state	**G1**	**G3**	G4	**G7**	G8	G10	G11	G13	**G16**	G18	G19	G20	**G22**	G23	**G24**	**G26**	G27	G32	**G33**	G41	G42	G43	G47	G50	G59	G62	G64	**G79**	
	L2	before	12.6	-	1.0	2.8	1.2	1.6	0.6	2.2	0.5	1.4	-	0.5	0.8	-	4.0	4.8	-	1.1	0.3	2.1	1.7	-	3.3	0.2	1.5	1.8	2.3	0.9	
		after	0.3	-	2.5	0.2	1.8	0.6	6.0	0.4	5.0	0.6	-	2.2	5.1	-	0.4	0.9	-	1.7	8.0	0.9	0.7	-	0.5	2.7	0.0	0.0	0.1	5.1	
	L5	before	-	1.2	-	6.3	-	-	2.8	2.5	-	-	0.6	2.9	1.3	1.3	-	2.7	2.3	0.6	-	0.5	-	0.1	-	-	2.5	-	-	0.9	
		after	-	9.1	-	1.1	-	-	1.1	0.6	-	-	1.5	1.0	0.4	1.1	-	1.0	0.4	2.7	-	1.6	-	1.4	-	-	0.3	-	-	5.1	
drift 2 (day 61)	reactor	time (d)	**G5**	**G7**	**G12**	G13	G16	G17	**G18**	**G19**	G20	G22	**G24**	G26	G27	G32	G41	G51	G64	G79											
	L3	before	0.9	0.5	0.6	0.4	1.2	1.5	0.8	5.2	1.0	1.2	2.5	1.2	0.50	3.3	1.9	1.3	2.7	2.0											
		after	2.2	4.1	2.2	1.5	1.9	0.9	2.3	0.6	1.9	1.3	0.4	3.7	1.6	0.2	0.8	0.3	0.4	0.6											
	L5	before	0.6	0.5	-	-	0.8	-	0.6	5.5	0.7	-	3.3	-	0.6	5.2	2.0	1.3	3.7	2.7											
		after	2.4	2.6	-	-	1.8	-	1.4	0.4	1.5	-	0.3	-	2.2	1.1	1.0	0.2	0.4	0.8											
drift 3 (day 100)	reactor	time (d)	G2	**G3**	**G4**	**G5**	**G7**	G8	G11	**G12**	G13	G15	G17	**G18**	**G20**	G22	**G24**	G26	G28	G30	G31	G32	**G38**	G40	G41	G51	G56	G57	G62	G64	G68
	L1	before	-	0.0	0.3	0.6	0.2	-	4.3	-	1.0	-	6.8	-	7.0	8.4	0.9	0.6	1.6	1.6	-	-	21.0	9.6	0.0	1.1	-	-	0.0	0.1	1.3
		after	-	11.4	3.6	3.2	3.3	-	0.5	-	1.8	-	1.2	-	0.5	1.1	10.9	1.6	0.8	0.2	-	-	0.4	0.3	1.9	2.9	-	-	2.3	7.4	0.3
	L3	before	0.6	0.0	0.3	1.2	-	1.9	-	2.2	-	0.2	4.0	0.6	3.5	-	0.7	-	-	2.6	0.2	2.1	17.5	7.3	0.0	-	0.4	1.7	-	0.0	-
		after	2.8	11.2	2.4	11.5	-	1.2	-	0.7	-	1.5	0.9	4.1	0.6	-	5.2	-	-	0.5	2.2	0.9	0.8	0.5	2.1	-	1.8	0.1	-	3.3	-

Step 4: Partitioning of β-diversity to reveal turnover and nestedness of SCs

The community composition variation was partitioned into species replacement and species loss to determine turnover and nestedness values using a method developed for microbial community flow cytometric data (14). The method was used to study the temporal pattern of intra- and inter-community β-diversity loss when the recycling rate RC was increased. Using multiple-site measures in the R package 'betapart', the turnover β_{SIM} and nestedness β_{NES} components of Sørensen dissimilarity were calculated (15, 16) (Fig. S8.6 and Table S8.3). Multisite intra-community β-diversity was calculated over all samples from the balanced period per phase per community. Multisite inter-community β-diversity was calculated over five local communities (L1-L5) per time point. The lowest intra-community β-diversity values for turnover β_{SIM} were always at RC_{80} with a mean value of 0.34 ± 0.02 and the highest values for nestedness β_{NES} were also always at RC_{80} with a mean value of 0.14 ± 0.02. The inter-community β-diversity values for turnover β_{SIM} were also lowest at RC_{80} (0.11 ± 0.04) during the balanced periods, while the values for nestedness β_{NES} remained roughly the same (Table S8.3).

We also investigated which SCs were nested. Nested SCs were determined if they remained dominant at all time points over the balanced period in the respective reactor and phase (relative cell abundance > 1.25%, Table S8.4). Generally, fewer nested SCs were observed in insular phases than in RC phases. In insular phases, nested but different SCs were found in the various local communities, while in RC phases, some of the SCs were nested in all reactors L1-L5 per phase or over all phases, that is, G2 in RC_{10}; G2, G9, G3, G4 and G11 in RC_{50}; and G2, G9, G4, G5, G12 and G14 in RC_{80}.

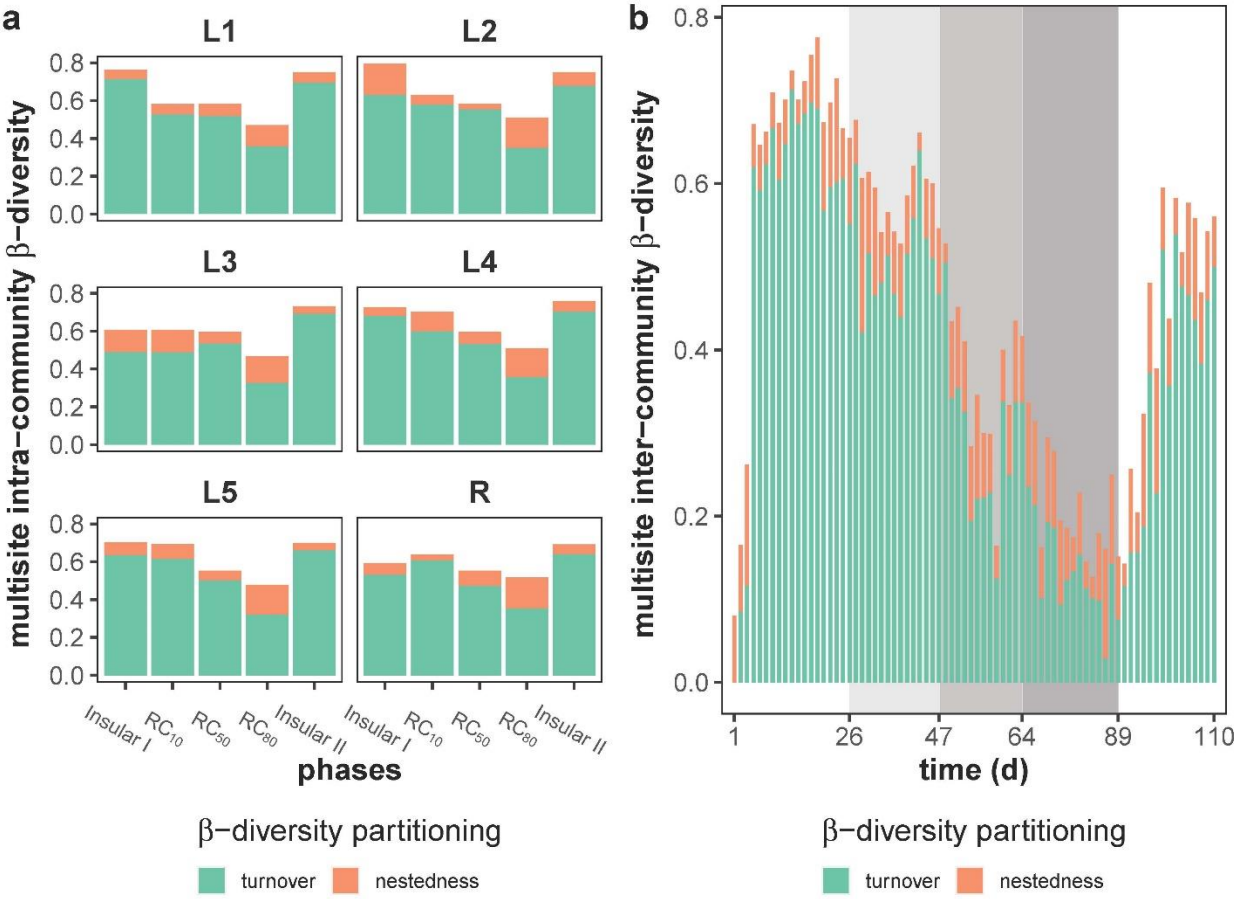

Figure S8.6 Partitioning of β-diversity into turnover (green) and nestedness (orange) components. a) Multisite intra-community β-diversity was calculated over all samples from the balanced period per phase per community and b) multisite inter-community β-diversity was calculated over five local communities (L1-L5) per time point. The shaded areas represent different phases with changed RC.

Table S8.3 Summary of turnover and nestedness components of multisite intra- and inter-community comparisons [Liu & Müller (14)] as mean ± standard deviation (sd) per phase. The mean ± sd values were all calculated among local communities L1-L5 during balanced periods if not clarified otherwise. Asterisks indicate that the diversity values in these phases were significantly different from those in any other phases, at $*p \leqslant 0.05$, $**p \leqslant 0.01$ or $***p \leqslant 0.001$.

comparison	components	Insular I	RC_{10}	RC_{50}	RC_{80}	Insular II
multisite intra-community	turnover	0.63 ± 0.09	0.56 ± 0.05	0.53 ± 0.02	0.34 ± 0.02**	0.68 ± 0.02
	nestedness	0.09 ± 0.05	0.08 ± 0.03	0.05 ± 0.01	0.14 ± 0.02	0.05 ± 0.01
multisite inter-community	turnover	0.64 ± 0.05***	0.52 ± 0.06*	0.24 ± 0.07**	0.11 ± 0.04**	0.43 ± 0.09*
	nestedness	0.07 ± 0.03	0.07 ± 0.02	0.08 ± 0.03	0.07 ± 0.04	0.09 ± 0.03

Table S8.4 List of nested subcommunities (SCs) in respective reactors and phases. Nested SCs were determined if they remained dominant (relative cell abundance > 1.25%) at all time points over the balanced period in the respective reactor and phase. Nested SCs are marked with the number '1' and a pink background. The SCs were ranked from left to right according to the descending order of frequencies of being nested (numbers of pink squares).

reactor	phase	G2	G9	G3	G4	G11	G8	G18	G22	G5	G12	G14	G24	G1	G33	G64	G15	G32	G13	G17	G19	G20	G26	G38	G43
L1	Insular I	0	0	0	0	0	0	0	0	0	0	0	0	0	0	0	0	0	0	0	0	0	0	0	0
L2	Insular I	0	0	1	0	0	0	0	0	0	0	0	0	0	0	0	0	1	0	0	0	0	0	0	0
L3	Insular I	1	1	0	1	1	0	1	0	0	0	0	0	0	0	0	1	0	0	0	0	0	0	0	0
L4	Insular I	0	0	0	0	0	0	0	1	0	0	0	0	0	0	0	0	0	0	0	0	0	0	0	0
L5	Insular I	0	0	0	0	0	0	0	1	0	0	0	0	0	0	0	0	0	0	1	0	0	0	1	0
R	Insular I	1	1	0	0	1	0	1	1	0	0	0	1	0	0	0	1	0	0	0	0	0	0	0	0
L1	RC_{10}	1	0	1	1	0	1	0	0	0	0	0	1	0	0	0	0	0	0	0	0	0	0	0	0
L2	RC_{10}	1	0	1	0	0	0	0	0	0	0	0	1	0	0	1	0	0	0	0	0	0	0	0	1
L3	RC_{10}	1	1	1	0	0	0	1	0	0	0	0	1	0	0	1	0	0	0	0	0	0	0	0	0
L4	RC_{10}	1	0	0	0	1	0	0	0	0	0	0	0	0	0	0	0	0	0	0	0	0	0	0	0
L5	RC_{10}	1	0	0	0	0	0	0	0	0	0	0	0	0	0	0	0	0	0	0	0	1	0	0	0
R	RC_{10}	1	0	1	0	0	0	0	0	0	0	0	1	0	0	1	0	0	0	0	0	0	0	0	0
L1	RC_{50}	1	1	1	1	1	1	0	0	0	0	0	0	0	0	0	0	0	0	0	0	0	0	0	0
L2	RC_{50}	1	1	1	1	1	0	0	0	0	0	0	0	0	0	0	0	0	0	0	0	0	0	0	0
L3	RC_{50}	1	1	1	1	1	1	0	0	0	0	0	0	0	0	0	0	0	0	0	0	0	0	0	0
L4	RC_{50}	1	1	1	1	1	1	0	0	0	0	0	0	0	0	0	0	0	0	0	0	0	0	0	0
L5	RC_{50}	1	1	1	1	1	1	0	0	0	0	0	0	0	0	0	0	0	0	0	0	0	1	0	0
R	RC_{50}	1	1	1	1	1	1	0	0	0	0	0	0	0	0	0	0	1	0	0	1	0	0	0	0
L1	RC_{80}	1	1	1	1	0	0	1	0	1	1	1	0	0	0	0	0	0	0	0	0	0	0	0	0
L2	RC_{80}	1	1	0	1	0	0	0	0	1	1	1	0	0	0	0	0	0	0	0	0	0	0	0	0
L3	RC_{80}	1	1	1	1	0	0	1	0	1	1	1	0	0	1	0	0	0	0	0	0	0	0	0	0
L4	RC_{80}	1	1	0	1	0	0	0	0	1	1	1	0	0	1	0	0	0	0	0	0	0	0	0	0
L5	RC_{80}	1	1	1	1	0	0	1	0	1	1	1	0	0	1	0	0	0	0	0	0	0	0	0	0
R	RC_{80}	1	1	1	1	0	0	1	0	1	1	1	0	0	1	0	0	0	0	0	0	0	0	0	0
L1	Insular II	0	0	0	0	0	0	0	0	0	0	0	0	1	0	0	0	0	0	0	0	0	0	0	0
L2	Insular II	0	1	0	0	0	0	0	0	0	0	0	0	1	0	0	0	0	1	0	0	0	0	0	0
L3	Insular II	0	1	0	0	0	0	0	1	0	0	0	0	0	0	0	0	0	0	0	0	0	0	0	0
L4	Insular II	0	1	0	0	0	0	0	1	0	0	0	0	0	0	0	0	0	0	0	0	0	0	0	0
L5	Insular II	0	1	0	0	0	1	0	1	0	0	0	0	1	0	0	0	0	0	0	0	0	0	0	0
R	Insular II	0	1	0	0	0	1	0	1	0	0	0	0	1	0	0	0	0	0	0	0	0	0	0	0

S9: Taxonomic composition of whole communities and sorted SCs

Step 1: Taxonomic composition of communities

A total of 96 whole-community samples were chosen for taxonomic analysis with two aims: 1) to confirm the variation in flow-cytometric-analysis-based community composition caused by mass transfer, for which samples of inoculum (day 0), for the 2nd and the 8th days as well as the final day for each phase were chosen for all local communities L1-L5 and the regional pool R (starting at day 9); and 2) to confirm the drifts identified by flow-cytometric-analysis-based intra-community variation, for which samples of three time points at which drifts occurred in at least two local communities were chosen (Tables S8.1, S8.2), namely, RC_{10}: drift at day 47 in L2 and L5, RC_{50}: drift at day 61 in L3 and L5, and Insular II: drift at day 100 in L1 and L3. The samples of day 44 in L2 and L5, day 55 in L3 and L5, and day 97 in L1 and L3 were taken for comparison of community states. The sampling time points for each reactor are listed in Table S9.1.

Table S9.1 The time points (day) of samples for whole-community taxonomic analysis are listed per reactor and phase. The time points in bold are those used to study the impact of drifts on community variation. The shaded areas represent different phases with changed RC. The time points of days 26, 47, 64 and 89 were the days on which the phases ended as well as those on which the next phases started; therefore, drifts at day 47 happened at phase RC_{10}, while drifts at day 61 and day 100 happened at RC_{50} and Insular II.

reactor/ phase	inoculum	Insular I	RC_{10}	RC_{50}	RC_{80}	Insular II
L1	0	1, 8, 26	27, 34, 47	48, 55, 64	65, 72, 89	90, 97, **100**, 107
L2		1, 8, 26	27, 34, 44, **47**	48, 55, 64	65, 72, 89	90, 97, 107
L3		1, 8, 26	27, 34, 47	48, 55, **61**, 64	65, 72, 89	90, 97, **100**, 107
L4		1, 8, 26	27, 34, 47	48, 55, 64	65, 72, 89	90, 97, 107
L5		1, 8, 26	27, 34, 44, **47**	48, 55, **61**, 64	65, 72, 89	90, 97, 107
R	-	9, 26	27, 34, 47	48, 55, 64	65, 72, 89	90, 97, 107

The taxonomic composition of communities at genus level is shown in Fig. S9.1 (the relative abundance table of communities at species level is shown in Dataset S4). A total of 18 classes and 159 genera were identified over all whole-community samples. Generally, the communities were dominated by the classes Bacteroidia, Gammaproteobacteria and Alphaproteobacteria, which are typical members of activated sludge (17, 18). At phases Insular I, RC_{10} and Insular II, communities harboured more diverse genera, namely, *Leadbetterella*, *Azospirillum*, *Pseudacidovorax*, *Brevundimonas* and *Pedobacter*. Although the taxonomic compositions of the local communities L1-L5 and the regional pool R were fairly comparable within each of the five phases, the compositions clearly differed between the phases. Therefore, the 16S rRNA gene

sequencing data supported the findings obtained by flow cytometry. The 16S rRNA gene sequencing data showed for the RC_{50} and RC_{80} high-rate recycling phases high synchrony in community compositions (Fig. S9.1). An unassigned genus from *Sphingobacteriaceae* (family) accounted for about half of the genera in RC_{50} and RC_{80}, and *Leadbetterella* and *Azospirillum* persisted but at lower relative abundances (Fig. S9.1). Members of the *Sphingobacteriaceae* have been reported to degrade a variety of organic chemicals (19-21), indicating their ability to use complex 'leftover' substrates. Members of *Azospirillum* are known for the ability to fix nitrogen (22) and thus could help overcome nitrogen deficiency specifically in RC_{80}. These major genera indicated the key role of nutrient availability in community building and it appears that mass transfer supported this dominance.

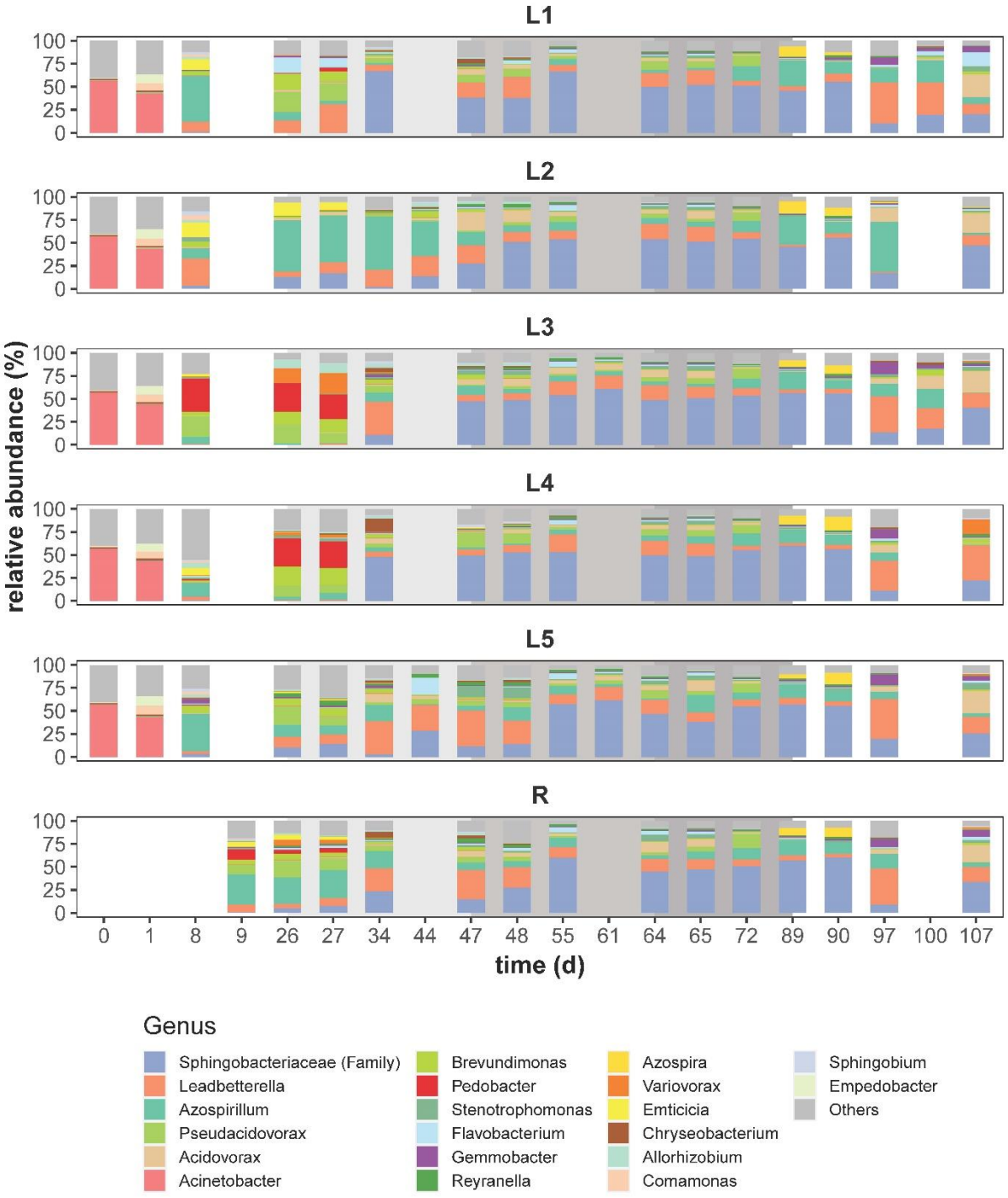

Figure S9.1 The taxonomic composition in relative abundance (%) of communities over time at the genus level. A total of 159 genera were identified. The top 20 most abundant genera are colour-coded and stacked from bottom to top per column in decreasing order of mean relative abundance over all samples. An unassigned genus from the family *Sphingobacteriaceae* is labelled by this family. The relative abundances

of genera other than the top 20 are summed up and represented as 'Others'. The shaded areas represent different phases with changed RC.

The NMDS analysis based on relative abundances of all 159 genera (Fig. S9.2) was supported by the R package 'vegan' (13) and visualized identically to the procedure used for the flow cytometric single-cell data shown in Fig. 2a. The trend of taxonomic composition of communities confirmed the trend revealed by flow cytometric fingerprints. The most extreme change was observed during the adaptation period of Insular I phase from day 1 to day 8, and all local communities L1-L5 evolved in similar directions at the end of Insular I phase. As RC increased from 10% to 80%, the communities became increasingly convergent on both regional and temporal scales. When recycling ended, community divergence increased slightly again compared with the levels at RC_{50} and RC_{80}. Thus, the data obtained by 16S gene sequencing clearly evidenced the influence of mass transfer on community composition demonstrated by the flow cytometric data.

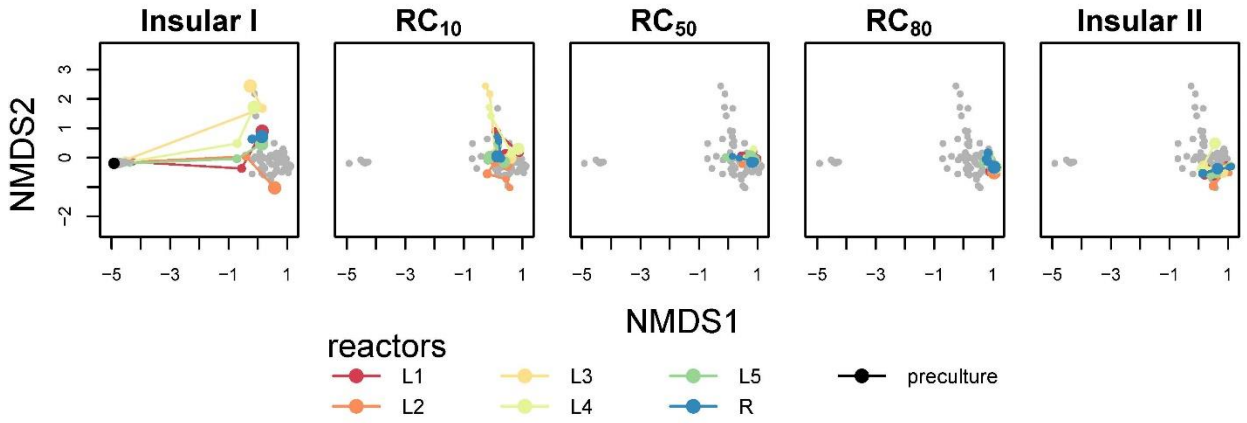

Figure S9.2 NMDS analysis using relative abundance of all genera (total of 159) based on Bray-Curtis dissimilarities (try = 100, trymax = 200). Successive and connected time points indicate the assembly trajectory of communities. Points in grey represent samples from the other phases.

Additional whole-community samples were analyzed at days 47, 61 and 100 to clarify changes in community composition occurring due to drift events previously determined by intra-community β-diversity based on flow cytometric data (Table S9.1). For comparison, the intra-community β-diversity based on the taxonomic composition of communities at the genus level was calculated following the workflow used for flow cytometric data (Supplementary Information S8, step 3). First, all genera with relative abundance > 0.63% (1/159, 1/total number of genera) were determined

as ‘dominant genera’. Second, the intra-community β-diversity was computed as the number of unique dominant genera, which were not shared by pairwise samples from successive time points per community. Third, owing to limited time points sampled for taxonomic analysis, the comparison could not be performed for short time intervals as was done for the much higher available sample numbers of flow cytometric data. Instead, the pairwise comparison could only be undertaken across long time intervals (varying from 1 to 18 days). To create a comparison with these data, the intra-community β-diversity based on SCs was therefore recomputed using the same pairwise samples at chosen time points (Table S9.1, unfilled circles in Fig. S9.3). We found that the variations of intra-community β-diversity based on the two analyses were similar and that the intra-community β-diversity values for both analyses decreased as RC increased, pointing to the fact that increasing RC is a means of preventing stochastic events.

The drifts events were calculated in the balanced periods of all phases. The values based on SCs were often higher than the corresponding values based on genus level, and the latter were so low at some time points that no drift could be detected. These findings showed that some drifts in SCs clearly detected by flow cytometric analysis were not revealed at the genus level. Thus, the β-diversity of SCs was more sensitive as indicator of community variation than the genus level. The background for these findings is that cells of the same genus may occupy different gates (SCs) in the gate template, whereas sequencing does not take into account physiological cell properties.

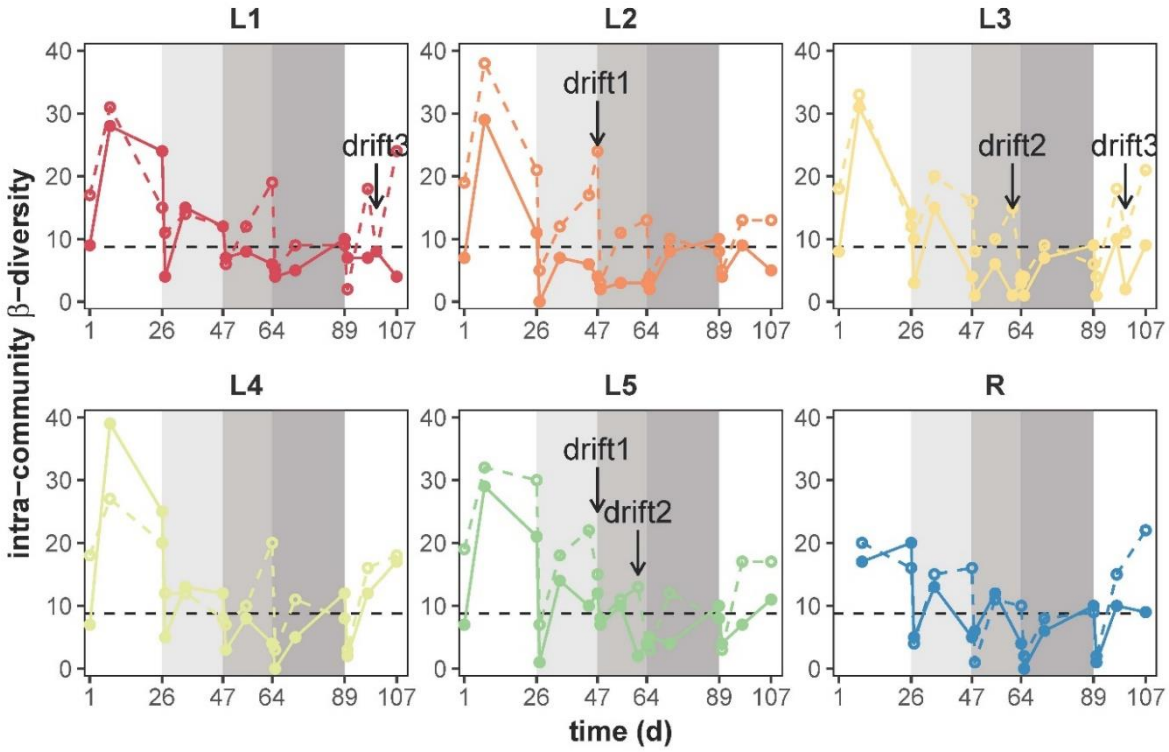

Figure S9.3 Drift events, detected by intra-community β-diversity variations based on flow cytometric data (SCs, open circles and dashed lines) and based on 16S rRNA amplicon sequencing data (genus, closed circles and closed line). The intra-community β-diversity was calculated as the number of unshared dominant genera (relative abundance > 0.63%) or dominant SCs (relative cell abundance > 1.25%) by pairwise samples from successive time points per community. The dashed black line marks the threshold determining drift (8.76), and the labels and arrows indicate three drifts from which cells were chosen for 16S rRNA gene analyses. The following drifts were chosen: drift1: day 47 in L2 and L5, drift2 day 61 in L3 and L5, and drift 3: day 100 in L1 and L3. The shaded areas represent different phases with changed RC.

Step 2: Taxonomic assignment of sorted SCs

Cells of gates were cytometrically sorted only when their abundance was above 2%. Out of 35,840 SCs a total of 51 SCs were selected for cell sorting and taxonomic analysis based on four specific features: 1) *mass transfer*, to confirm the redistribution of SCs from R to L1-L5 (e.g. G5, G12, G14 and G33) during RC_{80}, which were also correlated with RC (Fig. S12.1 and Fig. S8.3); 2) *net growth rate*, to investigate the taxonomy of cells in SCs, which grew (i.e. $\mu' SC_x > 0$ in $\geqslant$ 4 reactors) at RC_{80} in L1-L5 (Fig. 4): G1, G5, G9, G13, G18, G25, G33. In addition, we were interested in cells that did not grow but were rescued from R at RC_{80} in L1-L5 (i.e. $\mu' SC_x = 0$ in $\geqslant$ 2 reactors, Fig. 4): G2, G4, G11, G12, G14; 3) *nestedness*, to investigate the taxonomy of cells in the most nested SCs, that is, at RC_{50}: G2, G3, G4, G8, G9, G11 and at RC_{80}: G5, G12, G14 (Table S8.4); and 4) *drifts*, to investigate the taxonomy of cells benefitting from drifts (drift1: G3, G16, G22, G33, G79; drift2: G5, G7, G12, G18; drift3: G3, G4, G5, G7, G18, G24) or being disadvantaged by drifts (drift1: G1, G7, G24, G26; drift2: G19, G24; drift3: G12, G20, G38; Table S8.2). The sorted SCs are listed according to sample time and reactors in Table S9.2. The position of the sorted SCs in the gate template is shown in Fig. S9.4. The taxonomic composition of sorted SCs is shown at the genus level in Fig. S9.5 (Dataset S5). A total of 26 classes and 186 genera were identified over all sorted SC samples. Generally, most sorted SCs were dominated by only one or two classes, namely, Alphaproteobacteria, Gammaproteobacteria, Bacteroidia or Actinobacteria. At the genus level, most SCs were mono-dominant (marked in colour, Table S9.2). Only a few SCs comprised different genera (i.e., 047_G79_L2[4], 061_G5/G12_L3[4], 085_G5_L1/L3/R[1,2,3], 085_G14_L1[1,2,3], 086_G9/G25_L2[2]).

Table S9.2 Fifty-one cytometrically sorted SCs from respective time points (day) and reactors for taxonomic analysis. Each sample is named as 'time_gate_reactor'. The number labelled as superscript beside the sample name indicates the subjects it involved: 1, mass transfer; 2, net growth rate; 3, nestedness; 4, drifts.

Colour shades mark SCs dominated by *Azospirillum* ….., *Leadbetterella* ….., an unassigned genus from *Sphingobacteriaceae* (family) ….., an unassigned genus from PeM15 (order) ….., *Pseudacidovorax* ….., *Azospira* ….., *Acidovorax* ….., *Reyranella* ….., *Stenotrophomonas* ….., *Brevundimonas* ….., *Ochrobactrum* ….., *Sphingopyxis* ….. and *Microbacterium* …..

time (d)	gate	reactor					
		L1	L2	L3	L4	L5	R
26	G33		026_G33_L2[1]				
44	G1		044_G1_L2[4]				
44	G7					044_G7_L5[4]	
44	G24		044_G24_L2[4]				
44	G26		044_G26_L2[4]				
47	G3					047_G3_L5[4]	
47	G16		047_G16_L2[4]				
47	G22		047_G22_L2[4]				
47	G33		047_G33_L2[4]				
47	G79		047_G79_L2[4]				
58	G19			058_G19_L3[4]			
58	G24			058_G24_L3[4]			
61	G5			061_G5_L3[4]			
61	G7			061_G7_L3[4]			
61	G12			061_G12_L3[4]			
61	G18			061_G18_L3[4]			
63	G2	063_G2_L1[3]					
63	G3	063_G3_L1[3]					
63	G4			063_G4_L3[3]			
63	G8			063_G8_L3[3]			
63	G9			063_G9_L3[3]			
63	G11	063_G11_L1[3]					
71	G2					071_G2_L5[2]	
71	G4	071_G4_L1[2]					
71	G11					071_G11_L5[2]	
85	G5	085_G5_L1[1,2,3]		085_G5_L3[1,2,3]			085_G5_R[1,2,3]
85	G12	085_G12_L1[1,2,3]		085_G12_L3[1,2,3]			085_G12_R[1,2,3]
85	G14	085_G14_L1[1,2,3]		085_G14_L3[1,2,3]			085_G14_R[1,2,3]
85	G33	085_G33_L1[1,2]		085_G33_L3[1,2]			085_G33_R[1,2]
86	G1		086_G1_L2[2]				
86	G9		086_G9_L2[2]				
86	G13				086_G13_L4[2]		
86	G18		086_G18_L2[2]				
86	G25		086_G25_L2[2]				
99	G12			099_G12_L3[4]			
99	G20	099_G20_L1[4]					
99	G38	099_G38_L1[4]					
100	G3	100_G3_L1[4]					
100	G4	100_G4_L1[4]					
100	G5			100_G5_L3[4]			
100	G7	100_G7_L1[4]					
100	G18			100_G18_L3[4]			
100	G24	100_G24_L1[4]					

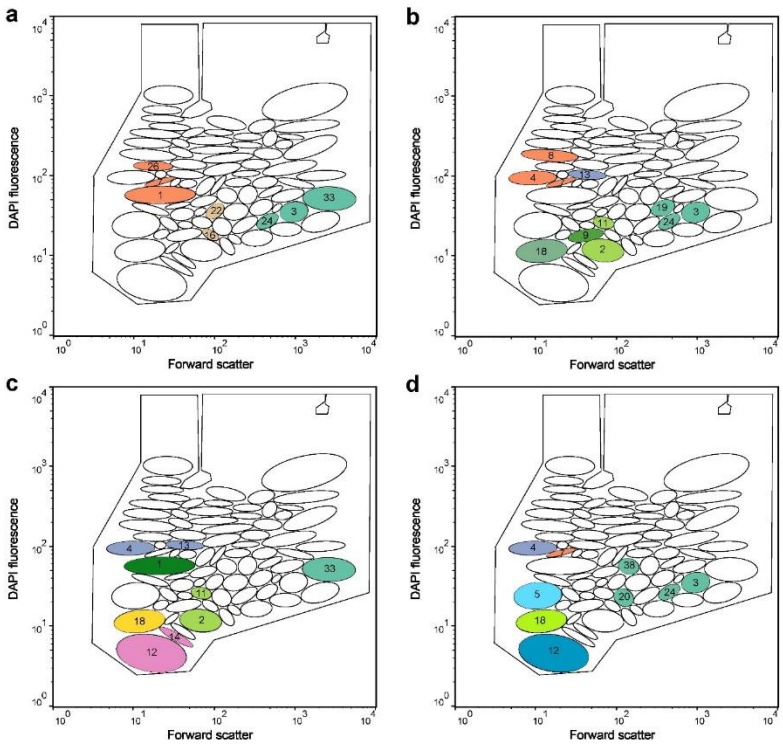

Figure S9.4 The sorted SCs from a: phase RC_{10} (days 26, 44, and 47), b: RC_{50} (days 58, 61 and 63), c: RC_{80} (days 71, 85 and 86) and d: Insular II (days 99 and 100) are coloured according to their mono-dominance of *Azospirillum* ….., *Leadbetterella* ….., an unassigned genus from *Sphingobacteriaceae* (family) ….., an unassigned genus from PeM15 (order) ….., *Pseudacidovorax* ….., *Azospira* ….., *Acidovorax* ….., *Reyranella* ….., *Stenotrophomonas* ….., *Brevundimonas* ….., *Ochrobactrum* ….., *Sphingopyxis* ….. and *Microbacterium* …..**.** The numbers (x) inside gates label the corresponding gate name: 'Gx'.

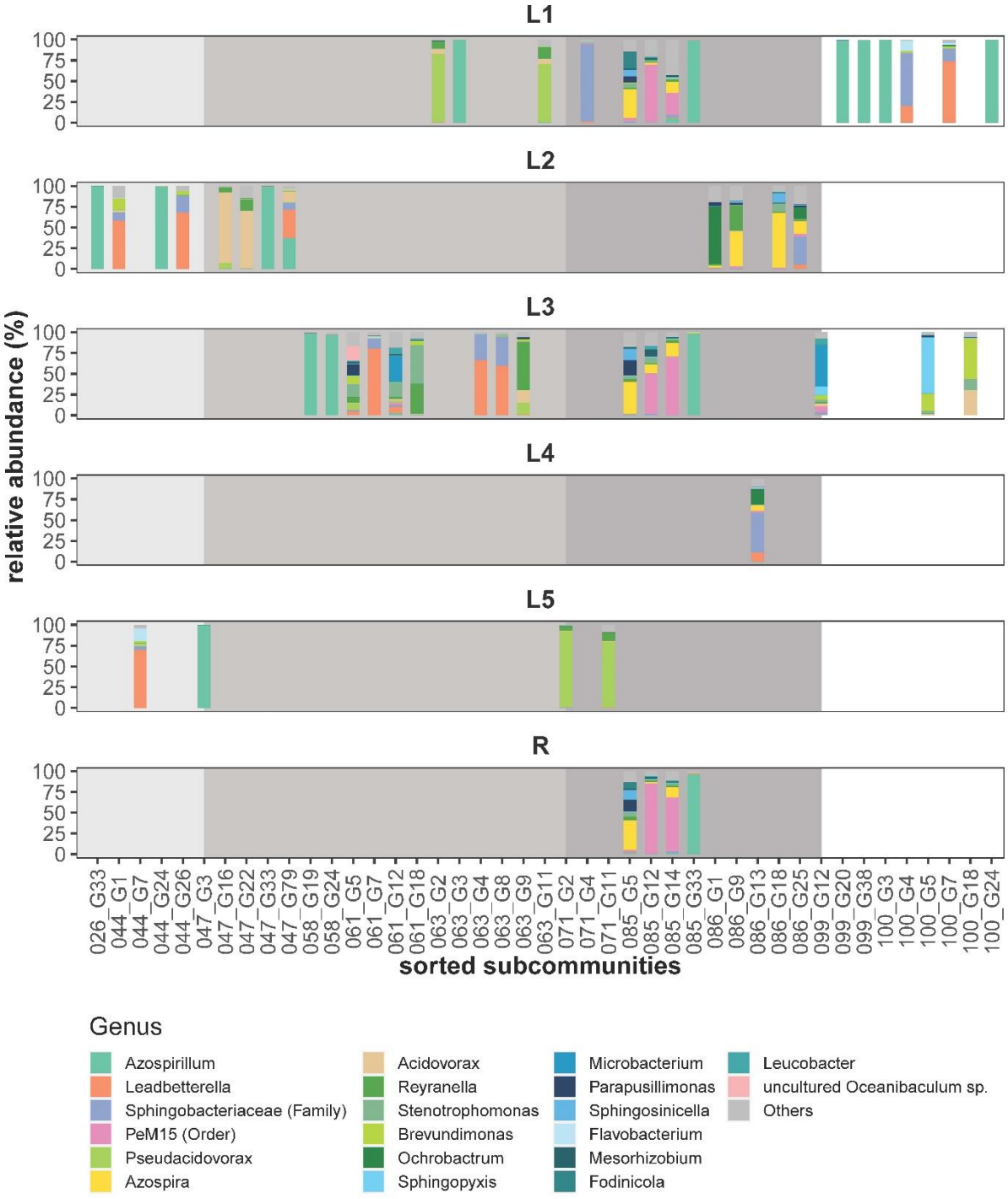

Figure S9.5 The taxonomic composition in relative abundance (%) of sorted SCs at the genus level. In total, 186 genera were identified. The top 20 most abundant genera are color-coded and stacked from bottom to top per column in decreasing order of mean relative abundance over all SCs samples. The unassigned genera are labelled with the respective family or order. The relative abundances of genera

other than the top 20 are summed up and represented as 'Others'. The shaded areas represent different phases with changed RC.

The genus assignments of cells in these SCs are discussed under the four specific features mentioned above:

Mass transfer & net growth rate: Mass transfer supported the persistence of SCs in local communities, either by enabling their local growth or by rescuing nongrowing SCs by their growth in the regional pool R. For example, at RC_{80}, *Azospirillum* (G33), *Azospira* (G9, G18), and *Ochrobactrum* (G1, Fig. S9.5, presenting only SCs > 2% cell abundance) followed the former mechanism ('growth'), and grew also at lower abundance in a set of local communities (Fig. 4), while an unassigned genus from PeM15 (order, G12 and G14), *Sphingobacteriaceae* (family, G4) and *Pseudacidovorax* (G2, G11, Fig. S9.5) followed the latter mechanism ('rescue') and did not grow in local communities in RC_{80}, but were rescued by growth in the regional pool R (Fig. 4). The mono-dominant SCs that showed net growth and that were rescued can be assumed to be superior local competitors. Some SCs that are also among the growing SCs (G5, G9, G25, Table S9.2) were multi-dominant and it can be assumed that the genera in each of the SCs can cooperate under RC_{80} conditions.

Nestedness: Generally, nested SCs were those that persisted in the different phases of the 114-generation experiment. For phase RC_{50}, we found for the flow cytometrically determined nestedness the SCs G2, G3, G4, G8, G9, and G11 (Table S8.4). Nearly the same gates were calculated as nested ones from the 16S rRNA gene sequencing data: genera *Azospirillum* (G3), *Leadbetterella* (G4, G8), *Pseudacidovorax* (G2, G11) and *Reyranella* (G9).

In $RC_{80,}$ flow cytometrically determined nested SCs were G2, G4, G5, G9, G12, and G14 (Table S8.4). Sequencing data found PeM15 (order, G12, G14) and *Pseudacidovorax* (G2) nested, while G5 and G9 were mostly multi-dominant and changed their proportions of contained genera from RC_{50} to RC_{80}.

In general, mass transfer supported genera such as G2, G12 and G14, which were nested and rescued by their ability to accumulate in the regional pool R (e.g., the unassigned genus from PeM15).

Drifts: Drifts are of stochastic nature when growth conditions are balanced. Three drift events occurring during 114 generations of cultivation were taxonomically investigated (Table S9.1). We found a flow cytometrically determined drift1 in RC_{10} where G1, G7, G24 and G26 decreased and G3, G16, G22, G33 and G79 increased in cell abundance (Table S8.2). 16S rRNA gene sequencing revealed the loss of *Leadbetterella* (G1, G7, G26) and the gain of *Acidovorax* (G16,

G22). Meanwhile, *Azospirillum* was lost from G24 and reappeared in G3 and G33. Drift2 (RC_{50}, day 61) showed cytometrically determined gates with decreased (G19, G24) and increased cell abundance (G5, G7, G12, G18). 16S rRNA gene sequencing revealed the loss of *Azospirillum* (G19, G24) and the gain of *Leadbetterella* (G7) and *Stenotrophomonas* (G18). Drift3 (Insular II, day 100) showed cytometrically determined gates with decreased (G12, G20, G38) and increased cell abundance (G3, G4, G5, G7, G18, G24). 16S rRNA gene sequencing revealed the loss of *Microbacterium* (G12) and the gain of an unassigned genus from *Sphingobacteriaceae* (G4), *Sphingopyxis* (G5), *Leadbetterella* (G7) and *Brevundimonas* (G18). *Azospirillum* was lost from G20 and G38 and was gained in G3 and G24.

Azospirillum showed its physiological flexibility by switching between different SCs, probably due to cell cycling states (23), rather than going extinct. Other genera also showed that flexibility, although the different SCs can also comprise different species or ecotypes. These findings support the lower intra-community β-diversity, calculated at the genus level, in comparison to the SCs calculated based on flow cytometric data (Fig. S9.3). This flexibility of some of the dominant genera that were also nested and that showed net growth or were rescued by mass transfer appears to have abolished the stochastic events occurring in the balanced periods under RC.

S10: Calculation of the net growth rate μ'

In this study, the biomass was quantified by counting cell numbers in local communities L1-L5 and the regional pool R (Fig. S5.2). The change of the total cell number during an interval Δt (d) was determined by cell numbers coming from the influent, cell numbers lost by the effluent and the net growth rate μ' of cells within Δt (d).

$$Change = Net\ growth + Influent - Effluent \qquad \text{Eq. S10.1}$$

The reactors of the five local communities L1-L5 and the regional pool R were fully mixed. Therefore, the cell numbers of the influent into local communities L1-L5 and into the regional pool R ($influent_{Lin}$ or $influent_{Rin}$) were equal to the cell numbers of the reactors from which the influent was pumped. In addition, the cell numbers in the effluent ($effluent_{Lout}$ or $effluent_{Rout}$) were equal to the cell numbers in that same reactor (L1-L5 or R). The net growth rate μ' of cells was calculated by the following equations:

$$\Delta n_{L,R} \cdot V_{L,R} = \mu' \cdot V_{L,R} \cdot n_{L,R} \cdot \Delta t + Q_{in} \cdot n_{in} \cdot \Delta t - Q_{eff} \cdot n_{eff} \cdot \Delta t \quad \text{Eq. S10.2}$$

$$\mu' = \frac{\Delta n_{L,R}}{\Delta t \cdot n_{L,R}} - \frac{Q_{in} \cdot n_{in}}{V_{L,R} \cdot n_{L,R}} + \frac{Q_{eff} \cdot n_{eff}}{V_{L,R} \cdot n_{L,R}} \quad \text{Eq. S10.3}$$

with:

symbol	description
$n_{L,R}$, n_{in} & n_{eff}	cell numbers (cells mL^{-1}) per reactor [local communities (n_L) and regional pool (n_R)], per influent (n_{in}) or per effluent (n_{eff})
$\Delta n_{L,R}$	difference of cell numbers (cells mL^{-1}) between successive samples in the respective reactors during an interval Δt (d)
$\overline{n_{L,R}}$	average of cell numbers (cells mL^{-1}) between successive samples in the respective reactors during an interval Δt (d)
$V_{L,R}$	working volume (mL) per reactor
Q_{in}	rate of influent volume per reactor (i.e., influent flow rate, mL d^{-1}), which is manually adjusted per phase in this study (Table S2.1)
Q_{eff}	rate of effluent volume per reactor (i.e., effluent flow rate, mL d^{-1})
μ'	net growth rate (d^{-1}) of cells in a local communities L1-L5 or the regional pool R

The difference in cell numbers ($\Delta n_{L,R}$) between successive samples on day i and day $i + \Delta t$ was determined during interval Δt (Eq. S10.4). The average of cell numbers $\overline{n_{L,R}}$ based on the cell numbers of successive samples and per day were calculated (Eq. S10.5) and used for the calculation of μ' during the interval Δt. This was performed for the cell numbers in local communities L1-L5 as well as the regional pool R ($n_{L,R}$).

$$\Delta n_{L,R} = n_{L,R\ at\ i+\Delta t} - n_{L,R\ at\ i} \quad \text{Eq. S10.4}$$

$$\overline{n_{L,R}} = (n_{L,R,at\ i} + n_{L,R,at\ i+\Delta t})/2 \quad \text{Eq. S10.5}$$

Calculation of the recycling rate RC

Calculation of the recycling rate RC for the local communities was based on the given dilution rate $D = Q_{eff}/V_{L,R}$. In this study, D was 0.72 d^{-1}. With fixed working volume $V_{L,R}$, Q_{eff} was balanced with the sum of the flow rates of the influent$_{Lin}$ from the regional pool R (Q_{in}) and the influent from

the medium (Q_{medium}). The influent$_{Lin}$ from the regional pool R (Q_{in}) contained cells. On each day, 576 mL was exchanged per reactor from which, during times of mass transfer, 10%, 50%, or 80% was taken from the regional pool R (Table S2.1). In the local communities L1-L5, with a given D and a given effluent$_{Lout}$ flow rate Q_{eff}, the influent$_{Lin}$ flow rate Q_{in} was dependent on the recycling rate RC.

$$Q_{in} = RC \cdot Q_{eff} \qquad \text{Eq. S10.6}$$

Relationship between net growth rate μ′ and mass transfer rate M

In completely mixed reactors, n_{eff} was considered equal to $n_{L,R}$, and for a local communities L1-L5, n_{in} was considered equal to n_R. For a local communities, Eq. S10.3 was simplified:

$$\mu' = \frac{\Delta n_L}{\Delta t \cdot n_L} - D \cdot RC \cdot \frac{n_R}{n_L} + D \qquad \text{Eq. S10.7}$$

The mass transfer rate M was quantified by the daily cell number entering the local community ($Q_{in} \cdot n_{in}$) in relation to the cell number present in the respective local community ($V_L \cdot n_L$):

$$M = \frac{Q_{in} \cdot n_{in}}{V_L \cdot n_L} = D \cdot RC \cdot \frac{n_R}{n_L} \qquad \text{Eq. S10.8}$$

By this, M was determined by the dilution rate and the recycling rate ($D \cdot RC$) and the relative difference of cell numbers between the regional pool and respective local community ($\frac{n_R}{n_L}$).

Then, Eq. S10.7 was replaced as:

$$\mu' = \frac{\Delta n_L}{\Delta t \cdot n_L} + (D - M) \qquad \text{Eq. S10.9}$$

The net growth rate μ′ is thus dependent on the difference between dilution rate D and mass transfer rate M, which characterizes the influence of emigration or immigration and the relative increase or decrease in cell numbers $\frac{\Delta n_L}{\Delta t \cdot n_L}$.

The ideal relationship among μ′, D and M is shown for a local community in the case of an increase of RCs (Fig. S10.1). In an ideal relationship, the net growth rate μ′ decreases when the mass transfer rate M increases at a given D (from $M1$ to $M3$). Under these circumstances, the increase in M would initially cause an increase in cell numbers (Fig. S10.2). After adaptation and when μ′ is equal to the newly adjusted $(D - M)$ under balanced growth conditions [i.e. μ′ –

$(D - M) = 0$], a successive phase-to-phase decrease of μ′ will occur with further increase of M. Instead, if there is no M and D remains unchanged, the cell numbers will remain stable with $\mu' = D$ after an adaptation period. If M is stopped after periods of various mass transfer rates, the net growth rate will equal D again ($\mu' = D$), which will also lead to a decrease in cell numbers to their original values (Fig. S10.2). In comparison to hypothesized patterns of cell number change (Fig. S10.2), the experimentally counted cell numbers (Fig. S5.2) showed a less clear pattern at phases 1-3. However at RC_{80} and Insular II, cell number changed drastically in the adaptation periods while fluctuating around a plateau in the balanced periods, which fitted our hypothesis (Fig. S5.2).

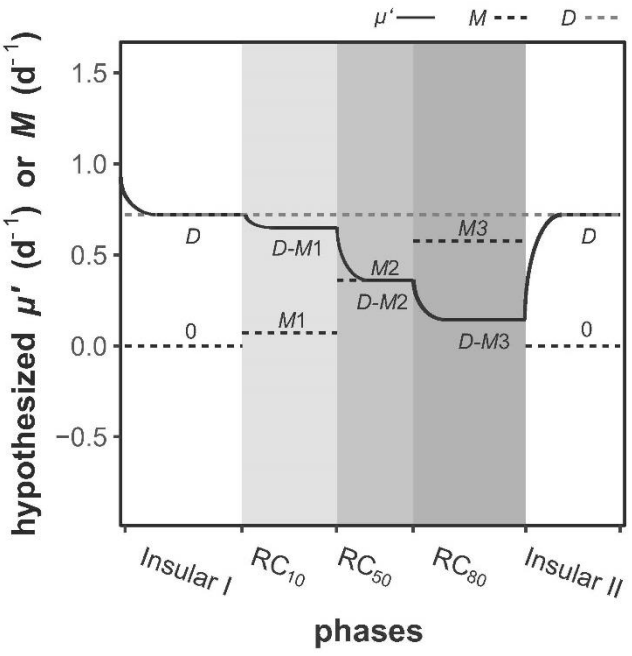

Figure S10.1 Hypothesized ideal dynamics of the net growth rate μ′ **(**the black line) and the mass transfer rate M (dotted black line) after increases in recycling rates RC in a local community. D: dilution rate (dashed grey line). Under ideal balanced conditions with unvarying cell numbers ($\Delta n_L = 0$) and if the cell number of the influent from the regional pool R (n_R) is equal to the cell number in the respective local community (n_L), then the transfer rate is $M = D \cdot RC$ and the net growth rate $\mu' = D - M$. M can be calculated for known RC values: $M1 = 0.1D$ (RC_{10}), $M2 = 0.5D$ (RC_{50}), $M3 = 0.8D$ (RC_{80}). The shaded areas represent different phases with changed RC.

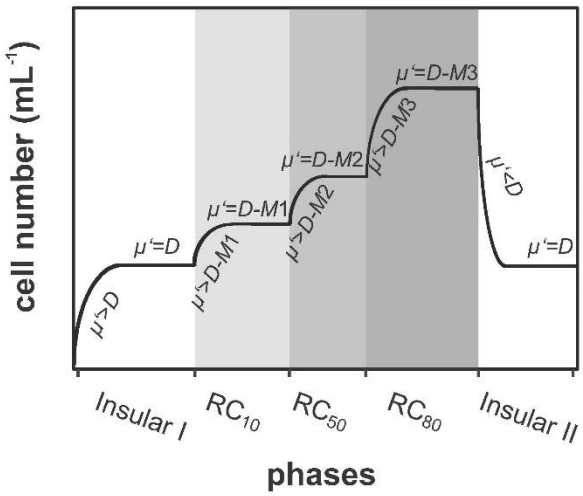

Figure S10.2 Hypothesized ideal dynamics of the cell number (cells mL^{-1}) in a local community after increases in recycling rates RC. μ': net growth rate, D: dilution rate, M: mass transfer rate. The cell numbers increase during the adaptation period when an increase in the mass transfer rate (M) causes an imbalance with $\mu' > D - M$. The net growth rate μ' will equal $(D - M)$ after the adjustment to balanced conditions $\mu' = D - M$. Under balanced conditions, cell numbers do not change ($\Delta n_L = 0$). The shaded areas represent different phases with changed RC.

In our study, the following ideal values for M were expected for the proposed experimental setup when conditions return to balanced situations ($\Delta n_L = 0$) and cell numbers of influent$_{Lin}$ (i.e. regional pool R) are equal to cell numbers in the local community ($n_R = n_L$). With changing RCs, M will also change, such as for $M1 = 0.1D$ = 0.072 d^{-1} (RC$_{10}$); $M2 = 0.5D$ = 0.36 d^{-1} (RC$_{50}$) and $M3 = 0.8D$ = 0.576 d^{-1} (RC$_{80}$). Corresponding to Eq. S10.9, $\mu' = D - M$, the net growth rate can theoretically be calculated to be 0.648 d^{-1} (RC$_{10}$), 0.36 d^{-1} (RC$_{50}$) and 0.144 d^{-1} (RC$_{80}$). For comparison, the average values of experimental M of L1-L5 were for RC$_{10}$ 0.06 ± 0.02 d^{-1}; for RC$_{50}$ 0.30 ± 0.06 d^{-1}; and for RC$_{80}$ 0.59 ± 0.05 d^{-1}, while the average values of calculated μ' were 0.69 ± 0.27 d^{-1}, 0.51 ± 0.42 d^{-1} and 0.20 ± 0.18 d^{-1} (Table S10.1, Dataset S6). Thus, the experimental M and μ' values nearly reached the hypothesized values of Fig. S10.1.

Produced cell numbers in local communities L1-L5

The absolute cell numbers increased from 1.28 ± 0.74 ×10^{12} cells per 800 mL in Insular I phase to 4.23 ± 1.11 ×10^{12} per 800 mL in RC$_{80}$ (Table S10.1). To determine whether this increase in cell number was caused by mass transfer or by real cell production within reactors, the production of individual cells (PC) per reactor per day (cells d^{-1}) was calculated. For this calculation, the net

growth rate μ′ per reactor was used. In addition, the term $\overline{n_{L,R}}$ was considered as the mean of the cell numbers in the same period for which μ′ was calculated.

$$\mathrm{PC} = \mu' \times V_{R,L} \times \overline{n_{L,R}} \qquad \text{Eq. S10.10}$$

The increase in M and the decrease in μ′ in recycling phases RC_{10}-RC_{80} did not markedly influence the number of produced cells per day and reactor (PC). Only in RC_{80} was the PC value slightly lower. The data indicate that nutrients placed no limitation on growth in most phases. Only the ammonium concentration decreased to lower values in RC_{80} and also in R (Fig. S3.1), which supports the lowered PC for RC_{80}. The values of PC, M and μ′ are shown in Table S10.1 and Dataset S6.

Table S10.1 Summary of experimental M, μ′ and PC values per day and at reactors L1-L5. The mean ± sd values were all calculated among local communities L1-L5 during balanced periods. All negative values were set to zero before averaging.

comparison L1-L5	Insular I	RC_{10}	RC_{50}	RC_{80}	Insular II
experimental M (d^{-1})	0	0.06 ± 0.02	0.30 ± 0.06	0.59 ± 0.05	0
experimental μ′ (d^{-1})	0. 71 ± 0.27	0.69 ± 0.27	0.51 ± 0.42	0.20 ± 0.18	0. 79 ± 0.31
cell numbers per reactor (800 mL, $\times 10^{12}$ cells mL^{-1})	1.28 ± 0.74	1.46 ± 0.52	1.97 ± 0.57	4.23 ± 1.11	1.26 ± 0.50
PC per reactor (800 mL, $\times 10^{12}$ cells d^{-1})	0.94 ± 0.56	0.99 ± 0.49	1.01 ± 0.74	0.85 ± 0.72	1.01 ± 40.49

S11: Quantification of the net growth rate per subcommunity μ′ SC_x

Similar to the community net growth rate (μ′, Supplementary Information S10), the net growth rate was calculated for each SC. At the SC-level, the net growth rate (μ′SC_x) of each SC per phase and reactor and time Δt was calculated only for the balanced growth phases (Dataset S7). Overall, 2,400 SCs were evaluated for each of the local and regional communities and per phase. In each phase, if an SC was never dominant ($\leqslant$ 1.25% relative cell abundance per SC), it was excluded from the evaluation. The criterion μ′$SC_x \geqslant 0$ was chosen to differentiate the various degrees of net growth μ′SC_x of cells in the SCs (Fig. 11.1d). For the determination of μ′SC, the absolute cell abundance per SC was used (Fig. S8.2).

The change in cell numbers per SC during interval ∆t (d) was determined by cell numbers per SC originating from the influent, cell numbers per SC lost by the effluent and the net growth rate $\mu' SC$ of the cells per SC within ∆t (d). According to the biomass balance shown in Eq. S11.1, the $\mu' SC$ can be calculated similar to μ' using Eq. S11.2 by specifying the values for SCx (x = 1-80 for 80 SCs in total):

$$\Delta nSC_{x,L,R} \cdot V_{L,R} = \mu' SC_x \cdot V_{L,R} \cdot nSC_{x,L,R} \cdot \Delta t + Q_{in} \cdot nSC_{x,in} \cdot \Delta t - Q_{eff} \cdot nSC_{x,eff} \cdot \Delta t$$

Eq. S11.1

with:

symbol	description
$nSC_{x,L,R}$, $nSC_{x,in}$ & $nSC_{x,eff}$	absolute cell abundances in SC_x (cells mL^{-1}) per reactor [local communities ($nSC_{x,L}$) and regional pool ($nSC_{x,R}$)], per influent ($nSC_{x,in}$) or per effluent ($nSC_{x,eff}$).
$\Delta nSC_{x,L,R}$	difference of absolute cell abundances in SC_x (cells mL^{-1}) between successive samples in the respective reactors during interval Δt (d)
$\overline{nSC_{x,L,R}}$	average of absolute cell abundances in SC_x (cells mL^{-1}) between successive samples in the respective reactors during interval Δt (d)
$\mu' SC_x$	the net growth rate (d^{-1}) of cells in SC_x in local communities L1-L5 or regional pool R

The difference in cell numbers per SC_x ($\Delta nSC_{x,L,R}$) between successive samples was determined for the interval Δt (Eq. S11.2). The average cell numbers per SC_x ($\overline{nSC_{x,L,R}}$) based on the cell numbers per SC of successive samples and per day were calculated (Eq. S11.3) and used for the calculation of $\mu' SC_x$ for interval Δt. This was done for the cell numbers of SC_x in local communities L1-L5 and in the regional pool R ($nSC_{x,L,R}$).

$$\Delta nSC_{x,L,R} = nSC_{x,L,R\ at\ i+\Delta t} - nSC_{x,L,R\ at\ i}$$

Eq. S11.2

$$\overline{nSC_{x,L,R}} = (nSC_{x,L,R\ at\ i} + nSC_{x,L,R\ at\ i+\Delta t})/2$$

Eq. S11.3

For a simplified determination of $\mu' SC_x$ in the local communities L1-L5, we assumed that the absolute cell abundance in the effluent$_{Lout}$ $nSC_{x,eff}$ is equal to the absolute cell abundance of the local communities L1-L5 $nSC_{x,L}$, and the absolute cell abundance in the influent$_{Lin}$ $nSC_{x,in}$ is equal

to absolute cell abundance in the regional pool R $nSC_{x,R}$. For SCx in a local community, Eq. S11.1 was simplified:

$$\mu' SC_x = \frac{\Delta nSC_{x,L}}{\Delta t \cdot nSC_{x,L}} - D \cdot RC \cdot \frac{nSC_{x,R}}{nSC_{x,L}} + D \qquad \text{Eq. S11.4}$$

For a simplified determination of $\mu' SC_x$ in the regional pool R, we assumed that the absolute cell abundance in the effluent$_{Rout}$ $nSC_{x,eff}$ is equal to the absolute cell abundance of the regional pool R $nSC_{x,R}$, and the absolute cell abundance in the influent$_{Rin}$ $nSC_{x,in}$ is equal to the absolute cell abundance in the local communities $nSC_{x,L}$. To calculate the cell numbers per SC entering the regional pool R ($nSC_{x,in}$) from five local communities (see setup of reactor in Fig. 1), the average of the cell numbers of SC_x [$SUM(nSC_{x,L})/5$] was used. Therefore, from Eq. S11.1, the calculation of $\mu' SC_x$ in the regional pool R was simplified:

$$\mu' SC_x = \frac{\Delta(nSC_{x,R})}{\Delta t \cdot nSC_{x,R}} - 5D \cdot \frac{SUM(nSC_{x,L})}{5 \cdot nSC_{x,R}} + 5D \qquad \text{Eq. S11.5}$$

Calculation of $\mu' SC_x$ on the basis of experimental data

In our study, $\mu' SC_x$ was determined on the basis of cell numbers per SC_x. The cell number per SC_x was measured under the influence of the mass transfer at varying RCs on a daily basis. The balanced periods of the different phases were chosen as Δt. For the calculation of $\mu' SC_x$ over Δt, the starting days i (days 7, 33, 54, 71, 96) and ending days $i + \Delta t$ (days 26, 47, 64, 89, 107) were chosen. The detailed values for $\mu' SC_x$ per SC_x during the balanced periods of the different phases are presented for the local communities and the regional pool in Dataset S7. For each phase, $\mu' SC_x$ (x = 1-80) was calculated for the dominant SCs (relative cell abundance > 1.25 in at least one sample during the corresponding periods) in L1-L5 and R (Fig. 4).

The $\mu' SC_x$ of most of the SCs showed positive growth in the local communities L1-L5. Others showed zero growth (blue dots in Fig. 4). Among those that showed zero growth were also those that were negative. The negative values originated from huge variations in cell numbers in the local communities L1-L5 compared to the relatively unchanged ones from the regional pool R (Table S5.1). To prevent an overestimation, we set all seemingly negative growth rates to zero.

Similar to μ' for the whole-community, $\mu' SC_x$ showed a decreasing trend with increased RC (Fig. 4). During phases of insular growth, $\mu' SC_x$ must have been at least equal to D in local communities; otherwise, SCs with $\mu' SC_x < D$ would run the risk of being washed out. Once the

mass transfer M had diminished the danger of a wash out due to back-cycling of cells, $\mu' SC_x$ was adjusted to the actual $D - M$. Thus, cells in SC_x were present in the system with a $\mu' SC_x$ smaller than D. In the regional pool R, there was no influent of fresh medium, and most SCs showed no net growth ($\mu' SC_x$, blue circles in Fig.4) due to severe limitations in nutrients (e.g. ammonium decreased from 27.18 ± 11.22 mg N L^{-1} in local communities to 12.46 ± 8.50 mg N L^{-1} in the regional pool R). Cells entered R at high rates from the local communities L1-L5 where the nutrients were already limited. Consequently, there was minimal capacity for growth.

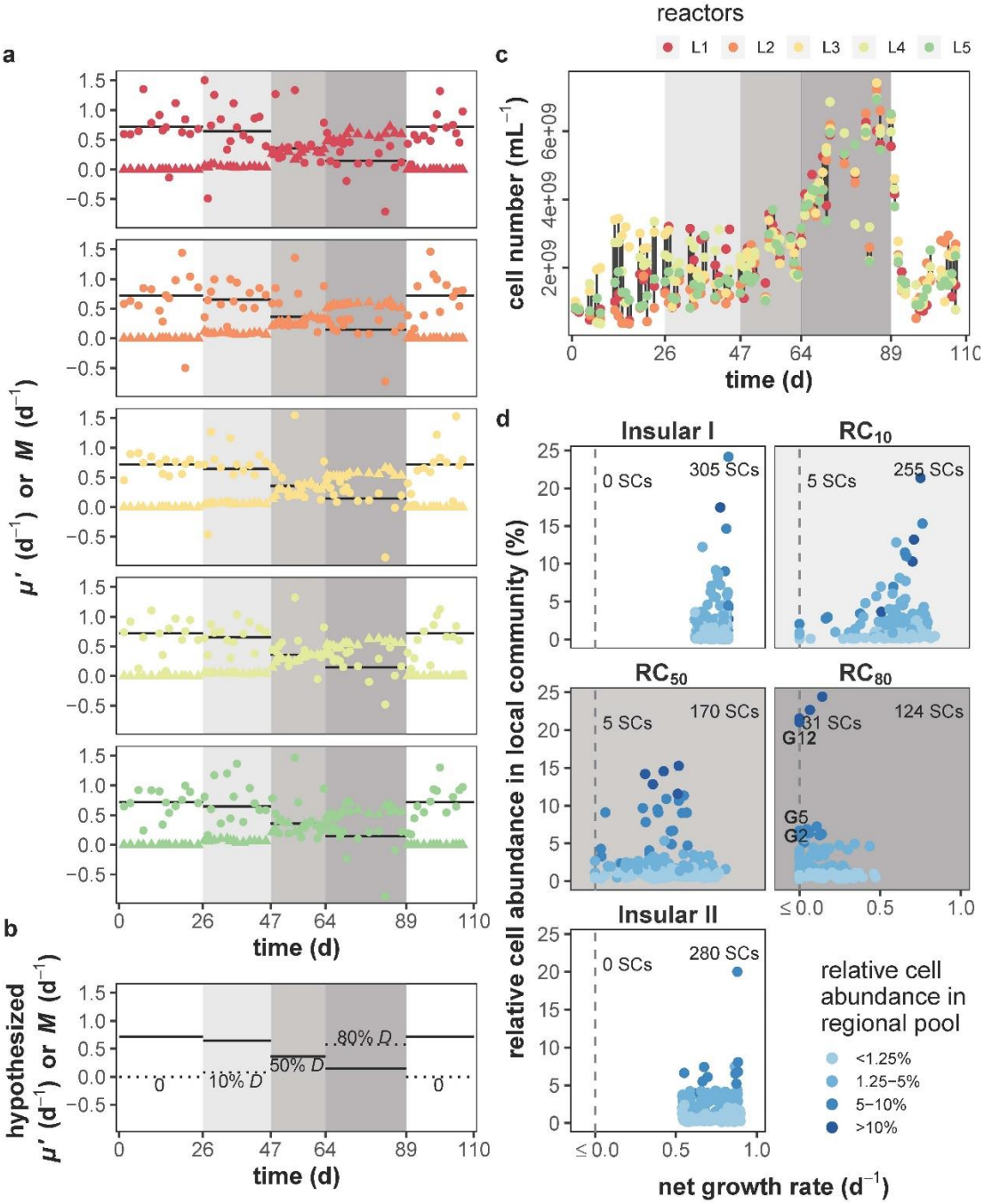

Figure S11.1 Net growth rates of microbiomes and subcommunities during increasing recycling rates RC and mass transfer rates M. **a)** Net growth rate μ′ (closed circles) and mass transfer rate M (closed triangle) of the local microbiomes L1-L5. The hypothesized values for μ′ (black line) are also shown. **b)** Hypothetical M (black dotted line) and μ′ (black line) values calculated for the experimental setup. **c)** Absolute cell numbers for each of L1-L5. **d)** Net growth rates of all dominant SCs ($\mu' SC_x$) of L1-L5. Each point stands for one SC. Heights of points on the y-axis indicate relative average cell abundance per SC during the balanced period per local community. The blue shades show the relative average cell abundance of the same SC in the regional pool R. The vertical grey dashed line indicates $\mu' SC_x = 0$. The numbers of dominant SCs with $\mu' SC_x = 0$ and $\mu' SC_x > 0$ are marked. With $\mu' SC_x = 0$, G12, G5 and G2 were the most abundant ones (relative average cell abundance > 5%) in L1-L5 at RC_{80}. The grey shades in the background of all graphs indicate the five phases Insular I phase, RC_{10}, RC_{50}, RC_{80} and Insular II phase.

S12: Effect of the recycling rate RC on the presence of SC

To determine the influence of the recycling rate RC on absolute cell abundance per SCs (cell number, mL^{-1}), the R package 'Hmisc' (24) and the Pearson's correlation test were used. All SCs from local communities L1-L5 and balanced periods were tested (Fig. S12.1). The test revealed a total of five SCs, which increased their absolute cell numbers to at least 10^8 cells mL^{-1} with increasing RC and showed a high correlation coefficient |rho| $\geqslant$ 0.55, $p \leqslant 0.05$. Theses gates were G5, G12, G13, G14 and G33. All of them were shown to be involved in net growth and rescue under mass transfer (Supplementary Information S11, Fig. 4).

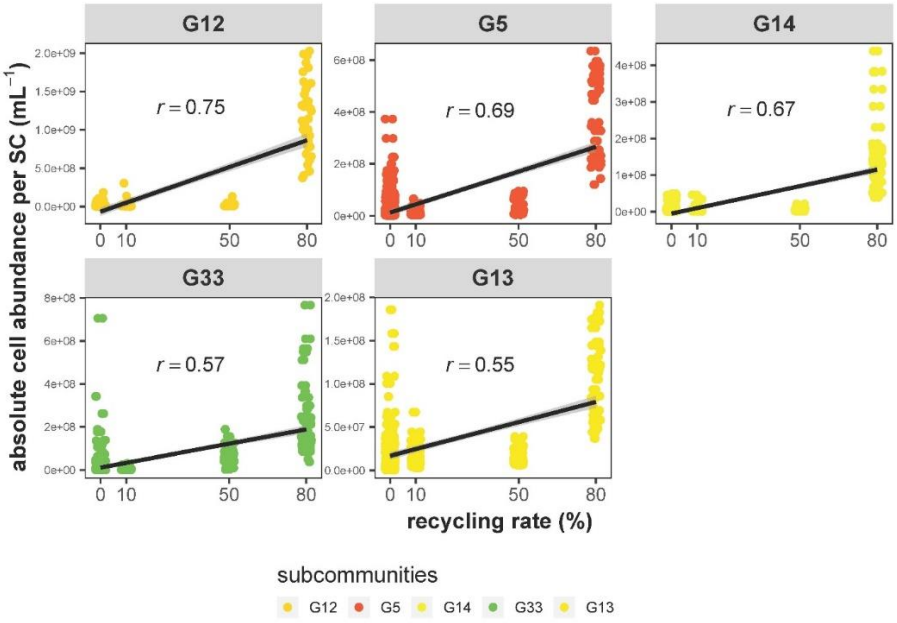

Figure S12.1 The correlations between absolute cell abundance per SC and RC. Only samples from the balanced period were used for analysis, and only correlations with a Pearson's correlation coefficient (r) > 0.55 and SCs with absolute cell numbers increased to at least 10^8 cells mL^{-1} are listed ($p \leqslant 0.05$). The line in each sub-plot indicates linear fitting, while the r value represents Pearson's correlation coefficient. The colors indicate the SCs.

In addition, the strength of the regional pool R to shape local communities L1-L5 in their different phases via mass transfer was tested for all communities including all SCs (from both the adaptation and balanced periods, Fig. S12.2). The data show that, as RC increased (particularly at RC_{80}), fewer SCs responded to mass transfer, but they did so with higher relative abundance per SC. At the same time, SCs tended to have similar relative cell abundances between L1-L5 and R. This is another indication that mass transfer synchronized L1-L5 via R. At Insular I and II phases, there was no correlation of cell abundance per SC between L1-L5 and R and an increase in the variety of dominant SCs. Clearly, the regional pool R shaped the local communities L1-L5.

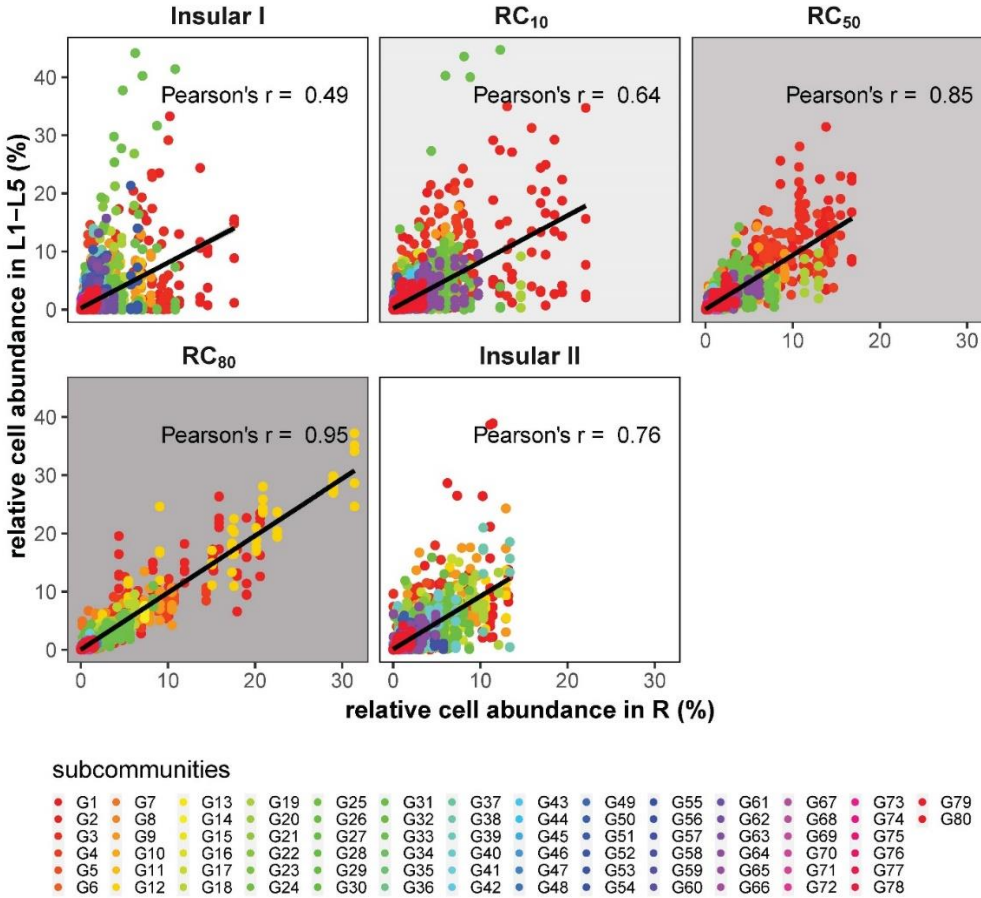

Figure S12.2 Relationship between relative cell abundance per SC in local communities L1-L5 and the regional pool R. The line in each sub-plot indicates linear fitting, labelled with Pearson's correlation coefficient r. The shaded areas represent different phases with changed RC.

S13: Relationship between biotic and abiotic parameters

To analyze whether operational reactor conditions influenced the communities structures over 114 generations, the correlations of SCs versus biotic or abiotic parameters (SC vs. Para) but also between SCs (SC vs. SC) were tested. Spearman's rank order correlation coefficient was used for this purpose. For this analysis, the relative cell abundances of SCs from both the adaptation and the balanced periods were used. The following biotic and abiotic parameters were included in the analysis: pH, electrical conductivity (EC), ammonium, total phosphate (PHOt), total chemical oxygen demand (CODt), supernatant chemical oxygen demand (CODs), biological chemical oxygen demand (CODb), OD and cell number (Fig. S3.1). The lists of all strong correlations [Spearman's rank order correlation coefficient |rho| $\geqslant$ 0.75, $p \leqslant$ 0.05, corrected according to the Benjamini-Hochberg method (25)] are given as Dataset S8 for SC vs. SC correlations and Dataset S9 for SC vs. Para correlations. The numbers of those correlations are summarized in Table S13.1. Both analyses were performed with the R package 'Hmisc' (24).

Table S13.1 The numbers of significant correlations of SC vs. SC and SC vs. Para are summarized for the local communities L1-L5 and the regional pool R per phase. Numbers of correlations in L1-L5 are averaged as mean ± sd. The significant correlations were estimated using Spearman's rank order correlation coefficient |rho| $\geqslant$ 0.75, $p \leqslant$ 0.05, corrected according to the Benjamini-Hochberg method (25). Relative cell abundances were used for the analyses. SC: all subcommunities, Para: biotic and abiotic bulk parameters (Fig. S3.1, without DW).

community	Insular I phase		RC_{10}		RC_{50}		RC_{80}		Insular II phase	
	SC vs. SC	SC vs. Para.	SC vs. SC	SC vs. Para.	SC vs. SC	SC vs. Para.	SC vs. SC	SC vs. Para.	SC vs. SC	SC vs. Para.
L1	234	11	149	20	284	52	259	37	320	52
L2	250	14	272	28	308	71	193	56	182	24
L3	227	8	234	17	363	64	316	47	263	35
L4	234	26	364	45	359	72	246	41	210	53
L5	158	21	228	18	255	64	274	55	277	51
mean ± sd	221 ± 36	16 ± 7	249 ± 78	26 ± 12	314 ± 47	65 ± 8	258 ± 45	47 ± 8	250 ± 55	43 ± 13
R	283	69	292	30	295	68	335	44	319	99

To test whether the newly assembled community members also established an interconnected relationship and changed their interaction potential due to mass transfer, the numbers of

significant correlations of SC vs. SC and between SC and the immediate environment of the microorganisms, SC vs. Para (biotic and abiotic parameters) were counted based on relative cell numbers in SCs. Generally, more significant correlations were found for SC vs. SC and of those more in the recycling phases RC (Table S13.1). The highest number of strong correlations for SC vs. SC in L1-L5 was found for RC_{50} (mean = 314 ± 47) and RC_{80} (mean = 258 ± 45; Wilcoxon test: pairwise comparison, $p = 0.012$ [Insular I vs. RC_{50}], 0.222 [RC_{10} vs. RC_{50}], 0.151 [Insular II vs. RC_{50}] and 0.143 [Insular I vs. RC_{80}], 0.691 [RC_{10} vs. RC_{80}], 1 [Insular II vs. RC_{80}], respectively). The number of correlations was much lower for SC vs. Para; however, the trend was the same for RC_{50} (mean = 65 ± 8) and RC_{80} (mean = 47 ± 8; Wilcoxon test: pairwise comparison, $p =$ 0.112 [Insular I vs. RC_{50}], 0.012 [RC_{10} vs. RC_{50}], 0.027 [Insular II vs. RC_{50}] and 0.008 [Insular I vs. RC_{80}], 0.032 [RC_{10} vs. RC_{80}], 0.548 [Insular II vs. RC_{80}], respectively). These results show the highest interaction potentials of SC vs. SC and SC v. Para in phases RC_{50} and RC_{80}, suggesting newly assembled communities by mass transfer.

A number of SCs profited exclusively from the increase in the recycling rates RC in phases RC_{50} and RC_{80} (Fig. S12.1, linear correlation coefficient |rho| $\geqslant$ 0.55, $p \leqslant 0.05$). Of those, gates G5, G12, G14 and G33 showed the highest cell numbers (> 1×10^8 cells mL^{-1} on average in RC_{80}, each) and among them G5, G12 and G14 were also those that were nested during RC_{50} or RC_{80} (Table S8.4). The cells of these SCs were sorted and analyzed by 16S rRNA gene sequencing (Supplementary Information S9, step2). The number of interactions between the various SCs was found to be generally higher than the interactions between SCs and operational parameters. The low number of interactions between SCs and the operational parameters was probably caused by the continuous setup of the reactor system. Instead, the high number of interactions between SCs under these conditions is contrary to the expected unaltered cell states typical of continuous cultivation of pure cultures.

However, the connected net growth and rescue qualities of certain SCs under mass transfer, especially at RC_{50} and RC_{80} (Fig. S12.1), can be considered responsible for reinforcing their selection and, concomitantly, the (reversible, phase Insular II) decline of the other SCs (Fig. S12.2) can be considered a process that increased the interaction potential between the SCs.

Finally, we performed a partial Mantel test as used by Wu et al. (26) to statistically test if the removal efficiency of CODs, NH4, and PHOt (Supplementary Information S3: Tables S3.2-S3.4) is connected to community compositional change (via relative cell abundance of all subcommunities per sample) caused by increasing mass transfer rates. First, we tested the strength of the Spearman correlation between Cell count and CODs, NH4, or PHOt. The resulting

Spearman correlation coefficients were: Cell count vs. CODs: IrhoI = -0.52, $p = 0$; Cell count vs. NH4: IrhoI = 0.23, $p = 3\times10^{-4}$; Cell count vs. PHOt: IrhoI = -0.08, $p = 0.2057$. The result shows that there is only one relatively strong correlation, namely between Cell count and CODs removal efficiency.

Second, to perform a partial Mantel test between community compositional data and community functional data, we excluded the potential autocorrelation with Cell count (using the R package 'vegan', 13). For the calculations we used the balanced periods of all phases of all reactors, and correlations were performed with 999 permutations. The Bray-Curtis dissimilarity matrix of community composition and Euclidean dissimilarity matrixes of Cell count and removal efficiency were calculated using the R package 'vegan' (13). The partial Mantel test correlation coefficient r_m shows that neither CODs, NH4, nor PHOt (here at least not strongly) removal efficiency was significantly correlated with community composition (partial Mantel test, $r_m = -0.0838$, $p = 0.999$ for CODs removal; $r_m = 0.0144$, $p = 0.697$ for NH4 removal; $r_m = 0.1066$, $p = 0.002$ for PHOt removal).

As an outcome, although the mass transfer rates changed, we found that the CODs, NH4, and PHOt removal efficiencies did not change. Therefore, the partial Mantel test verified that community changes did not influence community function in our metacommunity setup. We can assume that this behavior is caused by the functional redundancy that is typical for wastewater communities.

S14: Assessment of the proportions of deterministic and stochastic processes during mass transfer

Recently, it has been acknowledged that deterministic and stochastic processes shape the community assembly together. Rather than qualitatively determine the community assembly, quantitative tools have been developed to calculate the ratios of deterministic and stochastic processes (27). More specifically, several processes can be defined within ecological frameworks, termed as 'variable/heterogeneous selection', 'homogenizing/homogeneous selection', 'dispersal limitation', 'homogenizing dispersal' and 'undominated/drift' (28-30).

To better understand the community assembly processes under different levels of mass transfer, following our previous work (1, 31), we used three different quantitive tools: NST (Normalized Stochasticity Ratio, 27) analysis was based on flow cytometric data, while the other two tools require phylogenetic information from ASVs (amplicon sequence variants), such as QPEN

(Quantifying assembly Processes based on Entire-community Null model analysis, 28) and iCAMP (Community Assembly Mechanisms by Phylogenetic-bin-based null model analysis, 30). All three methods were performed at each time point, comparing pairwise local communities L1-L5 or local communities with the regionl pool R that were within the bounded metacommunity (27).

Normalized Stochasticity Ratio (NST) analysis

According to Ning et al. (27), the NST analysis considers two scenarios of deterministic processes that cause communities to be more similar (type A) or more dissimilar (type B) than the simulated communities based on null model (a community is assembled by random forces only, and stochasticity is theoretically 100%). Community simulation is the computational process in which virtual communities are created multiple times (1000 times):

1) The relative cell abundance data of the subcommunities are converted to presence-absence data of cells in dominant subcommunities (relative cell abundance > 1.25%);

2) The observed occurrence frequency of cells in each of the dominant subcommunities in all samples is calculated using all samples;

3) Then, a virtual assembly of the simulated community is performed by a repeated random selection of individuals from these dominant subcommunities, and the probabilities of how often individuals of these subcommunities are included in the assembly of a simulated community are proportional to the observed occurrence frequencies of these subcommunities.

The Jaccard dissimilarities are calculated between pairwise simulated communities, and an average of these values is computed. Therefore, the difference between the observed values from our data and the average values of the simulated community, representing the theoretical null model (stochasticity = 100%), was used to assess the strength of deterministic processes of community assembly in the observed community. The strength of stochastic processes was assessed by subtracting the determinism of the observed community from 100% (these values were further normalized to scale to 100%, taking into account the extreme values at full deterministic and stochastic assembly). The resulting NST values were tested by bootstrapping (1000 times) and represented by mean values (black dots) with error bars (black lines) from the bootstrapping test in Fig. S14.1.

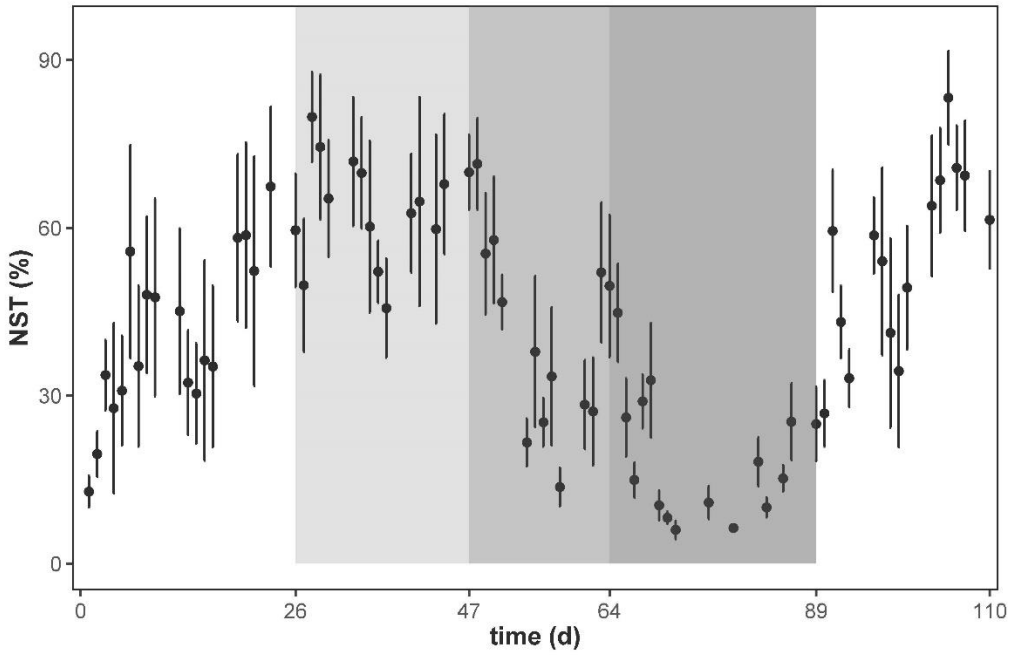

Figure S14.1 The relative importance of stochastic processes in community assembly over time, indicated by the index NST (Normalized Stochasticity Ratio, 27), by comparing local communities L1-5 based on flow cytometric data.

The community assembly was determined by both stochastic and deterministic processes (Fig. S14.1). Stochastic processes were particularly high in the insular phases (maximum 83% in the Insular II phase). While in the Insular I phase the stochasticity increased after the community adapted to the cultivation conditions, in Insular II phase the community reorganized itself after mass transfer to the insular conditions. Stochasticity was still high in phase 2 (RC_{10}), but decreased to minimum 6% during phase 4 (RC_{80}). The NST analysis of Ning et al. (27) supports our findings that mass transfer reduces stochasticity and synchronizes parallel running multiple communities. According to the definition of Ning et al. (27), which states that community assembly is more deterministic when NST< 50%, and more stochastic when NST >50%, we can conclude that through mass transfer at RC_{50} and especially at RC_{80}, a community is mainly assembled by deterministic processes and stochastic processes hardly play any role anymore.

Quantifying assembly processes based on Entire-community Null model analysis (QPEN)

Using QPEN, Stegen et al. (28) investigated both phylogenetic turnover and turnover of ASV composition of the entire communities, using βNTI (β-nearest taxon index) and βRC_{bray} (Raup-Crick metric based on Bray-Curtis dissimilarity), respectively, to determine ecological processes

(homogenizing selection, variable selection, dispersal limitation, homogenizing dispersal and undominant). In principle, high phylogenetic turnover indicates differentiation of niches that select for taxa with corresponding habitat preferences, based on the finding that habitat preferences of closely phylogenetically related taxa are more similar to each other than habitat preferences of distant relatives (32). Therefore, phylogenetic turnover between communities, quantified by βNTI, is calculated to determine whether an ecological proccess is driven by environmental selection:

1) The (abundance-weighted) β-mean-nearest taxon distance (βMNTD) is calculated between pairwise communities, quantifying the phylogenetic distance between each ASV in one community and its closest relative in a second community.

2) The βMNTD value of the null model is calculated by first randomizing ASV names and frequencies at the tips of the phylogenetic tree, and then recalculating βMNTD to obtain a null value. The randomization and recalculation are repeated 999 times.

3) The β-nearest taxon index (βNTI) is calculated as the difference between observed βMNTD and average null value of βMNTD.

4) βNTI < -2 or > +2 means that phylogenetic turnover is significantly smaller or larger than the null model.

In the calculation of βRC_{bray}, a null model test is also performed using a procedure similar to that used in the NST analysis (27). One difference is that a null model in the βRC_{bray} calculation uses the relative abundances of ASVs. The probabilities that ASVs are included in a simulated community are proportional to the average relative abundances of ASVs over all samples. The other difference is that Bray-Curtis dissimilarity is used instead of Jaccard dissimilarity. The deviation between the observed Bray-Curtis dissimilarity value and the null model value is standardized as the βRC_{bray} value. $\beta RC_{bray} < -0.95$ or $> +0.95$ provide the criteria to determine if the observed ASV composition turnover significantly deviates from the null model.

Stegen et al. (29) summarized the ecological processes as: 1) Homogeneous selection when βNTI < -2, meaning that communities occur in the same selective environment and selection is strong. 2) Variable selection when βNTI > +2, implying that communities are assembled in different selective environments. 3) Dispersal limitation when $|\beta NTI| < 2$ and $\beta RC_{bray} > +0.95$, which means a community has no influence on other communities and drift acts alongside dispersal limitation. 4) Homogenizing dispersal when $|\beta NTI| < 2$ and $\beta RC_{bray} < -0.95$, which means a high rate of dispersal homogenizes communities. 5) Undominated when $|\beta NTI| < 2$ and $|\beta RC_{bray}| < 0.95$, which means there is a moderate rate of dispersal and selection is relatively weak (28, 29).

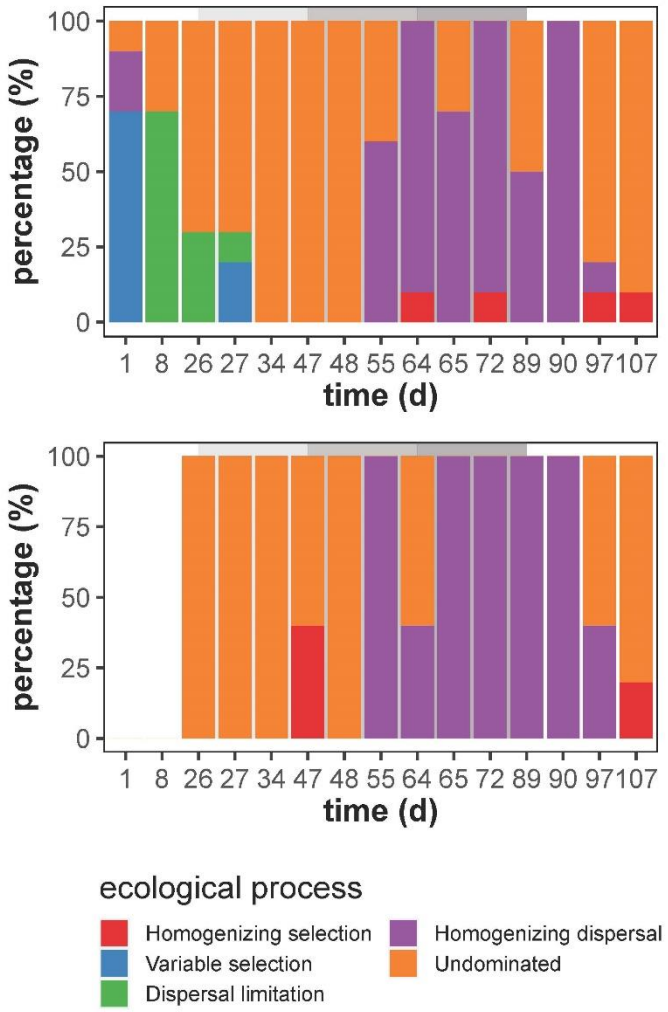

Figure S14.2 The percentages of ecological processes (28, 29) of community assembly over time, comparing between local communities (top), and between local communities and regional pool (bottom), based on 16S rRNA gene amplicon sequencing data.

At each time point, 10 pairwise comparisons between local communities (L vs. L) and 5 pairwise comparisons between local communities and the regional pool (L vs. R) were performed. Each comparison undergoes the criteria described above and the relative importance of each of the five ecological processes are calculated. The result is presented as Fig. S14.2.

The assembly of communities was mainly governed by dispersal-related processes: dispersal limitation or homogenizing dispersal. 1) Homogenizing selection was low and never dominated at any time point, while 2) variable selection was only dominated at day 1, when communities adapted to the reactor conditions through complex biotic and abiotic interactions. 3) Dispersal limitation dominated the ecological processes during the Insular I phase, confirming our

expectation that zero mass transfer supports stochastic process such as drift. 4) Homogenizing dispersal was particular dominant at late RC_{50} and at RC_{80}, which fits our hypothesis that high mass transfer synchronizes communities. The homogenizing dispersal was still prevalent into the early Insular II phase, so we hypothesize that a historical effect of RC_{80} delayed the development of insular communities which then became divergent in their structures. 5) Undominated process (i.e., moderate dispersal and weak selection) governed community assembly during RC_{10} and RC_{50}, a period of transition from zero to high mass transfer.

Infer Community Assembly Mechanisms by Phylogenetic-Bin-Based Null Model Analysis (iCAMP)

Ning et al. (30) modified the quantitative framework created by Stegen et al. (QPEN, 28, 29), creating the iCAMP approach. iCAMP assesses the ecological processes at the level of taxa lineages rather than the entire community. Ecological processes may differ between different microbial groups in a community, e.g., within a community certain microbial groups are under selection while others are under drift. The first step is phylogenetic binning, which divides taxa into different groups ('bins') based on their phylogenetic relationships. The iCAMP calculates phylogenetic diversities (i.e., phylogenetic turnover, using beta Net Relatedness Index, βNRI) and taxonomic β-diversities (i.e, ASV composition turnover, using modified Raup-Crick metric, βRC_{bray}) between the same bins in pairwise samples, and the ecological process are determined according to similar criteria as used by QPEN (the difference is that phylogenetic turnover is calculated using β-mean-pairwise distance instead of β-mean-nearest taxon distance in QPEN). The relative importance of the five studied ecological processes (HeS, HoS, DL, HD, DR) between pairwise communities is represented by the mean relative abundance (across the pairwise samples) of bins (each representing a sum of relative abundances of ASVs). At each time point, 10 pairwise comparisons between local communities (L vs. L) and 5 pairwise comparisons between local communities and the regional pool (L vs. R) were performed and the relative importance of each ecological process was visualized separately as points in the five panels of Fig. S14.3.

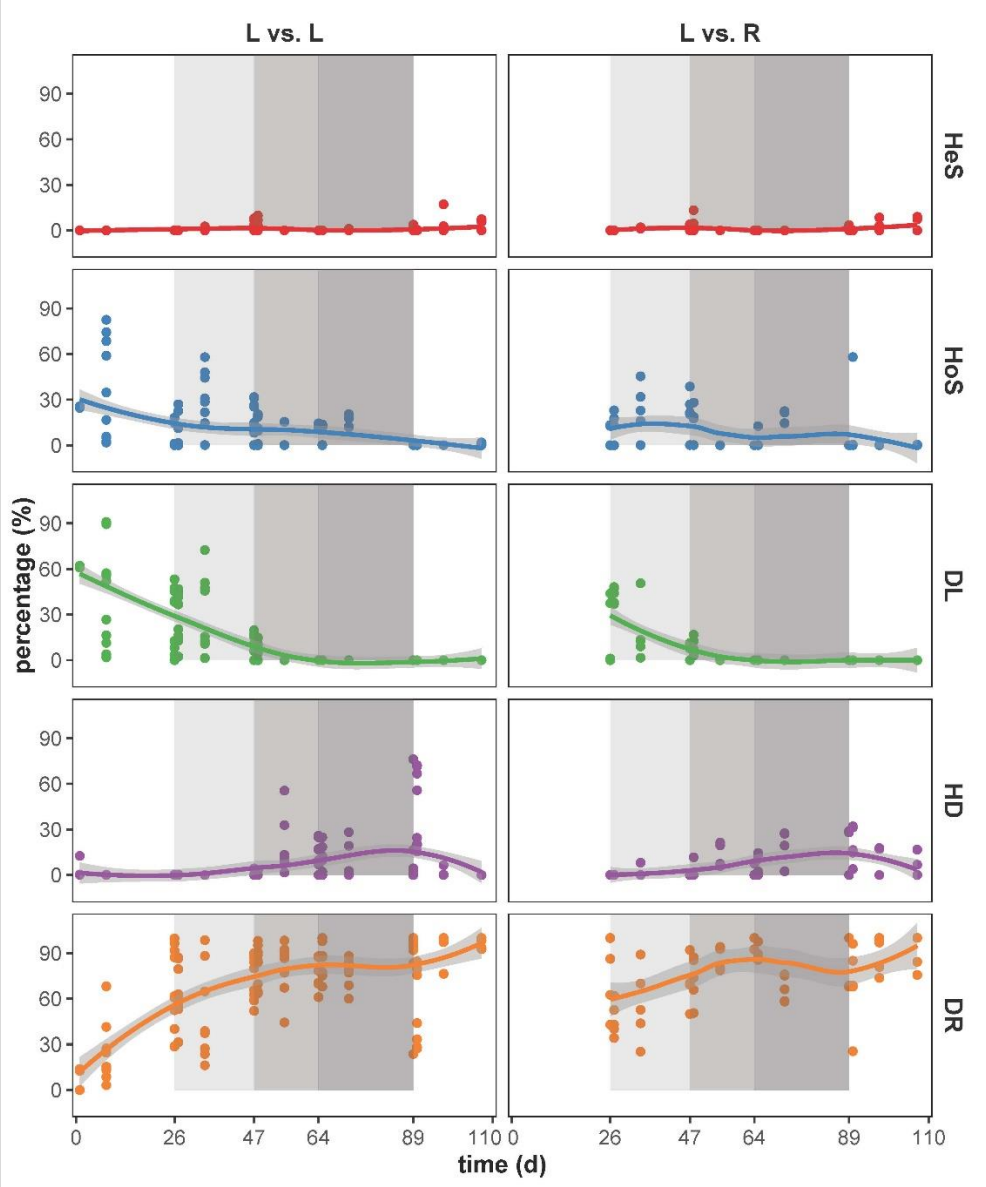

Figure S14.3 The percentages of community assembly mechanisms over time compared between local communities (L vs. L, left panel) and between local communities and the regional pool (L vs. R, right panel). According to Ning et al. (30), a phylogenetic-bin-based null model analysis (iCAMP) was used based on 16S rRNA gene amplicon sequencing data. HeS: heterogeneous selection; HoS: homogeneous selection; DL: dispersal limitation; HD: homogenizing dispersal; DR: drift, diversification, weak selection, and/or weak dispersal.

Trends in the relative importance of the five ecological processes of community assembly analyzed by iCAMP over time largely confirmed the results of QPEN (Fig. S14.2), such as those associated with dispersal, including dispersal limitation (DL) and homogenizing dispersal (HD).

Both heterogeneous selection (HeS) and homogeneous selection (HoS) were low after the community adapted to continuous cultivation conditions.

The three tools (QPEN, 28; NST, 27; and iCAMP, 30) all confirmed the results of our study that mass transfer homogenized local communities and the regional pool and reduced stochastic processes to as low as 6% (corresponding determinism = 94%). Similar to Stegen's method QPEN, the values calculated with iCAMP indicated homogenizing dispersal (HD) and progressive (decreasing) stochastic variation in phases 2 to 4 (27, Fig. S14.1). Selection was found to be exceptionally low in phase 4 (RC_{80}) by all three tools.

References

1. Z. Liu *et al*., Neutral mechanisms and niche differentiation in steady-state insular microbial communities revealed by single cell analysis. *Environ Microbiol* **21**, 164-181 (2019).
2. A. Cydzik-Kwiatkowska, D. Nosek, Biological release of phosphorus is more efficient from activated than from aerobic granular sludge. *Sci Rep* **10,** 11076 (2020).
3. N. Cichocki *et al*., Bacterial mock communities as standards for reproducible cytometric microbiome analysis. *Nat Protoc* **15**, 2788-2812 (2020).
4. C. Koch, S. Günther, A.F. Desta, T. Hübschmann, S. Müller, Cytometric fingerprinting for analyzing microbial intracommunity structure variation and identifying subcommunity function. *Nat Protoc* **8**, 190-202 (2013).
5. S. Takahashi, J. Tomita, K. Nishioka, T. Hisada, M. Nishijima, Development of a prokaryotic universal primer for simultaneous analysis of bacteria and archaea using next-generation sequencing. *PLoS One* **9** e105592 (2014).
6. D.P.R. Herlemann *et al*., Transitions in bacterial communities along the 2000 km salinity gradient of the Baltic Sea. *ISME J* **5**, 1571-1579 (2011).
7. E. Bolyen *et al*., Reproducible, interactive, scalable and extensible microbiome data science using QIIME 2 (vol 37, pg 852, 2019). *Nat Biotechnol* **37**, 1091-1091 (2019).
8. B.J. Callahan *et al*., DADA2: High-resolution sample inference from Illumina amplicon data. *Nat Methods* **13**, 581-583 (2016).
9. C. Quast *et al*., The SILVA ribosomal RNA gene database project: improved data processing and web-based tools. *Nucleic Acids Res* **41**, D590-D596 (2013).
10. S. McGinnis, T.L. Madden, BLAST: at the core of a powerful and diverse set of sequence analysis tools. *Nucleic Acids Res* **32**, W20-W25 (2004).
11. P.J. McMurdie, S. Holmes, phyloseq: an R package for reproducible interactive analysis and graphics of microbiome census data. *PLoS One* **8**, e61217 (2013).
12. Z. Liu *et al*., Ecological stability properties of microbial communities assessed by flow cytometry. *mSphere* **3** (2018).
13. J. Oksanen *et al*., Community ecology package. *R package version* **2** (2013).
14. Z. Liu, S. Müller, Bacterial community diversity dynamics highlight degrees of nestedness and turnover patterns. *Cytometry A* **97**, 742-748 (2020).
15. A. Baselga, Partitioning the turnover and nestedness components of beta diversity. *Glob Ecol Biogeogr* **19**, 134-143 (2010).
16. A. Baselga, The relationship between species replacement, dissimilarity derived from nestedness, and nestedness. *Glob Ecol Biogeogr* **21**, 1223-1232 (2012).

17. Q. Feng *et al*., Treatment of shale gas fracturing wastewater using microbial fuel cells: Mixture of aging landfill leachate and traditional aerobic sludge as catholyte. *J Clean Prod* **269**, 121776 (2020).
18. B. Shao *et al*., Enhanced treatment of shale gas fracturing waste fluid through plant-microbial synergism. *Environ Sci Pollut Res Int* **28**, 29919–29930 (2021).
19. P.L. Steyn *et al*., Classification of heparinolytic bacteria into a new genus, *Pedobacter*, comprising four species: *Pedobacter heparinus* comb, nov., *Pedobacter piscium* comb. nov., *Pedobacter africanus* sp. nov. and *Pedobacter saltans* sp. nov. Proposal of the family *Sphingobacteriaceae* fam. nov. *Int J Syst Bacteriol* **48**, 165-177 (1998).
20. T.A. Pankratov, B.J. Tindall, W. Liesack, S.N. Dedysh, *Mucilaginibacter paludis* gen. nov., sp. nov. and *Mucilaginibacter gracilis* sp. nov., pectin-, xylan- and laminarin-degrading members of the family *Sphingobacteriaceae* from acidic *Sphagnum* peat bog. *Int J Syst Evol Micr* **57**, 2349–2354 (2007).
21. S. Nagar *et al*., Phylogenetic relationships and potential functional attributes of the genus *Parapedobacter*: A member of family *Sphingobacteriaceae*. *Front Microbiol* **11**, 1725 (2020).
22. O. Steenhoudt, J. Vanderleyden, *Azospirillum*, a free-living nitrogen-fixing bacterium closely associated with grasses: genetic, biochemical and ecological aspects. *FEMS Microbiol Rev* **24**, 487-506 (2000).
23. S. Müller, Modes of cytometric bacterial DNA pattern: a tool for pursuing growth. *Cell Proliferat* **40**, 621-639 (2007).
24. F.E. Harrell, C. Dupont, Hmisc: harrell miscellaneous. *R package version* **3** (2008).
25. Y. Benjamini, Y. Hochberg, Controlling the false discovery rate - a practical and powerful approach to multiple testing. *J R Stat Soc Ser B* **57**, 289-300 (1995).
26. L. Wu *et al*., Global diversity and biogeography of bacterial communities in wastewater treatment plants. *Nat Microbiol* **4**, 1183–1195 (2019).
27. D. Ning, Y. Deng, J. M. Tiedje, J. Zhou, A general framework for quantitatively assessing ecological stochasticity. *Proc Natl Acad Sci USA* **116**, 16892-16898 (2019).
28. J. C. Stegen *et al*., Quantifying community assembly processes and identifying features that impose them. *ISME J* **7**, 2069-2079 (2013).
29. J. C. Stegen, X. Lin, J. K. Fredrickson, A. E. Konopka, Estimating and mapping ecological processes influencing microbial community assembly. *Front Microbiol* **6**, 370 (2015).
30. D. Ning *et al*., A quantitative framework reveals ecological drivers of grassland soil microbial community assembly in response to warming. *Nat Commun* **11**, 4717 (2020).
31. S. Günther *et al*., Species-sorting and mass-transfer paradigms control managed natural metacommunities. *Environ Microbiol* **18**, 4862-4877 (2016).
32. J. B. Losos, Phylogenetic niche conservatism, phylogenetic signal and the relationship between phylogenetic relatedness and ecological similarity among species. *Ecol Lett* **11**, 995–1003 (2008).